UNIVERSITY OF LIVERPOOL

Nitric Oxide Releasing Implants for Orthopaedic Applications

Thesis submitted in accordance with the requirements of

The University of Liverpool

for the degree of

Doctor of Philosophy

By Man Li

March, 2021

Abstract

The pathogenesis of many orthopaedic infections is related to the presence of biofilms on device surfaces, which are currently combatted, primarily by use conventional antibiotic therapies once the infection has occurred. However, the overuse and misuse of antibiotics has led to antimicrobial resistance (AMR) and therefore it is of great important to develop non-antibiotic approaches to efficiently treat biofilm-related bacterial infection for orthopaedic applications.

In this study, two different materials were investigated that are relevant to orthopaedic applications: titanium (Ti, non-degradable) and polycaprolactone/gelatine (PCL/GT, degradable). NO is used as an efficient antibacterial and antibiofilm agent as well as acting as a regulator of bone tissue engineering. Three NO-releasing systems have been designed and fabricated. The mechanisms of NO release kinetics and the antimicrobial properties of these systems are the key points to study in the main experimental chapters. The chemical modification of NO-releasing coatings on three platforms inhibits bacterial adhesion, resulting in impediment of biofilm formation on surfaces.

In Chapter 3, NO-releasing flat Ti surfaces were developed for antibiofilm and bone-integrating studies. Two different aminosilane precursors (6-Aminohexyl-3-aminopropyl trimethoxysilane (AHAP3) and 11-Aminoundecyltriethoxysilane (AUTES)) were immobilised onto the surface allowing the necessary amino functionality required to subsequently tether diazeniumdiolates. The structure of aminosilane precursors affected the resultant NO releasing properties in terms of payload and release kinetics. Both AHAP3/NO and AUTES/NO displayed similar biofilm inhibition efficiency against *Staphylococcus aureus (S. aureus)* and *Pseudomonas aeruginosa (P. aeruginosa)* after 6 h. And AUTES/NO was shown not to be cytotoxic towards human primary bone cells.

In Chapter 4, Ti foams were fabricated with a novel Lost Carbonate Sintering (LCS) process, and different layers of AUTES (the best performing silane precursor in Chapter 3) have been used as aminosilane precursors to silanise the Ti foams. The layers of AUTES played roles on the NO-releasing kinetics and the antimicrobial efficacy of the Ti foams. 5%AUTES/NO displayed the optimal antibiofilm/antimicrobial properties against both *Escherichia coli (E. coli)* and *S. aureus* after 4 and 24 h.

In Chapter 5, electrospun biodegradable scaffolds functionalised with NO were evaluated for their antimicrobial properties and bone cytocompatibility. Five ratios of PCL/GT polymer blends were electrospun into membranes and crosslinked with varying concentrations of genipin to control the degradation profile. The addition of PCL and crosslinking process improved the microstructure and the wettability of the membranes. In antibiofilm tests against *E. coli* and *S. aureus*, the crosslinked NO-releasing membrane that contained more gelatine displayed higher efficacy on both surface biofilm inhibition after 4 h owing to the higher loading of NO on these membranes. The crosslinked NO-releasing membranes with longer degradation profiles also performed better in terms of antibacterial response than the non-crosslinked equivalents.

Acknowledgements

First of all, I would like to thank my supervisor Dr. Raechelle D'Sa for her complete support, guidance, motivation and encouragement throughout my PhD course. Her door is always open anytime I need help and advice on either academia or life. The experience in the group is my treasure for a lifetime.

I am extremely grateful to Dr. Jenny Aveyard for her mentoring since the first day of my PhD journey, and for her constant emotional support and encouragement. Her passion, erudition and devotion in and out lab inspire me being a more positive person for my future.

Many thanks to Dr. Jude Curran and her group members for helping me address every issue I have encountered in my cell work, from purchasing the cell medium to capturing beautiful cell images.

I would also like to thank all the members of D'Sa Lab, present and past, for your support, and for the time we spent together during the long days of work.

I wish to express my gratitude to all the colleagues and staff at University of Liverpool for the help with different techniques employed in my study.

Thank you to all my friends, and the many students across the University of Liverpool and beyond who have helped to make this experience so much more enjoyable.

I am thankful to the financial support from China Scholarship Council.

And finally, I would like to dedicate this work to Mufeng and mom and dad, who have always supported any decision I have made, and believed in me to achieve my best. Thank you for being my constant rocks.

Table of Contents

Nomenclature

AFM	Atomic force microscopy
AHAP3	6-Aminohexyl-3-aminopropyl trimethoxysilane
AMR	Antimicrobial resistance
at. %	Atomic % concentration
AUTES	11-Aminoundecyltriethoxysilane
CFU	Colony forming unit
d	Day
DMEM	Dulbecco's Modified Eagle Medium
DTMS	n-Decyltrimethoxysilane
ECM	Extracellular matrix
E. coli	*Escherichia coli*
EDX	Energy dispersive X-ray spectroscopy
eV	Electron volt
FBS	fetal bovine serum
FTIR	Fourier-transform infrared spectroscopy
GBR	Guided bone regeneration
GT	Gelatine
HAc	Acetic acid
h	Hour
K_a	Acid dissociation constant
LB	Luria-Bertani
LCS	Lost carbonate sintering
min	Minute
MRSA	methicillin-resistant *Staphylococcus aureus*
NaAc	Sodium acetate
NO	Nitric oxide
$[NO]_m$	Maximum instantaneous NO release concentration
P. aeruginosa	*Pseudomonas aeruginosa*
PBS	Phosphate buffered saline
PCL	Polycaprolactone

R_a	Average roughness
RNOS	Reactive nitrogen oxide species
R_q	Root mean square roughness
RSNO	Nitrosothiol
S. aureus	*Staphylococcus aureus*
SEM	Scanning electron microscopy
$t_{1/2}$	half-life of NO release
t_d	NO release duration
Ti	Titanium
t_m	Time required to reach $[NO]_m$
t[NO]	Total concentration of NO after 1 h
UV-Vis	Ultraviolet visible spectroscopy
wt%	Mass fraction
XPS	X-ray photoelectron spectroscopy

Chapter 1: Introduction

Orthopaedic implants are widely used for fixation of long bone fracture, correction and stabilisation of spine deformities, replacement of joints, and cranio-maxillofacial applications. According to National Joint Registry,[1] for joint replacements alone over 2.5 million surgeries have been performed in the UK, and the number is still growing annually, especially given the increase the ageing demographic. The result of this is a significant economic burden on the NHS. Furthermore, morbidity and mortality rates may actually increase implants fail. Two leading causes of orthopaedic implant failure are aseptic loosening (18%) and infection (20%).[2] Aseptic loosening originates from poor integration of implants. Infections result from pathogens (mainly biofilm-forming bacteria) on implant surfaces, in which, *Staphylococcus* species, prominently *Staphylococcus aureus* (*S. aureus*) and *Staphylococcus epidermidis* (*S. epidermis*), account for approximately 70% of the infections. *Pseudomonas aeruginosa* (*P. aeruginosa*) accounts for another 8%.[3] *Escherichia coli* (*E. coli*) is also one of the most frequently isolated microorganism in orthopaedic implant infections with a portion of approximately 6-23%.[4-5]

The pathogenesis of many orthopaedic infections is related to the presence of biofilms on device surfaces, and current, primary treatment involves the use of conventional antibiotic therapy which can lead to antimicrobial resistance (AMR).[6] Once a biofilm forms on a surface it is much more difficult to eradicate than planktonic bacteria as biofilm cells are inherently more tolerant to antibiotics (up to 1000x higher concentration of antibiotics are needed to achieve efficient treatment).[7-8] The overuse and misuse of antibiotics has however resulted in the rise

of AMR which necessitates larger doses and last resort antibiotics for treatment. AMR is predicted to kill 10 million people annually by 2050 and have a global economic burden of over 100 trillion USD.[9] Moreover, no new classes of antibiotic have been discovered since 1987.[10] As such there is an urgent need to develop new alternatives to antibiotics that can treat infections without contributing to AMR.

In the body of this thesis, non-antibiotic antimicrobial materials, with specific focus on nitric oxide (NO)-releasing materials are designed and fabricated for potential orthopaedic applications.

1.1 Aims and Objectives

NO is a potent antimicrobial agent that is produced endogenously as a response to invading pathogens and not developing antimicrobial resistance. The antimicrobial efficacy of NO is dependent upon the NO release kinetics, resulting from NO delivery strategy. Both the antimicrobial capacity and cytotoxicity of NO are needed to be concerned in designing NO release platforms for biomedical applications. The aim of this thesis is to develop NO releasing systems that can treat infections on non-degradable (titanium) and degradable (electrospun membranes) surfaces for use in orthopaedic implant material development.

The aim of this thesis is achieved via these objectives:

1. To fabricate a range of bone-integrating, silane-modified titanium implant surfaces that can release NO for the purpose of treating orthopaedic infections without the use of antibiotics

2. To investigate the mechanism of NO release of these silane-modified NO releasing surfaces in order to control the rate and payload of active agent delivered.
3. To investigate the feasibility of tethering NO-releasing silane-precursor molecules onto titanium foams fabricated using lost carbon sintering (LCS) as a viable antimicrobial bone-integrating porous scaffold.
4. To investigate the fabrication of a range of electrospun biodegradable PCL/gelatine scaffolds for bone tissue engineering applications.
5. To investigate tethering of NO-releasing diazeniumdiolates, along with subsequent release kinetics and payload onto these electrospun scaffolds.
6. To evaluate the antimicrobial efficacy and cytocompatibility of these NO releasing materials.

1.2 Structure of the Thesis

The structure of this thesis follows the antimicrobial structure design strategy, ranging from surfaces to porous structure to membranes, using different fabrication techniques. The chapter orders are as follows:

- **Chapter 2**: Literature Review
- **Chapter 3**: Nitric Oxide Releasing Titanium Surfaces for Antimicrobial Bone-Integrating Orthopaedic Implants
- **Chapter 4**: Antimicrobial Nitric Oxide Releasing Porous Titanium Foams
- **Chapter 5**: Fabrication and Characterisation of Antimicrobial Guided Bone Regeneration (GBR) Electrospun Membranes
- **Chapter 6**: Conclusions and Suggestions for Future Work

1.3 Publications During PhD Study

- **Li, M.**, Aveyard, J., Fleming, G., Curran, J.M., McBride, F., Raval, R. and D'Sa, R.A., 2020. Nitric Oxide Releasing Titanium Surfaces for Antimicrobial Bone-Integrating Orthopaedic Implants. *ACS Applied Materials & Interfaces*, 12, pp.22433-22443.

- Qian, B., Zheng, Z., Liu, C., **Li, M.**, D'Sa, R.A., Li, H., Graham, M., Michailidis, M., Kantserev, P., Vinokurov, V. and Shchukin, D., 2020. Microcapsules Prepared via Pickering Emulsion Polymerisation for Multifunctional Coatings. *Progress in Organic Coatings*, 147, p.105785.

Chapter2: Literature Review

2.1 Biofilm-Related Infections in Orthopaedic Implants

2.1.1 Antimicrobial Resistance

Antimicrobial resistance (AMR) is a substantial global challenge associated with high rates of morbidity and mortality.[11-13] The misuse and overuse of antibiotics in clinical therapy for bacterial infection have been regarded as the primary drivers that causing AMR.[14-16] It has been reported that the rate of the surgical failure in orthopaedic implants due to bacterial infection is approximately 20%.[17] AMR occurs across worldwide regardless of the income level and inflicts the increasing clinical and financial burden.[18] Currently, there are 700,000 deaths annually are attributed to AMR infections. It also has been estimated to have a globally rise to 10 million people die from AMR and 100 trillion USD costs by 2050 if current trends continue.[9, 19] In the past 10 years, the World Health Organisation (WHO) and many other organisations have filed reports on the importance of studying and finding protocols in tackling the global rise of AMR.[9, 19]

Bacterial resistance is intensively related to the abuse of antibiotic in hospitals or community. An increased mortality rates of patients with bloodstream infections has been reported to be associated with resistant *Escherichia coli* (*E. coli*), *Pseudomonas aeruginosa* (*P. aeruginosa*), *Staphylococcus aureus* (*S. aureus*) and *Klebsiella pneumoniae* (*K. pneumoniae)*, etc.[20] In addition, infections caused by the methicillin-resistant *S. aureus* (MRSA) also has been widely observed in the community.[21]

The resistance in bacteria that develop from initial antibiotic-sensitivity, but then gradually adapt, to ultimate antibiotic-resistance. When bacterial cells are exposed

to an antibiotic, susceptible cells will die, but those insensitive ones will survive. Once the insensitive cells are regrown, all of the bacterial cells in culture will be a resistant cluster.[22] **Figure 2.1** shows the formation of resistant bacterial cells.

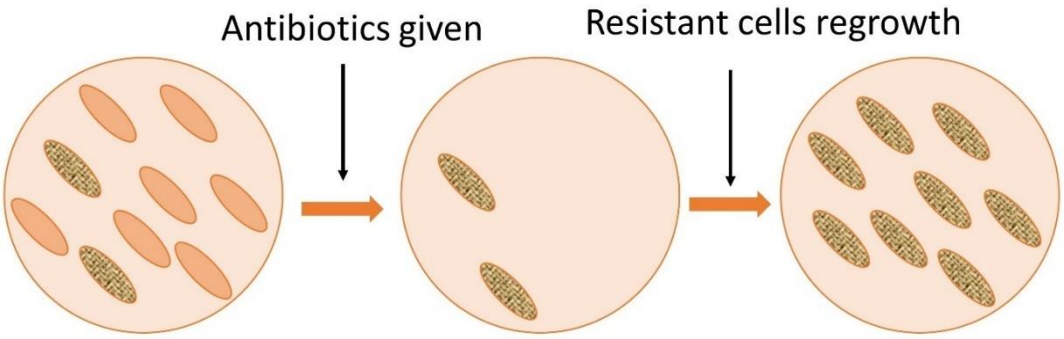

Figure 2.1: Growth of resistant bacterial cells. When cells are exposed to an antibiotic (could be repeated several times), the sensitive cells are killed and the survivals are resistant cells. All of the regrown cells are antibiotic resistant.[22]

The resistance can be an intrinsic resistance or an acquired resistance in bacteria.[23] Intrinsic resistance is a general characteristic within one bacterial species with genes encoded with resistance mechanisms. For example, altering the permeability of the membrane and active drug efflux are two intrinsic resistance methods that bacteria have developed.[24] While the acquired resistance which associates to resistance mechanisms of drug target modification, drug uptake limitation and drug efflux, relies on the resistance genes that transferred from other bacteria.[25] Different origins of resistance work with different mechanisms. Therefore, the antimicrobial resistance mechanisms of bacterial cells can be divided into four categories: (1) antibiotic inactivation; (2) drug target modification; (3) altered permeability of cells;

(4) active drug efflux. The mechanism scheme is illuminated in **Figure 2.2**. As they have different structures, gram-negative bacteria (such as *E. coli* and *P. aeruginosa*) vary in terms of their resistance mechanisms in comparison with gram-positive bacteria (i.e. *S. aureus*). Gram-negative bacteria use the four resistance mechanisms listed above. Gram-positive bacteria on the other hand, lacking of lipopolysaccharide (LPS) outer membranes and thicker cell wall and therefore possess a limitation in using altered membrane permeability and drug efflux mechanisms.[26-27]

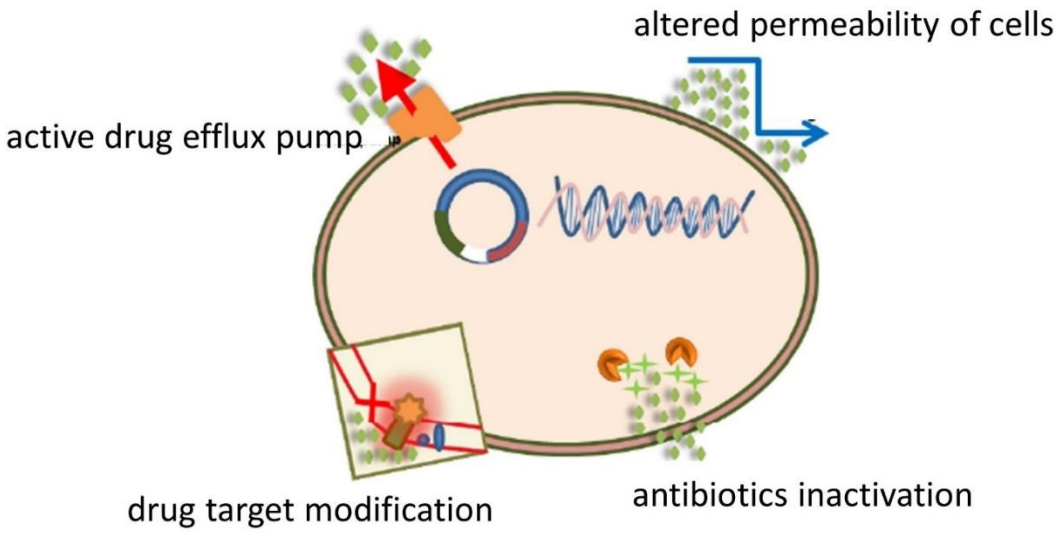

Figure 2.2: Main mechanisms of antimicrobial resistance. Image reproduced from Reygaert *et al*.[22] with permission from AIMS Press.

2.1.2 Biofilm-related Infections

Biofilms contribute to the spread of antimicrobial resistance. An established biofilm is a dynamic three-dimensional extracellular matrix (ECM) consisting of polysaccharides and proteins. Biofilms provide a protective environment for bacterial population, which is associated with resistance to antibiotic chemotherapy in subsequent infections.[28] The first biofilm related infection was identified by Costerton[29] and coworkers in 1982 using an electron microscopy study of *S. aureus* bloodstream infection. Since then, it has been found that bacterial biofilms could exist on almost all type of devices.[30] Bacteria commonly isolated from the biofilms on medical devices include both gram-positive and gram-negative species.[31] In terms of medical device, the main species of gram-positive bacteria include *S. epidermidis* and *S. aureus*; the common species of gram-negative bacteria are multidrug-resistant *E. coli* and *P. aeruginosa*. Some of the common medical devices that prone to biofilm infection and the relevant causative bacterial species are listed in **Table 2.1**.

Table 2.1: Common medical devices and biofilm related pathogen species.

Medical Device	**Biofilm Related Bacteria**	**Ref.**
Central venous catheters	*S. epidermidis*, *S. aureus*, *P. aeruginosa*, *Candida albicans*, *K. pneumoniae*, and *Enterococcus faecalis*	32-33
Urinary catheters	*S. epidermidis*, *Enterococcus faecalis*, *E. coli*, *Proteus mirabilis*, *P. aeruginosa*, *K. pneumoniae*	34
Contact lenses	*Acanthamoeba* spp., *P. aeruginosa*	35-36
Breast implants	*S. aureus*, coagulase-negative staphylococci, *Propionibacterium acnes* and *Citrobacter koseri*	37
Prosthetic cardiac valves	coagulase-negative staphylococci, *S. aureus*, *Candida albicans* and enterococci	38
Endotracheal tubes	*S. aureus*, *P. aeruginosa*, *Proteus mirabilis*, and *S. epidermidis*	39
Orthopaedic implants	*P. aeruginosa*, *S. epidermis*, *S. aureus*, *P. mirabilis*, *E. coli*, Streptococci, and Enterococci	40

Once a biofilm is formed on the surface of a medical device, they become difficult to remove and are less susceptible to a variety of physicochemical killing mechanisms, such as acidity, UV light, changes in salinity or hydration, heavy metal and phagocytosis.[41-45] There are 5 stages of the biofilm formation which are illustrated in **Figure 2.3**: (1) initial reversible attachment of cells onto the surfaces; (2) production of ECM to solid the attachment; (3) early development of biofilm structure (microcolony); (4) maturation of biofilm; (5) dispersion of free-swimming cells from the biofilm into environment. After stage 5, some of the dispersed planktonic bacteria may detach and disperse to another surface and begin a new cycle of biofilm formation.

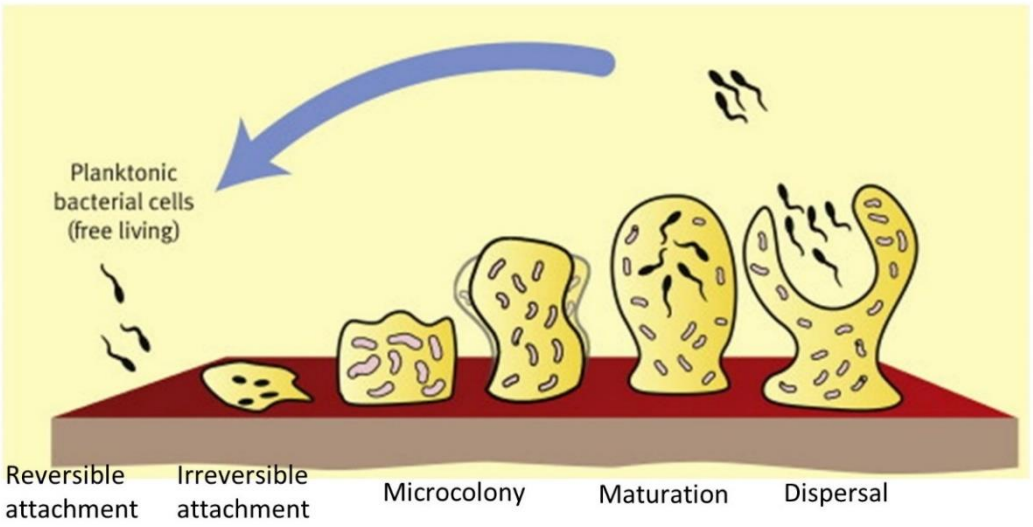

Figure 2.3: Schematic development of a biofilm in five stages: (1) initial reversible attachment of cells onto the surfaces; (2) production of ECM to solid the attachment; (3) early development of biofilm structure (microcolony); (4) maturation of biofilm; (5) dispersion of free-swimming cells from the biofilm into environment. After stage 5, some of the dispersed planktonic bacteria from biofilm to initiate a new cycle of biofilm formation elsewhere. Image reproduced from Galanakos *et al*.[46] with permission from Elsevier.

Bacteria in biofilms secrete an extracellular polymeric substance (EPS) which is adhesive also forms a physical barrier preventing antibiotics and other active agents from penetrating.[47] The EPS in biofilms as a filter that retain the host-produced serum components or minerals.[31, 34] It has been reported by Anwar et al.[48] that when using the same dosage of tobramycin (with drug levels far exceeding the minimum inhibitory concentration (MIC)) in the treatment on *P. aeruginosa*, the reduction of *P. aeruginosa* biofilm cells only reached approximately 2 logs, while there was >8-log decrease in planktonic cells. The resistance mechanism is due to the bacteria residing in a biofilm.[49] Three main mechanisms have been hypothesised:[28] slow penetration of antibiotics into the biofilm, altered microenvironment within the biofilm, and resistant phenotype of the bacteria. As biofilms display a high level of tolerance toward antibiotics, bacterial adhesion should be primarily prevented to inhibit biofilm formation on devices.[50-51] Moreover, once a biofilm forms on a medical device, planktonic bacteria can break off a mature biofilm and easily flow into the bloodstream or to infect a secondary location.[50-51] Whereas these dispersed planktonic bacteria can be eradicated through the combination of antimicrobials treatment and host immune responses, some highly tolerant biofilm bacteria may not be eliminated easily and this can lead to recurrence of infection.[52] In most cases, once a biofilm forms, replacing the bacterial colonised device or surgically removing the infected tissue is the only effective way to eradicate biofilm-related infections.[50, 53]

2.2 Antimicrobial Strategy

The susceptibility of bacteria to antimicrobials can be measured on bacteria in planktonic (free-floating) or biofilm states.[54-55] The initial effectiveness of antimicrobials is normally evaluated with the planktonic microorganisms.[56] However, the antimicrobial test on biofilm bacteria are believed to be more appropriate because this resembles real world settings more where a higher concentration of antibiotics are required in killing the mature biofilms.[57]

Bacteria can be classed into two categories: gram-positive and gram-negative bacteria; a classification based on the detailed illustration of the membrane structure differences between gram-positive and gram-negative bacteria was shown in **Figure 2.4**. Cellular machinery of each bacteria is surrounded by protective membranes. Gram-positive bacteria have a thicker and more rigid peptidoglycan cell wall outside the cytoplasmic membrane, while the gram-negative bacteria is protected by a thinner peptidoglycan layer sandwiched between a cytoplasmic membrane and an outer membrane. The addition outer membrane provides more permeability barriers for gram-negative bacteria, therefore, leading to more antimicrobials resistance.[58] Due to different cell surface characteristics, gram-positive and gram-negative bacteria displayed different susceptibility to various antibiotics and antimicrobial agents.

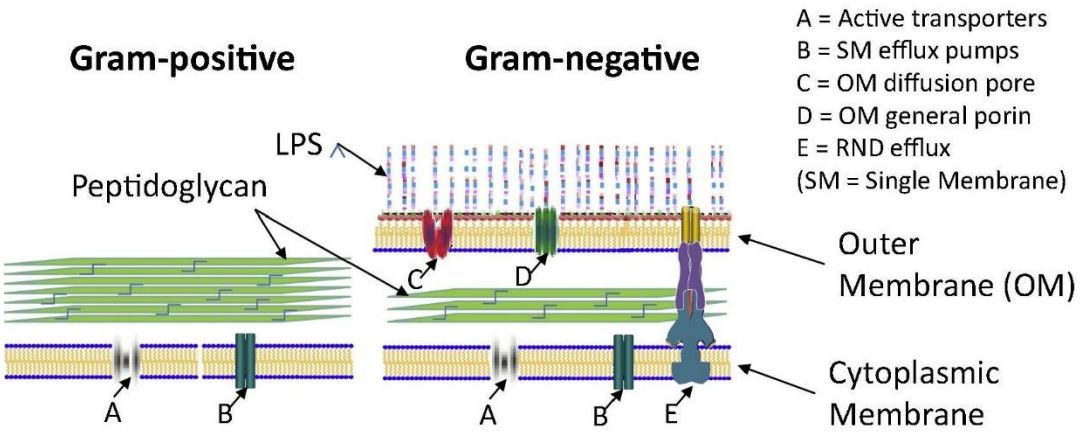

Figure 2.4: Differences of membrane permeability barriers between gram-positive and gram-negative bacteria. Image reproduced from Singh *et al*.[58] with permission from Elsevier.

Many strategies are being adapted to eliminate antimicrobial resistance, such as the use of new generation antibiotics, combination therapy, antibacterial substances and targeted drug delivery, etc.

2.2.1 Types of Antimicrobials

2.2.1.1 Natural Compounds

Natural antimicrobials generally are extracted from natural sources such as animals, microorganisms, and plants that use these compounds as a host-pathogen response. Examples of these compounds include things like antimicrobial peptides and enzymes such as lactoferrin, lysozyme, magainin, nisin lactoperoxidase, chitosan, pleurocidin, and spheniscin.[59-62] Nisin is an example of a microbial metabolic products. It is produced by the bacterium *Lactococcus lactis*, displayed an effective antimicrobial against gram-positive bacteria.[63] Plant derived antimicrobial products can also include essential oils such as eucalyptus, tea tree, lemongrass, etc.[62] The antimicrobial activity of essential oils is mainly attributed to the presence of phenolic

and terpenoid compounds which sensitise the cell membranes and impair microbial enzyme systems

2.2.1.2 Antibiotics

Antibiotics are a group of drugs that are used to treat bacterial infections. Since Alexander Fleming in 1928 discovered penicillin which is the first antibiotic, antibiotic therapy has achieved success against bacterial infections in clinics.[64] Development of new antibiotics is still one of the antimicrobial strategies to combat resistant pathogens and treat bacterial infections. However, the discovery of new antibiotics and the approval procedures of the new drugs has been slow in recent years and there has been no new class of antibiotic discovered in over 30 years.[65] Moreover, every class of antibiotics today has bacteria that have developed resistance towards it. Antibiotic combination therapy has been designed to improve the limitation of monotherapy in response to the problems of AMR. Some of the potentials of combination therapy has been reported, including the activity enhancement of antibiotics by synergy, prevention of resistance, inhibition the formation of biofilms, penetration improvement of antimicrobial agents into cells and tissues, and reductive production of toxin.[66]

2.2.1.3 Inorganic Bactericides

Inorganic antimicrobial agents are very attractive alternatives in doped biomaterials. They possess many advantages, such as good antimicrobial activity, biocompatibility, and adequate stability.[67] Silver and its ion form have broad antibacterial spectrum on both gram-positive and gram-negative bacteria by interrupting cell membrane transport and blocking cell DNA division.[68] However, it has been controversial over antibacterial silver. As an environment issues, concerns were raised about the

toxicity level of silver on organisms in marine ecosystem.[69-70] Gold nanoclusters has been reported to have wide-spectrum antimicrobial activity when the sizes controlled to 2 nm.[71] Copper nanoparticles also performed antimicrobial activity by destroying the cell wall of bacteria.[72]

2.2.1.4 Organic Bactericides

Synthetic organic antimicrobial agents including chlorhexidine, chloroxylenol, and poly(hexamethylene biguanide) are good alternatives if regarding antibiotic resistance.[73-74] Due to broad spectrum of antimicrobial action and lower risk of drug resistance, they are widely used in daily life, especially chlorhexidine. Chlorhexidine is known for its wide range of applications in dentistry, such as the combination use with gelatine for the treatment of periodontal infection.[75]

2.2.2 Modification of Biomaterials to Impart Antimicrobial Activity

Tethering of antimicrobial agents onto biomaterial has become a primary strategy in preventing bacterial-related infections of implanted medical devices in the past few decades.[76-77] The main strategy used for the development of antimicrobials is to prevent the colonisation of a surface before bacteria adhere. This is because once the bacteria adhesion to a device surface, biofilms would form on the surface and lead to biofilm-related infections, which are difficult to eradicate as described above. Therefore, the tailoring of surface modifications depends upon the antimicrobial strategies, including bacterial adhesion controlling, bacteria killing, and biofilms disrupting.[78] There are three main surface modification strategies to controlling bacterial adhesion preventing biofilm adhesion: antiadhesive surfaces, contact killing surfaces and biocide releasing surfaces.[79]

2.2.2.1 Antiadhesive Surfaces

Antiadhesive surfaces work on the principle of preventing microbes from sticking to the surface by physical rather than chemical means. These surfaces are sometimes called non-fouling or antifouling surfaces as the prevent contamination, protein adhesion and other routes to promoting the early phase of bacterial adhesion on surfaces. Surface contamination or proteins that adhere onto a surface can promote the adhesion of bacteria and the formation of biofilms.[80-81] Various surface modification techniques have been used in this regard such as polymer brush coatings,[82] self-assembled monolayers[83] and micro/nano structure, are carried out to develop these antiadhesive inert surfaces. Ge et al.[84] has fabricated micro/nano pillar arrays on a Si substrate, and the pillar patterns with a sub-micrometre level performed large reduction on bacterial retention and growth. Yang et al.[85] has developed another micro pattern which is called honeycomb-like structure. The fabricated honeycomb-like patterns with feature sizes of 1 μm notably inhibit bacterial adhesion, growth and biofilm formation against *E. coli* and *S. aureus*.

The antiadhesion on some charged surfaces performed by electrostatically interaction with ECM.[86] Superhydrophobic surfaces also act as antiadhesive surfaces and has been widely used for antifouling applications.

2.2.2.2 Contact Killing Surfaces

There are a broad range of antimicrobial molecules that possess antibiofilm activity have been introduced into coatings or been grafted onto surfaces.[87] These coatings that contain antimicrobials, such as antimicrobial peptides and quaternary amines, do not release bactericides, but killing bacteria on contact are the second strategy to develop on antimicrobial surfaces.[88-89] They work with different mechanisms:[87]

selectively degrading ECM of biofilms, killing metabolically quiescent bacteria within biofilms, disrupting Quorum sensing system, and reducing biofilm metabolism. The combination of different molecules has been proved to enhance the antibiofilm efficacy.[90] Furthermore, the biofilm treatment of antibiotics associated with the antibiofilm molecules also displayed the similar result in biofilm killing.[91] The advantage here of these coatings is that it can kill bacteria on contact without leaching into the environment. The disadvantage is that it has more of a localised effect.

Antimicrobial coatings on bulk materials aim to provide antimicrobial activity in biomaterial-tissue interface without compromising the mechanical property and biocompatibility of the bulk materials. However, some coating strategy would weaken the function of the host tissue by performing cytotoxicity or causing negative immune response. Therefore, it is of notable importance to balance the antimicrobial property and the biocompatibility in designing the coating.

2.2.2.3 Biocide Leaching Surfaces

Several bioactive antimicrobial coatings are based on leaching the active agent into the vicinity of the surface. These include releasing active antimicrobial such as reactive oxygen species,[92-93] nitric oxide,[94] thin films with organic/inorganic antimicrobials.[95] The advantage of these coating is that bacteria do not need to come into the surface of the material in order for the bactericidal application, however there might be a problem with leaching and toxicity of the material in the surrounding tissue.

2.3 Nitric Oxide

2.3.1 Nitric Oxide (NO) Molecule

Nitric oxide is a biological signal molecule that regulate cellular metabolic functions in physiological condition.[96-97] As an endogenously produced diatomic free radical with a short half-life (< 1 s in the presence of oxygen and haemoglobin), NO is associated with multiple physiological processes, including blood pressure regulation,[98] wound healing,[99] immune response[100-101] and skeletal homeostasis.[102-103] Endogenous NO is enzymatically produced from L-arginine by NO synthase (NOS).[104] NOS possesses three isoforms, including endothelia NOS (eNOS), inducible NOS (iNOS) and neuronal NOS (nNOS).[105] Low concentrations (10^{-12} – 10^{-9} M) of NO that promote vasodilation, angiogenesis and neurotransmission, are produced by eNOS and nNOS.[105] Larger concentrations (10^{-6} M) of NO that response to infections and inflammations, are produced in macrophages and neutrophils by iNOS.[105] NO will be oxidised by superoxide ($O_2^{\bullet-}$) to form peroxynitrite ($ONOO^-$) which is a more powerful oxidant in response to inflammatory.[94]

2.3.2 NO as an Antimicrobial and Antibiofilm Agent

The intrinsic broad-spectrum activity of NO against microorganisms is attributed to its reactive byproducts that produced through the spontaneous reaction of NO with oxygen or superoxide.[106-107] The nitrosation and oxidation of reactive nitrogen oxide species (RNOS) (i.e. nitrogen and oxygen intermediates) can cause nitrosative and oxidative damage to bacterial DNA, proteins, metabolic enzymes, and outer membrane structure.[108] The antimicrobial mechanisms are illuminated in **Figure 2.5**. Nitrosative species, such as dinitrogen trioxide (N_2O_3), that induce DNA deamination and thiols nitrosation cause bacterial death.[106, 109] Oxidative species, such as

peroxynitrite ($ONOO^-$) which is formed by NO reacting with superoxide, perform oxidative DNA damage and lipid peroxidation of pathogen cells.[109]

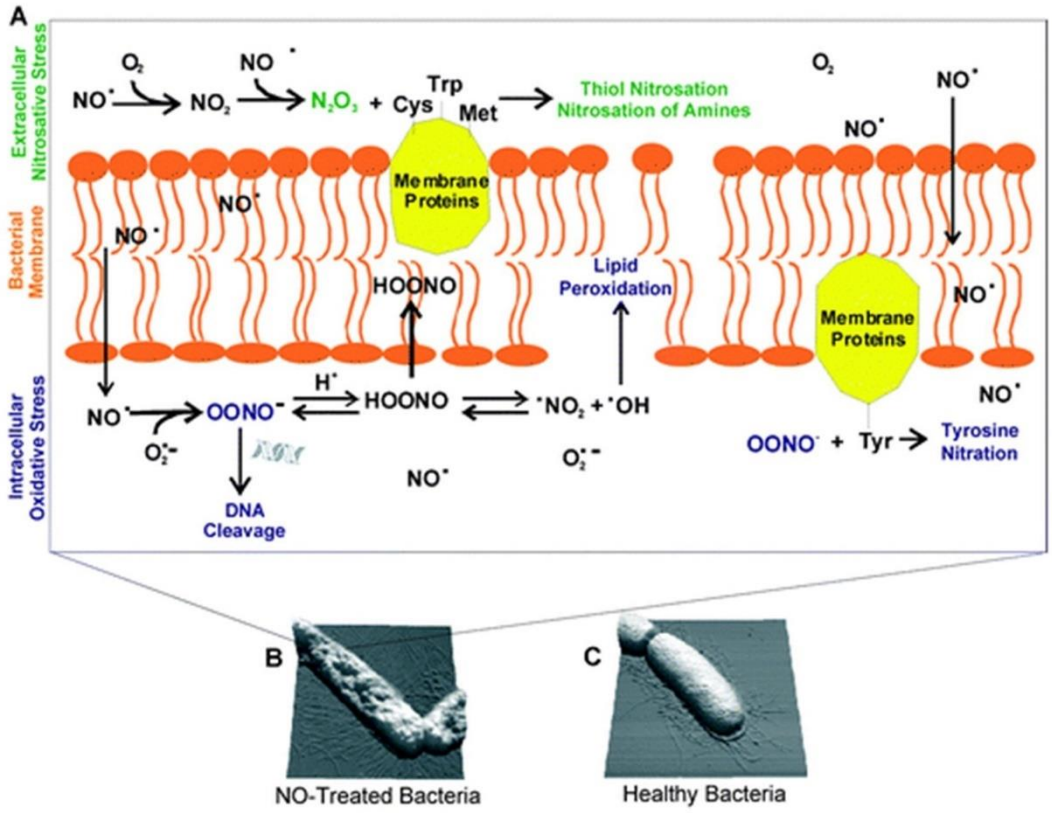

Figure 2.5: (A) Antimicrobial mechanisms of NO which acts as an antimicrobial agent. (B) AFM image of NO-treated bacteria. (C) The control group of bacteria. Images reproduced from Carpenter *et al*.[110] with permission from Royal Society of Chemistry.

Due to the small size of NO molecule and its multiple mechanisms in eradicating pathogens, there has been no reports of bacteria developing resistance to NO.[111] The antibacterial efficacy of NO has been shown to be capability of broad-spectrum antibacterial against gram-negative (e.g., *P. aeruginosa* and *E. coli*) and gram-positive (e.g., *S. aureus* and *S. epidermidis*) bacterial species, even drug-resistant bacteria (e.g., methicillin-resistant *S. aureus*).[112-113] Miller et al.[113] has intermittently exposed

drug-resistant strains of *E. coli* and *S. aureus* to gaseous NO (160-200 ppm for 30 min every 4 h) for one day *in vitro*. This protocol eradicated the drug-resistant bacteria without causing significant cytotoxicity. Similar results also can be seen in treating planktonic *P. aeruginosa in vivo*.[114]

Moreover, the study of antibiofilm activity of NO attracted a lot interest in recent years.[115-116] It has been illuminated in **Section 2.1.2** that the final dispersal stage in biofilm formation plays a key role in further colonisation and widespread the biofilm infection. NO acts as a signalling molecule in regulating the formation and dispersal of biofilms at a low NO levels of pico/nano molar concentration.[115] The detachment of *P. aeruginosa* from a mature biofilm has been triggered at NO concentration of 0.025-0.5 nM over 24 h.[116] The same NO donors also has been used in investigating a wider range of pathogenic biofilm dispersal. It has been concluded that low levels of NO possess capability of causing 30-90% biofilm dispersal without reducing its viability. Bacteria that dispersed from biofilm and transform back to a planktonic state via NO treatment normally displayed higher susceptibility to antimicrobial agents.[117-118] When using antimicrobials (tobramycin and hydrogen peroxide) for biofilm treatment, the addition of NO exposure performed 2-log higher reduction.[118] Although the low levels of NO performed no effects on viability reduction of biofilms, it significantly increased the susceptibility of biofilms to antimicrobials by dispersing biofilms and rising the susceptibility of planktonic bacteria.[117-118] High levels of NO concentration (micros/milis molar concentration) have completely eradicated biofilms in a previous research.[119] While the high concentration NO-mediated biofilm eradication has not been fully studied, one acceptable understanding is that the

physical destruction of biofilms associate to the altering of the EPS matrix by NO.[120-121]

2.3.3 Role of Nitric Oxide in Bone Tissue

Bone is a dynamic tissue that constantly undergoes remodelling.[122] Osteoblasts deposit new bone, while osteoclasts remove mineralised bone and organic tissue. Balanced activity of osteoblasts and osteoclasts is of great importance in maintaining bone function. For example, the reduced activity of osteoclast contributes to osteopetrosis, while the excessed osteoclastic activity can amplify bone loss.

Endogenous NO molecule has been found get involved in signalling pathways controlling bone cell physiology and bone remodelling.[123-126] Increased activity of the three NOS isoforms has been detected in bone fracture sites in human and rats.[127-128] nNOS and eNOS are calcium-dependent and constitutively expressed in human primary osteoblasts. iNOS is calcium-independent and iNOS-derived NO showed the capacity of activating osteoclasts in bone inflammatory process, which promotes the bone remodelling.[129] The production of NO enhanced osteoblastic proliferation and differentiation, promoting bone deposition.[130] A decreased eNOS-derived NO level has been shown to increase osteoclastogenesis and related bone resorption.[131] Mechanical strain on bone without causing fractures also stimulates NO production by osteoblasts for bone functional recovery.[132] In this case, activity of osteoclasts has been inhibited by increased local NO levels.

2.3.4 Role of Exogenous Nitric Oxide on Bone Cells

Endogenous NO is involved in bone repair process, therefore, NO concentration levels on regulating bone physiology should be taken into consideration in delivery strategy of exogenous NO.

To determine whether gaseous NO performs the same function on simulating bone cell growth as endogenous NO, S-nitroso-N-acetylpenicillamine (SNAP, a NO donor) has been used in osteoblast culture.[133] With the addition of SNAP, levels of alkaline phosphatase and cell numbers in osteoblasts have both increased, giving the promise of NO as a therapeutic for bone growth. Otsuka et al.[133] used diethylenetriamine/nitric oxide (DETA/NO) to incubate with osteoblasts and found no change in alkaline phosphatase level. However, a 3.5-fold increase in osteocalcin has been measured. Osteocalcin is an osteoblastic protein that promote the mineralisation of bone matrix. Furthermore, the NO releasing rate significantly impacted the local concentration of NO. To understand the NO releasing rate in regulating osteoblast behaviours, hence, slow release of NO from eNOS was modelled by DETA/NO while rapid release of NO from iNOS was mimicked by sodium nitroprusside (SNP).[134] At a low levels of donor concentration (10 μM), both DETA/NO and SNP displayed enhancement on osteoblasts proliferation. At a higher concentration (50 μM), osteoblasts performed proliferation on DETA/NO and apoptosis on SNP. Once the donor concentration increased to 100 μM, both DETA/NO and SNP displayed cytotoxicity on osteoblasts. It has been indicated that slow release of NO at low concentration is ideal for stimulating osteoblastic proliferation.

Effects of exogenous NO on osteoclasts dependent upon the NO release kinetics, including NO donor concentration and release duration, etc..[135] And elevated levels of NO have been found to cause osteoclastic apoptosis and inhibit osteoclastogenesis. Kanaoka et al.[136] has reported that bone stromal cells performed high osteoprotegerin (OPG), when supplemented with 15 μM DETA/NO, resulting in inhibition of osteoclastogenesis.

2.4 NO Donors

2.4.1 Classes of NO Donors

NO has efficacy in antibacterial and antibiofilm, the delivery of exogenous NO is often therapeutically difficult because NO is a reactive gas with a short half-life. As a result, much research has focused on the development of NO donors capable of controlled and sustained release in the therapeutic window. There are four common NO donors that have shown are commonly used: *N*-diazeniumdiolates, *S*-nitrosothiols, organic nitrates and metal nitrosyl.

N-diazeniumdiolates (containing $[N(O)=NO]^-$) are the NO adducts of precursor amines (**Figure 2.6**). The first *N*-diazeniumdiolates were reported by Drago in 1960, which involves the reaction of NO with selected nucleophiles.[137-138] The synthesis of *N*-diazeniumdiolates under high NO pressure was later refined by Keefer and coworkers.[139-140] *N*-diazeniumdiolates can form on both primary and secondary amines after NO treatment. Most of the studies focused on secondary amine *N*-diazeniumdiolates because if its higher stability.[139] *N*-diazeniumdiolates are formed by deprotonating secondary amines using a base such as sodium methoxide or sodium hydroxide.[138] The amine anion then nucleophilically attacks 2 molecules of NO and form the *N*-diazeniumdiolate moiety. Under physiological conditions, *N*-diazeniumdiolates spontaneously release two molecules of NO per.[138, 141] The mechanism diagram of *N*-diazeniumdiolates formation and NO release is shown in **Figure 2.6**. The kinetics of release of *N*-diazeniumdiolates can be controlled by pH or temperature dependent process.[142] For example, *N*-diazeniumdiolate-modified proline (PROLI/NO) displayed a NO-release half-life of 2s while *N*-diazeniumdiolate-modified diethylenetriamine (DETA/NO) for 24 h.[143] The terminal primary amines on

DETA are believed to stabilise *N*-diazeniumdiolate by forming intermolecular rings, therefore, allowing down the degradation rate and NO release. This class of NO donor is the most widely exploited for medical applications and indeed used in this thesis as the kinetics and payload of NO can be carefully controlled.

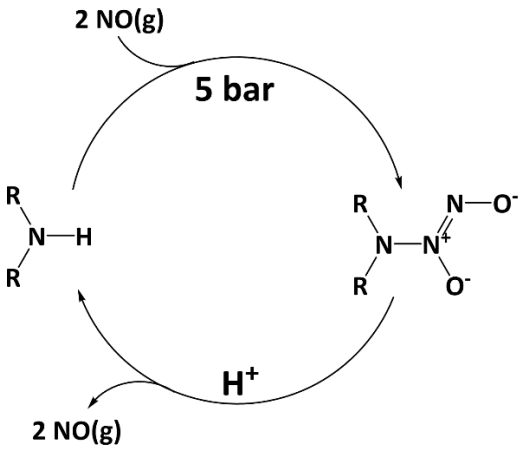

Figure 2.6: Mechanism diagram of *N*-diazeniumdiolates formation and degradation.

S-nitrosothiols are endogenous NO carriers. They are synthesised via nitrosation of free thiols with nitrosating agents.[144] NO release from *S*-nitrosothiols is also a spontaneous process. Some of the commonly used *S*-nitrosothiols include *S*-nitrosoglutathione (GSNO) and SNAP. Organic nitrates have been the oldest NO donors in clinical use.[145] However, some potential shortcomings of organic nitrates have been found in clinical applications. For example, nitroglycerin, the most used organic nitrate, efficiently release NO after being active. But patients often develop tolerances to nitroglycerin and can limit NO release capacity of nitroglycerin, resulting in low treatment efficacy.[146] Metal nitrosyl compounds are a family of

coordination complex containing NO ligands. SNP is the most common in metal nitrosyl class[145] and it has been used for treating high blood pressure.[147] Some common NO donors have been listed in **Table 2.2**.

Table 2.2: Common nitric oxide donors.

Donor type	**Chemical formula**	**NO donor examples**	**Notable NO-release triggers[121]**	**NO release half-life**	**Experimental parameters**
N-diazeniumdiolate	$R_2NN(O)NO$	PROLI/NO	Proton-initiated decomposition	1.8 s[148]	pH 7.4, 37°C
		DETA/NO		20 h[148]	pH 7.4, 37°C
S-nitrosothiol	RSNO	SNAP	Photolysis	1.7 h[149]	pH 7.4, 37°C, in dark
			Thermal decomposition		
			Cu(I)-catalysed reduction		
Organic nitrate	$RONO_2$	Nitroglycerin	Enzymatic decomposition	N/A[a]	
Metal nitrosyl	Varies	SNP	Photolysis	N/A[a]	

[a] Organic nitrates and metal nitrosyls do not spontaneously release NO at physiological pH and temperature

2.4.2 Comparison of NO Donors for Antimicrobial Applications

Each NO donor class presents its own NO loading mechanism and certain advantages for NO release. Based on the NO release mechanisms of the donors, the efficacy of each donor class on treating bacterial and biofilm related infections need to be evaluated. Organic nitrates require enzymatic activation and this hinders their utility for antimicrobial applications. Also the enzymes that present in surrounding tissue may deactivate the NO release from organic nitrites.[150] Metal nitrosyls, such as SNP, are photolytic NO donors; i.e. an external light trigger (e.g. UV or visible light) is needed for the release of NO release profile of metal nitrosyls, limiting its utility for implanted biomaterials. Additionally, metal nitrosyls have storage challenges owing to their light sensitivity. In addition, the toxicity of metal centres and ligands on tissue cells need to be considered in applications. Although *S*-nitrosothiols are used as NO donors for killing bacteria,[151] their decomposition is easily triggered by temperature, light, the presence of transition metal ions (e.g. copper) and the other thiols, hence resulting in relative instability.[152-153]

N-diazeniumdiolate spontaneously decomposition under physiological conditions to generate 2 molecules of NO. *N*-diazeniumdiolates generally need to be stored under in low temperature and moisture-free conditions to prevent its degradation. The NO-release kinetics and stability of *N*-diazeniumdiolates have been improved via modifications with other chemical structure.[154-155] The cytotoxicity of *N*-diazeniumdiolates precursors is of concern, aminosilane precursors have been used to tune antimicrobial efficacy towards bacteria and cytotoxicity to human primary

osteoblasts.[156] Therefore, *N*-diazeniumdiolates promise the most extensive usage for antimicrobial application due to their stability, functional ability and tunability.

2.5 *N*-Diazeniumdiolate Delivery Vehicles

Many low molecular weight *N*-diazeniumdiolates have limitations (e.g. short half-life and precursor cytotoxicity), hindering their broader antimicrobial applications.[143] *N*-diazeniumdiolates delivery vehicles have been developed to address these problems as listed below.

2.5.1 Inorganic Nanoparticles

Silica nanoparticles have been employed for NO storage and delivery due to its ease of synthesis, tuneable structure and nontoxic nature.[157] NO donor precursors (e.g. secondary amines or thiols organic functional groups) have been introduced onto silica nanoparticles for subsequent grafting of the NO donor.[158-159] Zhang et al.[160] has synthesised NO-releasing fumed silica particles (with size of 0.2-0.3 μm) followed by tethering alkylamines onto the silica surfaces, and functionalisation with an *N*-diazeniumdiolate moiety. Shin et al.[157] has reported a one-pot sol-gel method upon preparing NO-releasing nanoparticles that with the *N*-diazeniumdiolates distributed uniformly throughout the particles.

Gold nanoparticles and quantum dots have also been used as delivery vehicles for *N*-diazeniumdiolates.[112, 161-162] For example, Polizzi et al.[161] synthesised *N*-diazeniumdiolates-functionalised gold clusters (~3 nm) with modest NO-release for short durations (< 0.023 μmol, <1.5 h). These gold clusters (~5 nm) significantly enhanced NO release (0.386 μmol) and durations (16 h).

2.5.2 Biopolymeric Scaffolds

Biopolymers widely attract attention in fabricating tissue scaffolds due to their favourable nontoxicity, inherent biodegradability and biocompatibility. Chitosan, alginate, cyclodextrins and hyaluronic acid have been successfully modified with *N*-diazeniumdiolates.[163-166] Ahonen et al.[166] reported on the synthesis of NO release alginate scaffolds of different molecular weights. Those scaffolds demonstrated pathogen and biofilm eradication efficiency without causing toxicity towards human respiratory epithelial cells. Lu et al.[167] have reported on secondary amine functionalised chitosan oligosaccharides with varying molecular weights. The antimicrobial efficacy was determined to be a function of the size and ionic characteristic, with low molecular weight and cationic oligosaccharides showing a 5-log reduction in *P. aeruginosa* biofilms.

2.5.3 Dendrimers

Dendrimers are an interesting vehicle for NO delivery due to their hyper-branched nanostructures which allows for a high NO loading capability.[142] Schoenfisch and coworkers have shown that NO-functionalised poly(propyleneimine) (PPI) dendrimers demonstrated antibacterial activity against gram-positive and gram-negative bacteria including methicillin-resistant *S. aureus*. The antibacterial efficacy was correlated to the dendrimer size and exterior functionality with minimal cytotoxicity towards fibroblast cells with up to a 5-log reduction in all bacterial strains for the most optimised NO-functionalised PPI dendrimers.[168]

2.5.4 Liposomes

Liposomes are colloidal nanocarriers with a cell membrane-like structure that consisted of an inner aqueous core and a phospholipid bilayer outer shell. The encapsulation of NO donors into liposomes has been investigated as a strategy for NO storage and delivery.[169] The NO release kinetics of *N*-diazeniumdiolates encapsulated liposomes upon has been reported to be tuneable via altering NO donor molecular structure and/or phospholipid composition.[170] The hydrophobic phospholipid acted as a physical barrier which has been shown to slow down proton-initiated degradation rate of encapsulated *N*-diazeniumdiolates, therefore, enhancing the stability of this NO delivery vehicle.

2.5.5 NO Release Coatings

For some medical device applications, the development of a coating or thin film on an implantable device is the best solution to the reduction of biofilm-associated infections.[171-173] Three representative strategies for constructing *N*-diazeniumdiolates-functionalised surfaces, including noncovalent incorporating, covalent tethering and macromolecular doping, are summarily shown in **Figure 2.7**.

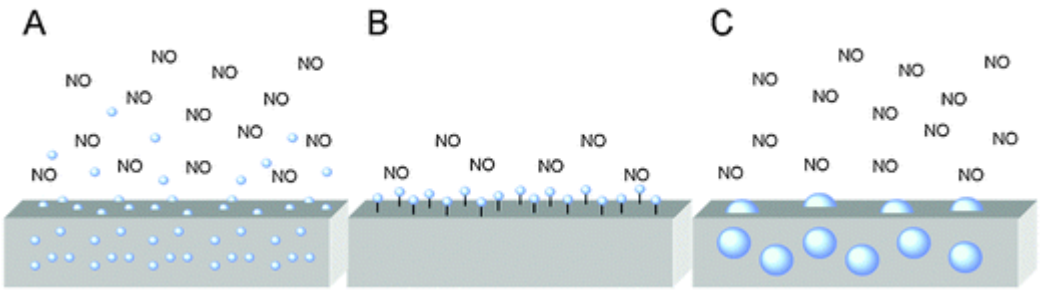

Figure 2.7: Representative strategies for constructing *N*-diazeniumdiolates-functionalised surfaces: (A) noncovalent incorporating of NO donors (small blue spheres); (B) covalent tethering of NO donors; (C) doping of NO-releasing macromolecular scaffolds (large blue spheres). Image reproduced from Riccio *et al*.[174] with permission from Royal Society of Chemistry.

Smith et al.[175] have fabricated NO-releasing thin film polymers by noncovalently doped *N*-diazeniumdiolated DETA within polycaprolactone (PCL), and detected NO release rate of 56 nmol/mg over 1 week. Covalent tethering of *N*-diazeniumdiolates into coatings have been reported by several groups.[175-176] For example, D'Sa group has reported on the ability of NO-releasing polymer coatings to prevent *P. aeruginosa* biofilm formation.[141] Poly (ethylene terephthalate) and silicone elastomer were oxygen plasma treated followed by diazeniumdiolate functionalisation and these coating demonstrated a 60–92% reduction in viable gram-positive and gram-negative bacteria.

Another approach that can be utilised to generate NO-releasing surfaces was proposed by Kumar and coworkers.[177] In their work, a solvent-free technique has been suggested to generate NO-releasing plasma polymer coatings using diazeniumdiolate. The amine-based coatings were deposited using plasma

polymerisation followed by NO gas exposure which resulted in a diazeniumdiolate-functionalised substrate. This coating demonstrated a controlled release of NO for over 2 days and was effective at preventing the formation of *P. aeruginosa* and *S. aureus* biofilms. Recent studies have evaluated the macromolecular scaffold doping strategy for NO storage and delivery from the coating. For example, Zhang and coworkers[160] prepared NO-releasing coating by doping 20 wt% pendant hexane diamine structure (i.e., Sil-2N[6]-N_2O_2Na) silica particles into polyurethane (PU) layer. Koh et al.[178] fabricated hybrid sol-gel/PU glucose biosensors which made up of two layers, including glucose oxidase and N-diazeniumdiolated silica particle doped layer. They reported NO release durations were associated to both the type and concentration of macromolecular dopants.

2.6 Biomaterials for Bone Healing and Regeneration

Guided bone regeneration (GBR) is a therapeutic method to repair bone defects or injuries. The basic principle of GBR method is to isolate the bone defect from the surrounding tissue.[179] A illustration of GBR for bone defect recovery is shown in **Figure 2.8**.

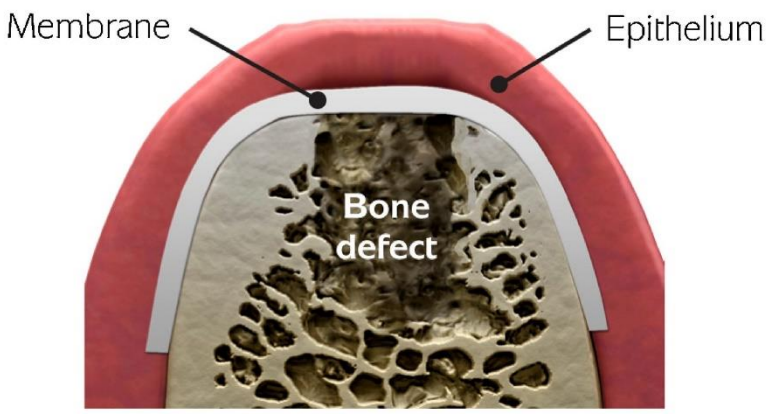

Figure 2.8: Illustration of GBR for bone defect recovery. Image reproduced from Bottino *et al*.[180] with permission from Elsevier.

GBR membranes act as barriers in treatment as well as encourage bone regeneration.[181] Normally, they are used as a medical device with dental implants[182] or bone grafting materials.[183] Therefore, the main design criteria of GBR membranes including biocompatibility, space maintaining, selective permeability, tissue integration and clinical manageability.[184] Several factors should be taken into consideration when selecting or manufacturing biomaterials for GBR, including biocompatibility, osseointegration and mechanical properties and biodegradability, wear resistance, etc..[185] A material with good biocompatibility will have low

cytotoxicity and not cause any inflammatory or allergic response in the human body.[186] The osseointegration inability of the material will cause implant loosening after surgery, resulting in implant failure and revision surgery.[187] The mechanical properties (e.g. hardness, tensile strength, modulus and elongation) determine the type of material that will be employed for a specific application.[185] GBR membranes can be grouped as non-resorbable or resorbable membranes in terms of specific area utility. Non-resorbable membranes, including polytetrafluoroethylene (PTFE) and titanium mesh, are capable of maintaining membrane shape for a sufficient period.[188] However, the drawback of this type is the need of a removal surgery. The use of resorbable membranes have avoid this shortcoming. A variety of natural or synthetic polymers, such as collagen and aliphatic polyesters, are used in fabricating resorbable membranes.[189]

2.6.1 Titanium Implants

2.6.1.1 Surface Structure and Properties of Titanium

Titanium (Ti) is a metal, first discovered in England by Gregor in 1790 and named by Klaproth in 1795. And its alloys have been used extensively as an orthopaedic and dental biomaterial due to its good biocompatibility, osteointegration, and suitable mechanical and corrosion resistance. Many of its favourable properties is associated to the presence of the surface oxide layer. A native titanium oxide film with only a few nanometres thick grows spontaneously on Ti surface upon exposure to air.[190] In detail, the amorphous or nanocrystalline oxide film with a thickness of 3-7 nm mainly contains stable TiO_2. A hydroxyl layer (i.e. physiosorbed water layer) is formed via hydroxide and chemisorbed water bond with Ti cations. In addition, to avoid a

contamination layer that can attach onto surface, Ti should be stored in clean condition. A diagram of titanium oxide film is illustrated in **Figure 2.9**.

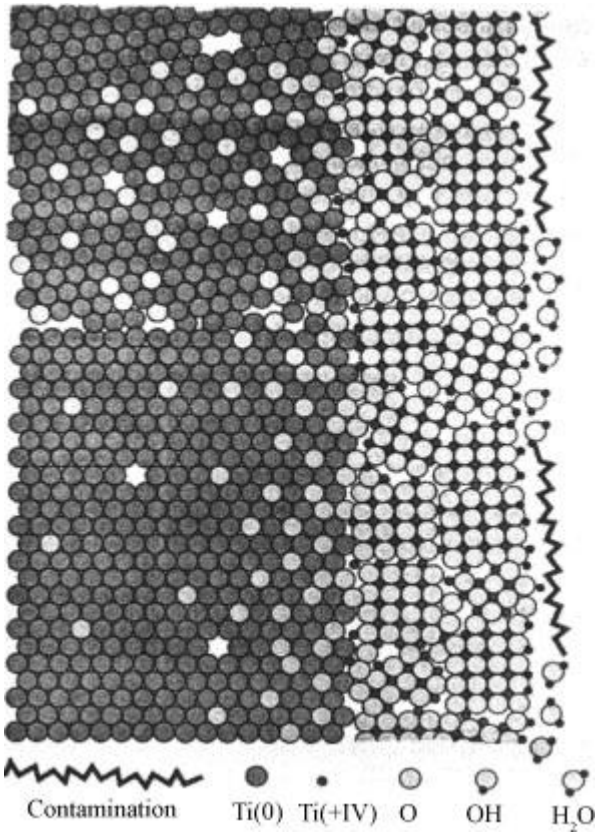

Figure 2.9: Illustration of titanium oxide film. Image reproduced from Liu *et al*.[191] with permission from Elsevier.

2.6.1.2 Ti Surface Enhancement by Silanisation

Surface modifications on Ti surfaces are known to improve cellular adhesion, differentiation and other cell-tissue response without adversely affect the bulk properties. The main strategies of surface modification include immobilisation of peptides, proteins or growth factors onto Ti surfaces.[192-193] A number of techniques (e.g. self-assembled monolayers, protein immobilisation) have been developed for Ti

surface modification.[194-195] However, as a result of existence of the inert TiO_2 layer, any modification needs to take place with this oxide layer. Aminosiliane, a strong coupling agent, is one of the a few available organic reagents that can form strong chemical bonds on TiO_2 layer.[196] In addition, silanised surface has achieved stability and wear resistant in clinical application.[197]

The formula of aminosilane is represented as

$R\text{-}Si(OR')_3$,

where OR' is the hydrolysable alkoxy group, and R is the backbone with amino-functional group(s).

At the initial stage of silanisation on Ti surface, the aminosilane is activated by hydrolysed

$$R\text{-}Si(OR')_3 + 3H_2O \rightarrow R\text{-}Si(OH)_3 + 3R'\text{-}OH \quad (1)$$

The reaction can be triggered by water molecules.

With the increase of the acidic silanol groups (-SiOH) in the solution, dimers are forming

$$R\text{-}Si(OH)_3 + R\text{-}Si(OH)_3 \rightarrow R\text{-}Si(OH)_2\text{-}O\text{-}Si\text{-}(R)\ (OH)_2 + H_2O \quad (2)$$

Titanium surface with a thin oxide layer possesses hydroxyl groups (-OH), therefore, enabling the formation of ≡Si-O-Ti≡ bonds.[198] Usually only one siloxane bone from each silicon atom link onto the inorganic substrate.[199] Heat treatment is the final step in silanisation, thermal curing has been reported to enhance the crosslinking of aminosilanes to form a siloxane film onto metal surfaces through eliminating H_2O.[200]

Since most silanes do not dissolve in water, ethanol (~90-95% vt%), this is an effective surface modification technique that has been a viable solution in clinic.[201]

There are several factors that affect the quality and stability of formed aminosilane layer on Ti surfaces, such as functionality of the amine to the silicon centre, type of the alkoxy group, and concentration of silanes.[202-204] Here, we only consider the case of single species aminosilane utility in surface silanisation.

a. The amine group is able to, both inter- and intramolecularly, catalyse the formation and hydrolysis of siloxane bonds. The intramolecular catalysis is achieved via the formation of a stable five-membered ring intermediate.[205]

b. The two alkoxy groups, methoxy group and ethoxy group, have different hydrolysis rates. The faster hydrolysis rate of methoxy groups results in a high variability of the silane layer, because the layer structure is more susceptible to the amount of water on substrate surfaces.[203]

c. The hydrophobic polysiloxane film is not a simple monolayer but usually with a thickness of ten molecular layers. The thickness of the film dependent upon the concentration of the silane solution but not the reaction time.[204]

2.6.1.3 Porous Titanium

While titanium and its alloys are widely employed in the orthopaedic and dental sector, dense forms of these materials can cause a mismatch of the Young's modulus leading to stress-shielding and poor interfacial connectivity between the bone and implant. Consequently, this can lead to fibrous tissue formation at the implant interface, poor osseointegration and the development of an inflammatory response. Porous titanium can avoid some of these issues such as decrease in Young’s modulus

(in comparison to bulk metals) that will match bone more. This will prevent stress shielding which can lead to bone resorption and implant loosening. The porous structure facilitate the migration of cells, effective transport of body fluids, and integration of newly grown bone.[206-208] It is generally accepted that a high porosity of interconnected pores which can allow for cell migration and growth and vascularisation should have pore sizes in the range of 100–400 µm. Given the importance of porosities in metallic biomaterials, researchers have investigated fabrication of porous titanium such as plasma spraying, additive manufacturing, furnace sintering, lost wax casting and vapor deposition has been used to manufacture porous titanium.[209-210] The lost carbonate sintering which is one of the sintering manufacturing processes has been developed and patented by Zhao et al..[211] It has been widely used for applications in energy, aerospace and civil engineering.[212-215]

2.6.2 Degradable Polymeric Scaffolds for Bone Regeneration

Several techniques have been used for degradable polymeric scaffolds for including film casting, dynamic filtration and electrospinning.[180, 216-219] Membranes made by film casting and dynamic filtration methods have been found lack of clinical manageability and component uniform.

2.6.2.1 Electrospinning

Electrospinning is a simple and economical method used for effectively fabricating continuous micro-/nano- fibres from a variety of polymer solutions.[220-223] Although, this technique was first developed over 100 years,[224] its widespread application in tissue engineering has only been realised in the last two or three decades.[225]

A typical electrospinning setup (as shown in **Figure2.10a**) consists of four following components:

a. High-voltage power supply: a direct current (DC) voltage in the range of several tens of kVs is applied to the system, and build up a surface charge on the polymer solution.[225]

b. Flow control pump: a flow control pump is used to adjust the flow rate of the fluid in the system, in order to generate fibres with controllable diameters.[221]

c. A capillary tube with a needle: when electrostatic repulsion force of surface charges overcome surface tension, the polymer droplet can be stretched into a conical shape known as the Taylor cone at the needle tip. The Taylor cone will be invisible, and fibres formation starts within the needle if the applied voltage is high enough.[226] The formation of Taylor cone is shown in **Figure 2.10b**.

d. A collector: For different fibre assemblies, collectors can be designed in various shapes, such as a plate or a rotating drum.

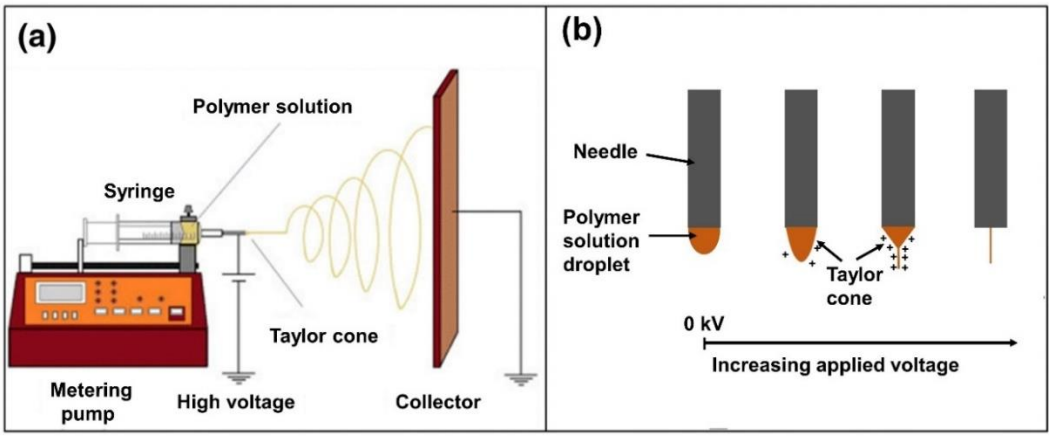

Figure 2.10: Illustrations of (a) typical electrospinning set-up and (b) the effect of voltage on Taylor cone formation. Image reproduced and adapted from Islam et al.[222] with permission from Springer.

Polymers are dissolved in volatile solvent before electrospinning. In the electrospinning process, the polymer solution is held at the needle tip by surface tension. Once the repulsive electrical force increases to a value sufficient to overcome the surface tension, the polymer droplet is stretched to form a conical shape called Taylor cone.[227] The charged cone then pulls into a charged jet of polymer solution, and then the jet rapidly and unstably whips between needle tip and collector to achieve evaporation of the solvent. Eventually, the polymer fibres are left behind onto collector.[223, 228-229]

The electrospinning process is governed by many parameters, those are summarised and listed in **Table 2.3**.

Table 2.3: Electrospinning parameters and their effects on fibres morphology.

Class of parameter	Parameters	Effects on fibres	Ref.
Electrospinning processing	Voltage	Decrease in fibres diameter with increase of voltage.	230
	Flow rate	Increase in fibres diameter with increase of flow rate; Generation of beads with too high flow rate.	228, 231
	Types of collector	Generation of beaded fibres on less/no conducting material collector; Generation of aligned fibres on rotating collector with alignment speed.	232-233
	Distance between needle tip and collector	Decrease in fibres diameter with increase in distance; Generation of beads with too small and too large distance.	230, 234
Electrospinning solution	Viscosity	Increase in fibre diameter with increase of viscosity; Generation of beads in low viscosity.	235-236
	Concentration	Increase in fibre diameter with increase of concentration.	237-238
	Molecular weight of polymer	Increase in beads amount with decrease in molecular weight.	239-240
	Conductivity	Decrease in fibre diameter with increase in conductivity.	241-242
Ambient	Temperature	Decrease in fibres diameter with increase in temperature.	243
	Humidity	Generation of small circular pores on fibre surface with increasing humidity.	244

The morphology and arrangement of fibres are controllable in an electrospinning fabrication. In addition, there are a wide range of polymers can be selected to use for this easy-setup and low-cost processing.[245] A unique character of electrospinning is that a large one-piece membrane can be fabricated at one time.[246] As GBR membranes are usually used in small pieces, the repeatability of membranes can be achieved by electrospinning. Electrospinning has greater potential in fabricating degradable GBR membranes out of a variety of polymers and can act effectively as vehicles for drug delivery applications. Hatton and coworkers have developed electrospun poly (ε-caprolactone) (PCL) membranes with bioactive glass composition (F18). These membranes displayed increased tensile strength with the addition of the bioactive glass and not cytotoxic and therefore showed promise as GBR membranes for small bone injuries.[247] Moreover, electrospun membranes also are versatile and have been used with dual functionality for tissue regeneration and drug delivery. For example, Colley et al.[248] have reported on the fabrication of an electrospun dual-layer mucoadhesive electrospun scaffold which consists of an outer hydrophobic polycaprolactone layer and an inner, mucoadhesive polyvinylpyrrolidone (PVP) and Eudragit® RS100, layer. These patches were effective in sticking to mucosal tissue without cytotoxicity and were successfully loaded with drugs for the treatment of oral lesions. Clitherow et al.[249] have demonstrated that PCL and PVP/RS100 (PVP/RS100) electrospun patches are effective antifungal drug delivery vehicles for oral thrush.

2.7 Summary

This literature review chapter provides a detailed background for the study and design of antimicrobial biomaterials for bone tissue engineering in this thesis. The strategy used in this thesis for addressing implant biofilm associated orthopaedics infections is to exploit the antimicrobial function of NO without using antibiotics which lead to drug resistant bacteria. As NO is a reactive gas molecule and has short half-life, the chemical properties and delivery mechanisms (e.g. coatings, scaffolds) of NO donors (mainly *N*-diazeniumdiolates) have been reviewed in this chapter. Two main types of biomaterials that are used to fabricated orthopaedic implants are also, reviewed in this chapter.

Chapter 3: Nitric Oxide Releasing Titanium Surfaces for Antimicrobial Bone-Integrating Orthopaedic Implants*

3.1 Introduction

Implant-associated infections represent a serious complication as once bacteria colonise the surface, they form biofilms, which are more difficult to treat, requiring up to a 1000-fold increase in the antimicrobial dose.[8, 250-251] Once an infection takes place on a titanium implant, repeated revision surgeries are often required and can lead to poor implant integration, bone loss and soft tissue defects.[252-253] Orthopedic implant infections are caused most often caused by *Staphylococcus species* (*S. aureus* and *S. epidermidis*) or *Pseudomonas aeruginosa* which can be acquired during surgery or subsequently through a hematogenous route.[3, 254] Moreover, implants that are transmucosal and percutaneous (e.g. dental and external fixation pins) are more susceptible to infection as opportunistic bacteria that reside on the skin mucosa can colonise the peri-implant soft tissue which can lead to a peri-implant bone infection.[255-256] Localised delivery of antibiotics via a coating layer on the implant is seen as a promising strategy to prevent infections and subsequent failure of the implant. However, given the rise in the global epidemic of antimicrobial resistance, much focus has changed to the development of alternative antimicrobials such as silver,[257-258] zinc ions,[259] bioactive antibodies,[260] antimicrobial peptides[261-262] and nitric oxide[36, 111] which have a low tendency to developing multi drug resistant bacteria.

Nitric oxide (NO) is a potent broad spectrum antimicrobial and part of the body's defense mechanism that is activated by inflammatory cells (neutrophils and macrophages) which are responding to invading pathogens such as bacteria,

*This chapter has been published. M. Li *et al*. *ACS Appl. Mater. Interfaces*, **2020**, 12(20), 22433–22443

protozoa and fungi.[116, 263] The antimicrobial activity of NO is attributed to the reactive nitrogen oxide species (RNOS) that are produced through the spontaneous reaction of NO with oxygen or superoxide that cause damage to bacterial DNA, proteins and lipid membranes.[106-107] The formation of these RNOS become significant or antimicrobial when the concentration of NO is >1μM.[106] Given that there are several mechanistic pathways for NO to inactivate bacteria, studies have shown that there is a low tendency for bacteria to develop resistance to this antimicrobial.[108, 121] Furthermore as eukaryotic cells have evolved mechanisms that are capable of scavenging these RNOS, it is thought that NO will exhibit a low toxicity on the host.[263]

Although NO is clearly identified as a potent antimicrobial, its clinical utility is challenging as NO is a highly reactive gas with a short half-life.[264] As such, there has been much research focused on the development of NO donors such as *N*-diazeniumdiolates, *S*-nitrosothiols, organic nitrates, metal nitrosyls which can store and release NO for more prolonged periods of time under requisite conditions.[145, 148, 265] The most commonly reported *N*-diazeniumdiolates (containing the $[N(O)=NO]^-$) are adducts formed from a NO dimer with a secondary amine nucleophile.[148, 264] These *N*-diazeniumdiolates can spontaneously decompose with tunable half-lives dependent on the structure of the nucleophile (amine), pH and temperature.[148] As secondary amine diazeniumdiolates are formed much easier, much work has focused on these rather than primary amine diazeniumdiolates.[177, 266-268] Although many of these studies have investigated how NO can be released for biomaterial/medical device applications, there is a paucity of information regarding the mechanism of release and the robustness of the coatings. For example, Ho and coworkers[177] focused on the feasibility of using plasma polymerisation to coat polymer surfaces

with allylamine and diallylamine coatings, followed by the incorporation of diazeniumdiolates. In this study, although they have looked at primary and secondary diazeniumdiolates and have obtained a higher NO payload with the secondary diazeniumdiolate, they have not evaluated the stability or shelf-life of the coatings or investigated the potential cytotoxicity of the materials. Moreover, the underlying coatings are not optimised to promote osseointegration.

Amino terminated silanes (as opposed to methyl, hydroxyl, or thiol) have been found to control cell responses, resulting in the formation of high quality de novo tissue.[269-270] These comprehensive investigations were performed with a variety of silanised glass surfaces to understand the effect of silane chain length on associated osteoinductive properties of the surface.[269] Within this chapter, only the longer chain silanes containing pendant amino groups resulted in the formation of an apatite-like layer on the surface that induced a significantly enhanced osteoinductive response across the entirety of the surface.

Therefore, amino-terminated silane (11-Aminoundecyltriethoxysilane, AUTES) with the most consistent and homogeneous osteoinductive property has been selected and used to tether NO. The hypothesis here is as the underlying surface is known to be osteoinductive, once the NO is released and any potential infection during implantation is averted, osseointegration can take place. Within this preliminary study we investigate the effect of NO on the initial and prolonged (after 7 days) viable adhesion of primary human osteoblasts to the modified surfaces. However, since primary diazeniumdiolates are not as well studied and do not release as much NO,[137] another potentially osseointegrative promoting silane containing a secondary amine

has been selected in order to investigate the effects of primary vs secondary amines in terms of antimicrobial efficacy.

In this chapter, Ti has been functionalised with two different aminosilanes and subsequently tethered diazeniumdiolates on. A comprehensive mechanistic study of developed NO releasing coatings has been carried out to understand the kinetics and payload of release as a function of the stability of the silane, the nature of the amino functional group and pH of release. This mechanistic understanding will allow fine tuning of the antimicrobial efficacy to prevent infection at 6 h (time frame for initial bacterial adhesion vs. mammalian cell adhesion) in the so called "race to the surface". The antimicrobial efficacy against *Staphylococcus aureus* and *Pseudomonas aeruginosa* have been studied at 6 and 24 h and cytocompatibility of the surfaces with primary human osteoblast cells was investigated in order to improve the integration of implants with bone.

3.2 Materials and Methods

3.2.1 Experimental Materials

Ti rods (ø 6.4mm, 99.7% metal basis) were purchased from Alfa Aesar and cut into pieces 1.5 mm in thickness. 6-Aminohexyl-3-aminopropyl trimethoxysilane (AHAP3, 95%), 11-Aminoundecyltriethoxysilane (AUTES, > 95%), n-Decyltrimethoxysilane (DTMS, 97%) were purchased from Fluoro Chem. Ethanol, acetic acid (HAc), sodium acetate (NaAc), Luria Bertani Broth (LB Broth), LB agar, Dulbecco's Modified Eagle Medium (DMEM), fetal bovine serum (FBS), Penicillin-Streptomycin, Trypsin-EDTA solution, formaldehyde solution and Triton™ X-100 were purchased from Sigma-

Aldrich. 4',6-diamidino-2-phenylindole (DAPI) staining mounting gel and ActinGreen ™ 488 reagent kit were obtained from Thermo Fisher Scientific.

3.2.2 Titanium Pretreatment

Ti discs were polished with SiC sand paper (1200-grit) and then washed with ethanol and DI water for 15 mins each. Washed Ti discs were then air dried at room temperature and stored in a desiccator until use.

3.2.3 Silanisation and Diazeniumdiolate-Functionalisation

Pristine polished Ti discs were immersed in 10 wt % silane solutions (Amino-silanes: AHAP3, AUTES and Control alkyl silane: DTMS) prepared in ethanol and shaken on a gyro-rocker (SSL3, Stuart) at 70 rpm for 4 h. Samples were then washed with ethanol 3 times to remove unreacted silane and cured in an oven at 80° C for 4 h. At the end of this time, samples were then stored in a desiccator until diazeniumdiolate functionalisation. Silanised samples are referred to as AHAP3, AUTES and DTMS, respectively. Silanised Ti discs were functionalised with diazeniumdiolates in an in-house built stainless steel NO reactor as previously reported.[141] Briefly, the reactor chamber was purged with 6 bar argon (BOC, Guildford, UK) for 5 mins (3 x) and 10 mins (3 x) to remove atmospheric oxygen and water. Then nitric oxide (NO) (BOC, Guildford, UK) was introduced into the reactor at 5 bar for 3 days. At the end of this time, residual NO was removed by flushing the chamber with 6 bar argon for 5 mins (2 x) and 10 mins (2 x). Diazeniumdiolate functionalised Ti samples were then stored at -20°C until use. Diazeniumdiolate functionalised samples are referred to as Ti/NO, AHAP3/NO, AUTES/NO and DTMS/NO, respectively. It should be noted that titanium samples will have an oxide layer on the surface and most likely exist as TiOx.

Moreover as Ti and DTMS do not possess any amine functionality, there is no possibility of forming *N*-diazeniumdiolates, and as such these are control samples. The nomenclature is kept as Ti/NO and DTMS/NO for consistency and ease of readership.

3.2.4 Characterisation

3.2.4.1 Contact Angle Analysis

Static contact angles (Attension ThetaLite, Biolin Scientific, Västra Frölunda, Sweden) were used to determine the changes in surface wettability of all samples. The sessile drop method was used and contact angle measurement images were taken using OneAttension software (Biolin Scientific, Västra Frölunda, Sweden). Three random spots were performed per sample type (n=3) and mean values ± standard deviations of the samples were recorded and repeated twice.

3.2.4.2 Atomic Force Microscopy Analysis

Atomic force microscopy (AFM) was used to observe the surface topography changes of silanised samples (Bruker Multimode 8 fitted with a NanoScope V controller; Bruker, Billerica, MA, USA). Samples were imaged in air in ScanAsyst mode using a silicon RTESPA-525 tip, operating at a scan rate of 0.9 Hz. At least three replicate regions including the centre and edge of 10 x 10 μm^2 of each sample were imaged and repeated twice. The mean roughness (R_a) and root mean square roughness (R_q) were measured using Bruker NanoScope Analysis 1.7 software.

3.2.4.3 X-ray Photoelectron Spectroscopy

Functionalised surfaces were analysed by X-ray photoelectron spectroscopy (XPS) on an Axis-Supra instrument from Kratos Analytical with monochromatic Al Kα radiation (225W). Survey scan spectra were recorded at a pass energy of 160 eV and a 1 eV

step size. High resolution scans were acquired at a pass energy of 20 eV and a 0.1 eV step size. The XPS spectra were recorded in normal emission. Three random areas on each sample were analysed and the results are reported as the mean average atomic percentage concentration (at. %) ± standard deviations. Spectra were processed using CasaXPS 2.3.19PR1.0 software (Casa software, UK) and charge calibrated to C 1s at 284.8 eV. Spectra were curve fitted with a mixed Gaussian-Lorentzian function after Shirley background subtraction.

3.2.4.4 NO Release Measurement

Nitric oxide release from samples was measured using a Sievers 280i Chemiluminescence Nitric Oxide Analyser (NOA280i, GE, USA). The instrument measures nitric oxide based on a gas-phase chemiluminescent reaction between nitric oxide and ozone:

$NO + O3 \rightarrow NO2^* + O2$

$NO2^* \rightarrow NO2 + hv$

Emission from electronically excited nitrogen dioxide is in the red and near-infrared region of the spectrum, and is detected by a thermoelectrically cooled, red-sensitive photomultiplier tube. Before measurement, calibration was carried out by using zero air filter and 89.2 ppm NO (g) (balance nitrogen). The diazeniumdiolate functionalised samples (6.4 mm diameter, 1.5 mm thick) were immersed in 5 ml of acetic acid buffer (pH 4) or phosphate buffered saline (PBS; pH 7.4 and pH 8.5) at room temperature in a three-neck round bottom flask. Nitrogen gas was continuously sparged though the buffer at a flow rate of 200 ml / min. A vacuum pump connected with the NOA is used to draw the mixed gases in to the reaction cell

and maintains the pressure of the reaction cell. Nitric oxide release was measured at an interval of 1 s over more than 20 h. Each sample was measured in triplicate.

3.2.5 Biofilm Assay and Morphology Analysis

3.2.5.1 LB Broth and Agar Plates Preparation

Fresh LB broth and LB agar plates were prepared prior to use. LB broth and LB agar powders were dissolved in deionised water with a concentration of 20g/L and 35g/L, respectively, followed by 15 minutes autoclave sterilisation at 121 °C. The sterilised LB broth was used after cooling down to room temperature. The sterilised LB agar plates were poured in aseptic condition and left to solidify at room temperature. All the broth and agar plates were stored at 4°C for further use.

3.2.5.2 General Bacterial Culture

Staphylococcus aureus (*S. aureus*) ATCC 25923 and *Pseudomonas aeruginosa* (*P. aeruginosa*) PA01 were used to evaluate the biofilm inhibition efficiency of the nitric oxide releasing surfaces. Overnight cultured bacteria were diluted to 10^6 CFU/mL according to McFarland Standards in LB broth. Samples were placed in a 48 well-plate and 500 µL diluted bacterial solution was added to each well before incubating at 37 °C to allow biofilm formation.

3.2.5.3 Biofilm Assay

After incubation, samples were gently washed with PBS once to remove any unattached planktonic bacteria and then 1 mL of fresh LB broth was used to remove and re-suspend the biofilms. The bacterial CFU was determined after serial dilution of the bacterial suspension using the Miles and Misra method on LB agar plates.[271]

3.2.5.4 Bacterial Morphology Analysis

After incubation with bacteria, the samples were gently washed with PBS to remove unattached bacteria, and fixed with 2.5% glutaraldehyde solution in sterile PBS for 4 h at 4 °C, then dehydrated with increasing concentrations of ethanol (30, 50, 75, 90, 95, and 100 v/v %) for 10 min. After drying the samples were coated with gold (Q150T ES sputter coater; Quorum, East Sussex, UK) before SEM imaging (JSM 7001F FEGSEM; JEOL, Tokyo, Japan).

3.2.6 *In Vitro* Cell Culture and Immunocytochemistry Analysis

Primary human osteoblast cells used in this thesis were obtained from Institute of Aging and Chronic Disease (University of Liverpool, UK). The original passage cultured from explants of human bone from ethically approved osteoarthritis surgery.[272] Cells were expanded and maintained *in vitro* in DMEM media supplemented with 10% FBS and 1% penicillin-streptomycin in a humidified atmosphere of 5% CO_2 at 37 °C and used between passages 5 and 10. Upon confluence cells were rinsed in sterile PBS and incubated with trypsin-EDTA for 3 minutes at 37 °C to remove the cells from tissue culture polystyrene (TCPS) and retain in solution, diluted to 1 x 10^5 cells/ml using the afore mentioned culture medium. Samples were incubated with 1 ml of cell suspension per well in 24-well culture plates. The media was replaced with fresh cell culture media every 3 days.

At day 7 of culture, cells were prepared for staining using the following protocols. Medium was removed from the wells and samples were rinsed with sterile PBS for 5 minutes at 37 °C. Cells were then fixed using 4% formaldehyde for 15 min at room temperature, followed by rinsing with PBS. Then cells were permeabilised with 0.5% Triton® X-100 for a further 15 min at room temperature. After washing 3 times with

PBS, cells were incubated with diluted Oregon Green PhallodinTM 488 kit (5µg/ml) for 30 min at 4°C followed by further rinsing with PBS prior to mounting with DAPI staining mounting medium (Vector, UK). Cell morphology images were obtained by confocal laser scanning microscopy (LSM 510, Zeiss, Germany). 6 images were taken per samples and representative images are shown. Images were processed using ImageJ 1.48 software.

3.2.7 Statistical Analysis

One-way analysis of variance (ANOVA) was used to analyse the differences among various treatment samples. The Student-Newman-Keuls (SNK) method was carried out to determine significance between treatment types. A value of $p < 0.05$ was taken as being statistically significant.

3.3 Results and Discussion

3.3.1 Synthesis of *N*-Diazeniumdiolate-Functionalised Titanium

The diazeniumdiolate functionalised Ti surfaces were synthesised via a two-step method illustrated in **Figure 3.1**. Polished Ti surfaces were functionalised with silanes with or without primary and secondary amines; 6-Aminohexyl-3-aminopropyl trimethoxysilane (AHAP3): 1 primary amine and 1 secondary amine, 11-Aminoundecyltriethoxysilane (AUTES): 1 primary amine and n-Decyltrimethoxysilane (DTMS): no amine. The silane-modified Ti substrates were then exposed to high pressures of NO (5 bar) over 72 h to allow formation of diazeniumdiolate NO donors.

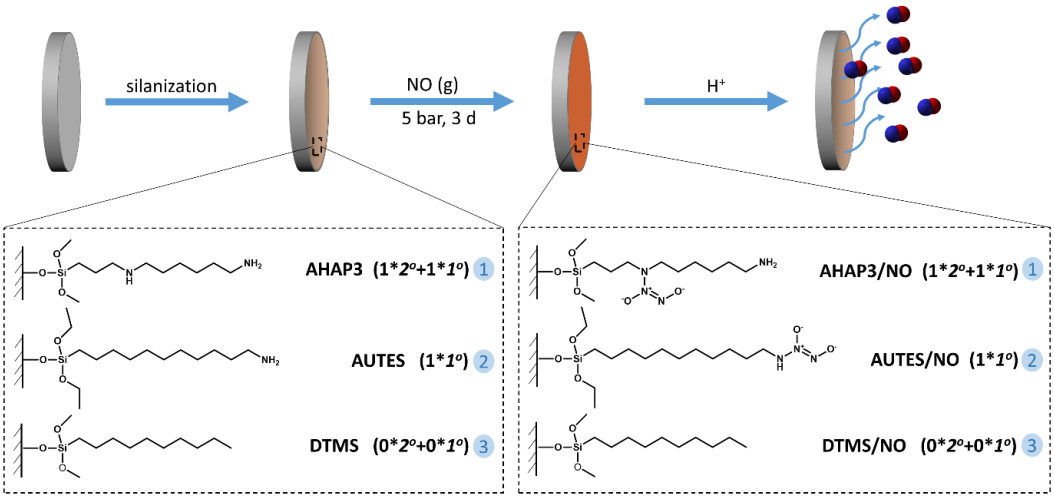

Figure 3.1: Diazeniumdiolate functionalisation of titanium surfaces.

3.3.2 Surface Wettability: Static Water Contact Angle

The wettability of the Ti substrates before and after functionalisation was determined using static contact angles with the results shown in **Figure 3.2**. Pristine Ti had an average contact angle of 64°. After silanisation, the contact angles for AHAP3, AUTES and DTMS films on Ti increased to 78, 83 and 101°, respectively. The increase in contact angle can be attributed to the presence of hydrophobic alkyl silane chains confirming functionalisation of the surface. DTMS displayed the most hydrophobic character, as there is no electronegative amino group present in the silane molecule.

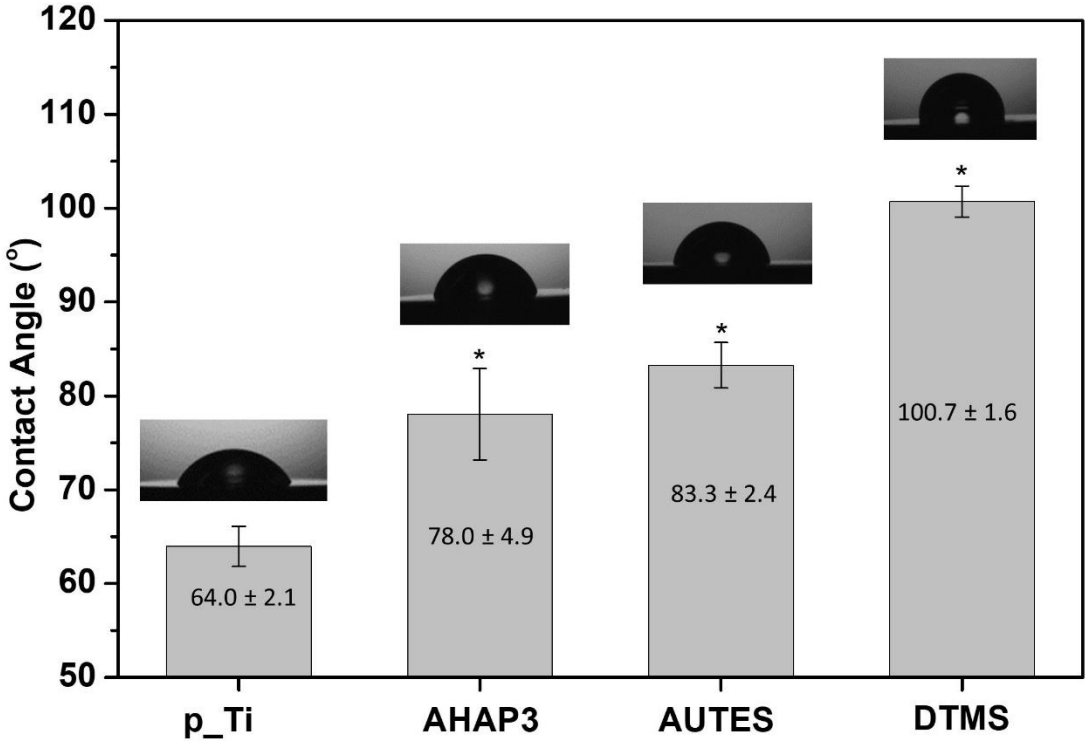

Figure 3.2: Measurement of contact angle with water drops at room temperature on pristine Ti (p_Ti) and silanised p_Ti with AHAP3, AUTES and DTMS. Each bar represents mean ± SD (n=3). *$p < 0.05$, relative to the control.

3.3.3 Surface Topography: Atomic Force Microscopy

The topography of Ti and functionalised Ti surfaces was investigated using AFM (**Table 3.1** and **Figure 3.3**). Pristine Ti has a roughness of 35.5 ± 0.8 nm (R_a) (**Figure 3.3a**) and all of the silanised surfaces showed a statistically significant increase in roughness (**Figure 3.3b- d**). This is indicative of the deposition of multiple layers of silane on the surface. Indeed there is visible aggregation of the silane observed on all of the silanised surfaces (**Figure 3.3b-d**). The silanised surfaces displayed roughness values (R_a) of: AHAP3 (108.1 ± 16.4 nm), AUTES (87.1 ± 8.7 nm) and DTMS (64.8 ± 17.4 nm) (also listed in **Table 3.1**).

Table 3.1: Topography of silanised surfaces.

roughness	p_Ti	AHAP3	AUTES	DTMS
***R*q (nm)**	46.4 ± 2.1	135.0 ± 26.0 [a]	109.2 ± 9.1 [a]	80.9 ± 22.0
***R*a (nm)**	35.5 ± 0.8	108.1 ± 16.4 [a]	87.1 ± 8.7 [a]	64.8 ± 17.4 [a]

[a] indicates statistical significance ($p < 0.05$) between the control and silanisation surfaces.

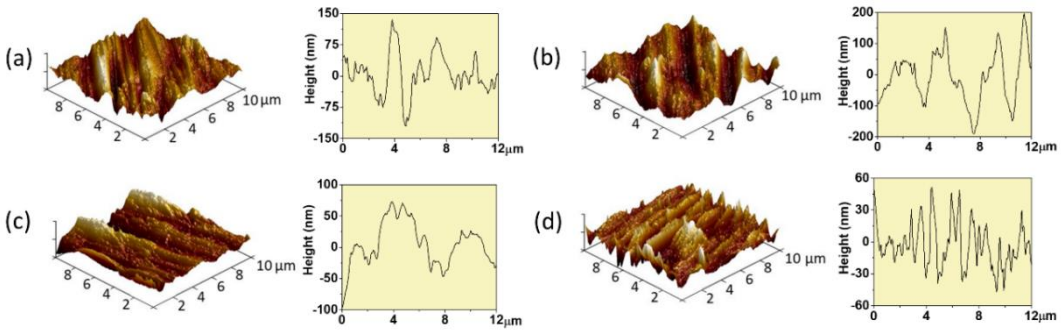

Figure 3.3: AFM height mode of silanised surfaces. The cross-sections of 10 × 10 µm^2 size images are shown at different z-axis maximum heights. a) p_Ti, b) AHAP3, c) AUTES, d) DTMS.

3.3.4 Surface Chemistry: X-ray Photoelectron Spectroscopy

The surface chemistry of the silanised surfaces pre- and post- diazeniumdiolate treatment were analysed by XPS with the resultant at. % shown in **Table 3.2**. XPS analysis shows that pristine Ti consists of Ti, C, O and N. After silanisation with all 3 silanes, the Ti 2p peak decreases with an increase in the C 1s peak and introduction of the Si 2p peak, confirming the silanisation of the surface. Following exposure of the silanised Ti surfaces to NO, the at. % of the C 1s peak decreases with a concomitant rise in the O 1s and N 1s peaks confirming formation of the N-diazeniumdiolate functional group.

Table 3.2: Atomic surface concentration (at. %) of pristine ti surface, silanised surfaces and diazeniumdiolates-functionalised surfaces.

sample	C (1s)	O (1s)	N (1s)	Ti (2p)	Si (2p)
p_Ti	28.2±1.4	52.2±0.8	0.6±0.5	18.9±1.1	-
AHAP3	63.9±5.3	15.2±5.4	9.6±1.4	1.3±2.3	9.9±1.2
AUTES	75.0±0.3	11.5±0.2	3.7±0.4	-	9.8±0.2
DTMS	47.9±0.8	34.4±0.5	1.7±0.3	11.7±0.5	4.2±0.3
Ti/NO	49.3±2.7	39.4±2.2	1.7±0.8	9.5±1.3	-
AHAP3/NO	57.1±1.2	26.4±1.1	10.3±0.3	0.6±0.5	5.5±0.2
AUTES/NO	71.5±0.2	17.8±0.2	1.8±0.5	0.1±0.1	8.8±0.4
DTMS/NO	62.2±3.5	25.8±4.9	0.8±0.4	4.1±2.0	7.0±1.4

Table 3.3: XPS derived N 1s curve fitted data for the surfaces.

sample	N 1s			
	N-H	N^+	N-O	by-products (NO_2^-, NO_3^-, NO_4^-)
p_Ti	69.1	30.9	-	-
AHAP3	83.1	16.9	-	-
AUTES	75.8	24.2	-	-
DTMS	75.1	24.9	-	-
Ti/NO	55.7	-	-	44.3
AHAP3/NO	12.1	22.9	25.4	39.6
AUTES/NO	14.7	28.8	31.5	25.0
DTMS/NO	-	72.0	28.0	-

The silanisation and functionalisation with diazeniumdiolate can also be corroborated by analysing the curve fitted high resolution N 1s spectra shown in **Figure 3.4** (with the associated quantitative information given in **Table 3.3**). The presence of nitrogen on pristine Ti (**Figure 3.4a**) is due to the nitrogen contamination of the raw material (N: 0.02% in Ti rod, data from certificate of analysis document, Alfa Aesar). Following silanisation with the aminosilanes, AHAP3 and AUTES, two additional states of nitrogen observed, with binding energies at ~400.5 eV (N-H) and ~401.6 eV (N^+) (**Figure 3.4c and e**). After exposure to high pressures of NO, diazeniumdiolate formation was confirmed via the presence of the new peaks observed, indicative of N-H (400.5 eV), N-O (402.3 eV), and NO_4^- (~407 eV) bonds. Moreover, the presence of the N-O bond is observed with a decrease in the N-H bond, confirming the nucleophilic attack of the amine group on the NO dimer forming

the diazeniumdiolate functional group. Interestingly, DTMS does not have any pendant amino groups but after exposure to NO gas, the N 1s envelope shows the presence of N-O peak (28%). This is probably due to some physisorbed NO on the surfaces that have been converted to nitrates and nitrites.

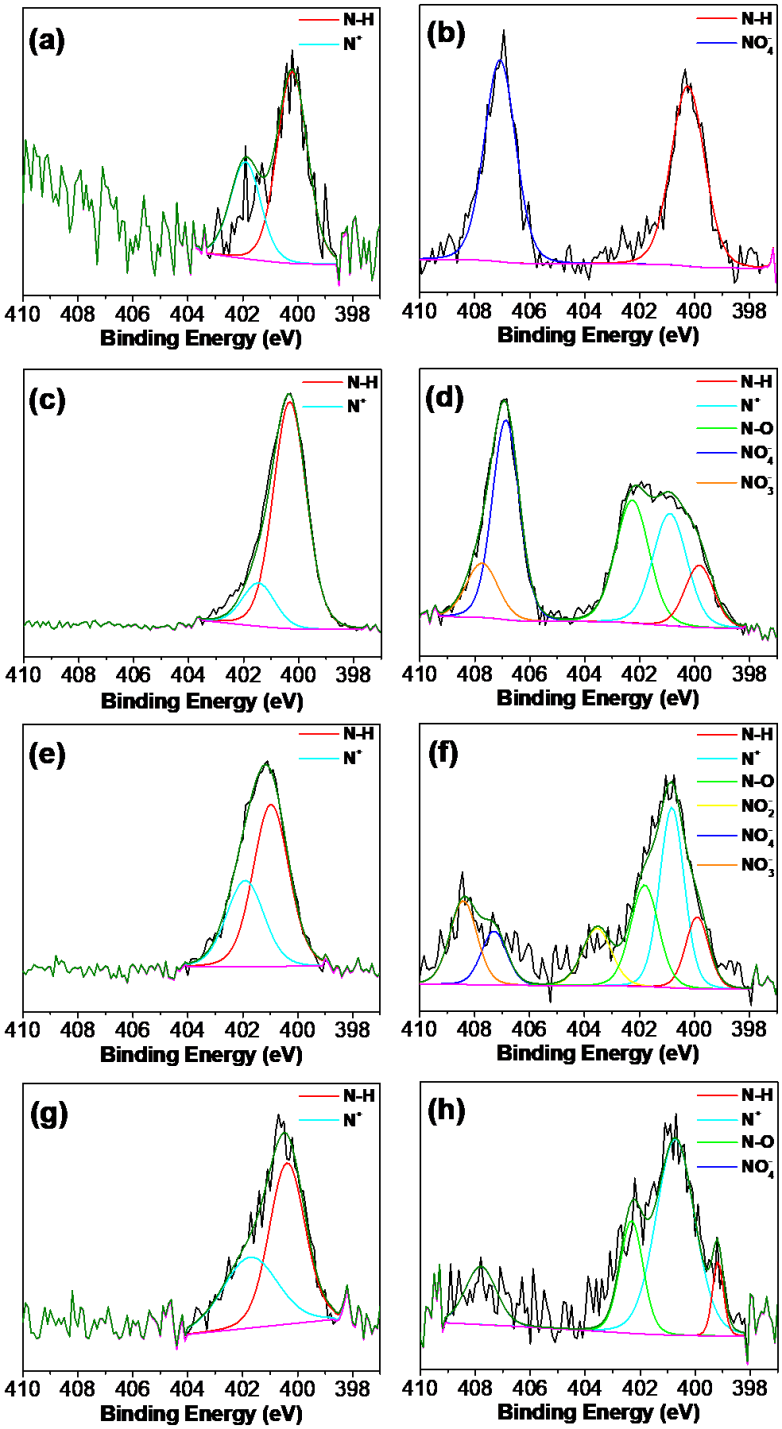

Figure 3.4: High-resolution N 1s spectra of (a) p_Ti, (b) Ti/NO, (c) AHAP3, (d) AHAP3/NO, (e) AUTES, (f) AUTES/NO, (g) DTMS and (h) DTMS/NO. The peak at ~401.6 eV represent $–N^+$ and the N-O bond shows a bonding energy at ~402.3 eV, shows successful formation of diazeniumdiolates.

3.3.5 NO Release from Diazeniumdiolate-Functionalised Surfaces

In order to understand the effects of pH on NO release, the NO-payload from the diazeniumdiolate-modified surfaces was determined using a chemiluminescence nitric oxide analyser in acetate and PBS buffers at pH 4, 7.4 and 8.5. The NO release profiles of Ti/NO, AHAP3/NO, AUTES/NO and DTMS/NO are shown in **Figure 3.5 (a-e)**. The total concentration of NO after 1 hr (t[NO]), half-life of NO release ($t_{1/2}$), maximum instantaneous NO release concentration ($[NO]_m$), time required to reach $[NO]_m$ (t_m) and NO release duration (t_d) from each surface were determined and the values are summarised in **Table 3.4**. The NO payload and release kinetics were dependent upon the number and class of amines in the silane, the pH of the release buffer and if a monolayer or multilayer of silane was present on the surface.

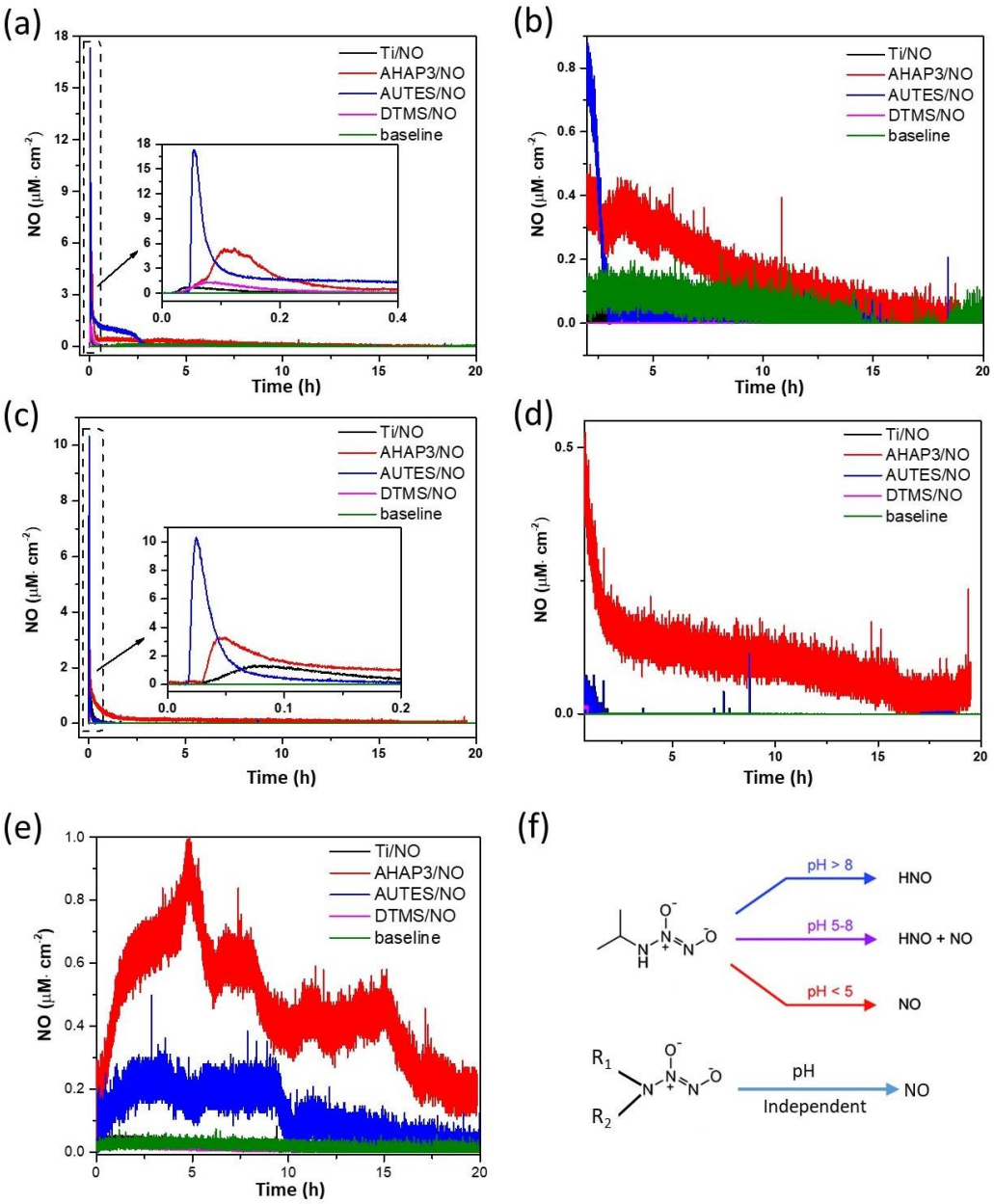

Figure 3.5: Chemiluminescence NO release profiles of (a) overall 20 h and the insert is rescaling of the first 0.4 hr at pH 4, (b) rescale detailing over 20 h at pH 4, (c) overall 20 h and the insert is rescaling of the first 0.2 hr at pH 7.4, (d) rescale detailing over 20 h at pH 7.4 and (e) overall 20 h at pH = 8.5 buffers at room temperature. The inserts have the same scaling units of the axis as the overall pictures. (f) primary and secondary amine based diazeniumdiolates decomposition as NO/HNO donor at different pHs.[267-268]

AHAP3/NO: At pH 4, AHAP3/NO surfaces released NO at a maximum instantaneous NO release concentration of 1.8 $\mu M \cdot s^{-1}$ with 1005.4 μM NO being released in a burst during the first hour. At pH 7.4, the concentration of NO released was less than that observed at pH 4, with 676.8 μM of NO released during the first hour. At pH 8.5, the AHAP3/NO surface released a NO concentration of 330.5 μM during the first hour.

AUTES/NO: At pH 4, AUTES/NO surfaces released a maximum instantaneous NO release concentration of 5.6 $\mu M \cdot s^{-1}$ and 1883.6 μM NO was released in a burst during the first hour. At pH 7.4, the concentration of NO released was less than that observed at pH 4. 476.2 μM of NO was released during the first hour. At pH 8.5, the AUTES/NO surface released 133.7 μM during the first hour.

DTMS/NO: At pH 4, DTMS/NO surface, released 231.1 μM of NO with a maximum instantaneous NO release concentration of 0.4 $\mu M \cdot s^{-1}$. At pH 7.4, the concentration of NO released was less than that observed at pH 4. The final concentration of NO released was 26 μM during the first hour. At pH 8.5, the DTMS/NO surface released no measurable NO. DTMS/NO has no amine in its backbone and therefore cannot form an *N*-diazeniumdiolate.

Table 3.4 NO release properties for diazeniumdiolate-functionalised surfaces prepared by using silane with different amine groups in pH 4, 7.4 and 8.5.

	Silane precursor	Number of amine		t[NO]	t[NO]	$t_{1/2}$	$[NO]_m$	t_m	t_d
		primary	secondary	(μM)	($\mu M \cdot cm^{-2}$)	(min)	($\mu M \cdot s^{-1} \cdot cm^{-2}$)	(min)	(h)
pH 4	AHAP3	1	1	1005.4	3122.4	34.2	5.6	7.4	18.1
	AUTES	1	0	1883.6	5849.7	52.8	17.4	3.2	3.2
	DTMS	0	0	231.1	717.7	8.0	1.3	4.5	0.8
pH 7.4	AHAP3	1	1	676.8	2101.9	16.3	3.1	2.7	16.5
	AUTES	1	0	476.2	1478.9	2.4	10.2	1.5	1.5
	DTMS	0	0	26.0	80.7	0.2	0.3	2.1	0.7
pH 8.5	AHAP3	1	1	330.5	1026.4	183.9	0.9	5.6	20+
	AUTES	1	0	133.7	415.2	159.8	0.3	5.3	10
	DTMS	0	0	-	-	-	-	-	-

3.3.6 Mechanism of NO Release

The mechanism of NO release is dependent on three factors as described below: pKa of the amine, class of amine (primary vs secondary) and quality of the silane layer formed on the surface.

pKa: The NO release from diazeniumdiolate occurs via protonation of the amine precursor and the release kinetics are dependent upon the pKa of the amine. As such, the higher the pKa the easier the protonation and the faster the release at physiological conditions. The rate of release of NO can also be increased by other factors such as the presence of neighboring amines which can act as a proton source[139] and an increase in temperature.[273] This is indeed what was experimentally observed for the AHAP3/NO and the AUTES/NO surfaces; at pH 4 these surfaces showed a burst release of NO.

Class of amine: Keefer and coworkers have demonstrated that primary amine diazeniumdiolates decompose to HNO and NO with the product ratio dependent on the pH and the basicity of the nitroso oxygen formed.[268] In contrast, secondary amines only undergo decomposition based on pH mediated protonation to produce exclusively NO.[268] A schematic has been shown in **Figure 3.5 (f)**. Keefer has shown that primary amine diazeniumdiolates decompose: (a) exclusively to NO at pH 5; (b) to a mixture of HNO and NO at pH 5-8, and (c) exclusively to HNO above pH 8. In this chapter, AHAP3/NO has the potential to form one secondary and one primary amine diazeniumdiolate and AUTES/NO has the potential to form only a primary amine diazeniumdiolate. Therefore, based on Keefer's mechanism,[268] AHAP3/NO and AUTES/NO will release the highest concentration of NO at pH 4 as

both the primary and secondary amines exclusively decompose to NO. The concentration of NO will then decrease as the pH of the release buffer increases due to the presence of primary amines and subsequent decomposition to HNO. Despite the AHAP3 releasing lower amounts of NO at pH 4 (1005.4 µM) than the AUTES (1883 µM), the release concentration exceeds the concentration released by AUTES at pH 7.4 due to the presence of a secondary amine in AHAP3.

Number of amines/Quality of silane layer: AHAP3 has one secondary amine and one primary amine and therefore the potential to form of two diazeniumdiolates and have double the payload of NO at pH 4. In solution, this is indeed what is observed, where AHAP3/NO (10 µl/5 ml PBS) shows a maximum NO release of 1993.3 $\mu M \cdot s^{-1}$, in comparison with AUTES (**Figure 3.6**). However, the opposite was observed when the silanes were immobilised on the surface, with AHAP3/NO and AUTES/NO having NO payloads of 1005.4 µM and 1883.6 µM within the first hour. The lower payload observed here is due to the quality of the silane monolayer formed.

A more cohesive silane coverage on Ti surfaces should yield a higher NO payload. AUTES forms a monolayer on the surface through hydrolysis of an ethoxy leaving group to generate silanol containing species that readily condenses on the surface. The faster the hydrolysis of the silane, the faster the condensation and the increase in the self-condensation/aggregation reactions (a less cohesive monolayer is formed on the surface). The rate of hydrolysis of the alkoxy groups are dependent on their size ($CH_3O > C_2H_5O > t\text{-}C_4H_9O$), meaning that a methoxysilane hydrolyses 6 - 10x quicker than an ethoxysilane.[202-203, 274-275] Therefore, as ethoxysilanes hydrolyse slower than methoxysilanes, they will form more cohesive monolayers on the surface. In this

chapter, AHAP3 is a methoxysilane and AUTES is an ethoxysilane. This explains why AHAP3/NO on the surface has a lower NO payload when on the surface compared with AUTES/NO, despite the situation being reversed in solution phase (**Figure 3.6**).

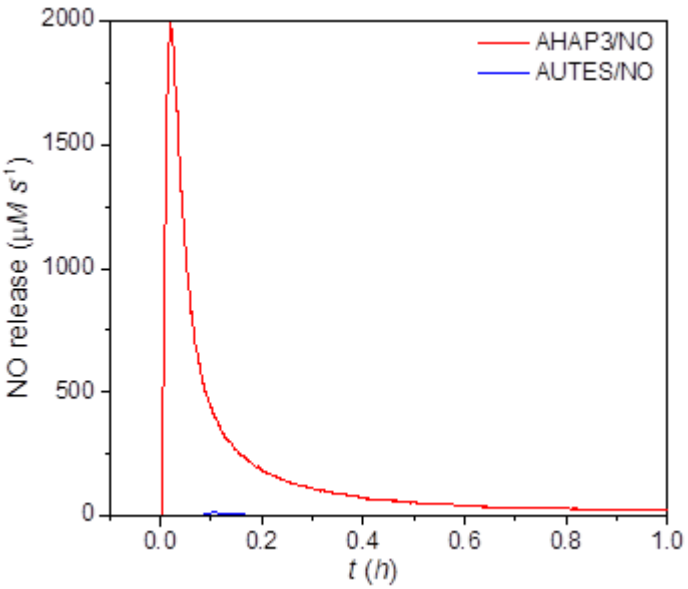

Figure 3.6: NO release of liquid AHAP3/NO and AUTES/NO measured in pH4 PBS.

3.3.7 Antimicrobial Analysis

Gram-positive *S. aureus*, and gram-negative *P. aeruginosa*, two relevant pathogens for orthopaedic infections,[53] were selected to measure the antimicrobial efficacy of NO releasing samples. The SEM micrographs of *S. aureus* and *P. aeruginosa* cultured for 6 h on Ti, AHAP3, AUTES and DTMS samples with/without NO release are shown in **Figure 3.7**. Bacterial clusters and biofilms can clearly be observed on pristine Ti (as shown in **Figure 3.7a (i)**), and all non-NO releasing silanised surfaces (AHAP3, AUTES, and DTMS, **Figures 3.7b-d (i)** respectively) demonstrating that these surfaces do not exhibit antimicrobial activity. Tethering of the diazeniumdiolate to the

aminosilanised surfaces AHAP3/NO (**Figure 3.7b (ii, iv)**) and AUTES/NO (**Figure 3.7c (ii, iv)**) demonstrate a reduction in the *S. aureus* and *P. aeruginosa* adhered to the surface, in comparison to Ti/NO (**Figure 3.7a (ii, iv)** and DTMS/NO (**Figure 3.7d (ii,iv)**). This is in agreement with the results presented in **Figure 3.5**, which demonstrates that the surfaces that release the highest payload of NO exhibit the most antimicrobial activity.

The prevention of biofilm formation on all surfaces at 6 and 24 h was determined by using a biofilm CFU assay and the results are presented in **Figure 3.7e** for *S. aureus*. The AHAP3/NO surface showed a reduction in the number of adhered *S. aureus* from 0.8×10^8 CFU/ml to ~10^6 CFU/ml at 6 h which corresponds to a 1.5 log reduction (**Figure 3.7e**). Likewise, the AUTES/NO surface showed a reduction in the number of adhered *S. aureus* from 4.1×10^7 CFU/ml to ~10^6 CFU/ml at 6 h which corresponds to a 0.8 log reduction (**Figure 3.7e**). At 24 h, the reduction in the adhered bacteria is approx. 1.5 log for AHAP3 to AHAP3/NO and 0.8 log for AUTES to AUTES/NO. This difference in antimicrobial activity is in agreement with the results presented in **Table 3.4** which show that the AHAP3/NO surface has a higher payload of NO at pH 7.4 (676.8 µM) vs AUTES/NO (476.2 µM). The surface of Ti/NO and DTMS/NO did not show any reduction in the adhered bacteria. A salient point here is that the NO release profiles were carried out in 5 mL of measurement buffer, whilst, the antimicrobial experiments were carried out in 500 µL of broth. Hence the bacteria in these experiments are exposed to 10x the payload observed in the NO release profiles and within the reported range need for antimicrobial activity by Friedman and coworkers.[106]

The prevention of biofilm formation on all surfaces at 6 and 24 h was determined by using a biofilm CFU assay and the results are presented in **Figure 3.7f** for *P. aeruginosa*. The AHAP3/NO surface showed a reduction in the number of adhered *P. aeruginosa* from ~10^5 CFU / ml to 1.6×10^4 CFU / ml at 6 h which corresponds to a 0.8 log reduction (**Figure 3.7f**). Likewise, the AUTES/NO surface showed a reduction in the number of adhered *P. aeruginosa* from 1.6×10^5 CFU / ml to 3×10^4 CFU / ml at 6 h which corresponds to a 0.8 log reduction (**Figure 3.7f**). At 24 h, the reduction in the adhered bacteria is approx. 0.3 log for AHAP3 to AHAP3/NO and there was no significant reduction for AUTES to AUTES/NO. This difference in antimicrobial activity is in agreement with the results presented in **Table 3.4** which show that the AHAP3/NO surface has a higher payload of NO at pH 7.4 (676.8 µM) vs AUTES/NO (476.2 µM). The surface of Ti/NO and DTMS/NO did not show any reduction in the adhered bacteria. As mentioned above, as the antimicrobial experiments are carried out in only 500 µl of broth, the bacteria are exposed to 10x the payload observed in the NO release profiles and within the reported range need for antimicrobial activity by Friedman and coworkers.[106]

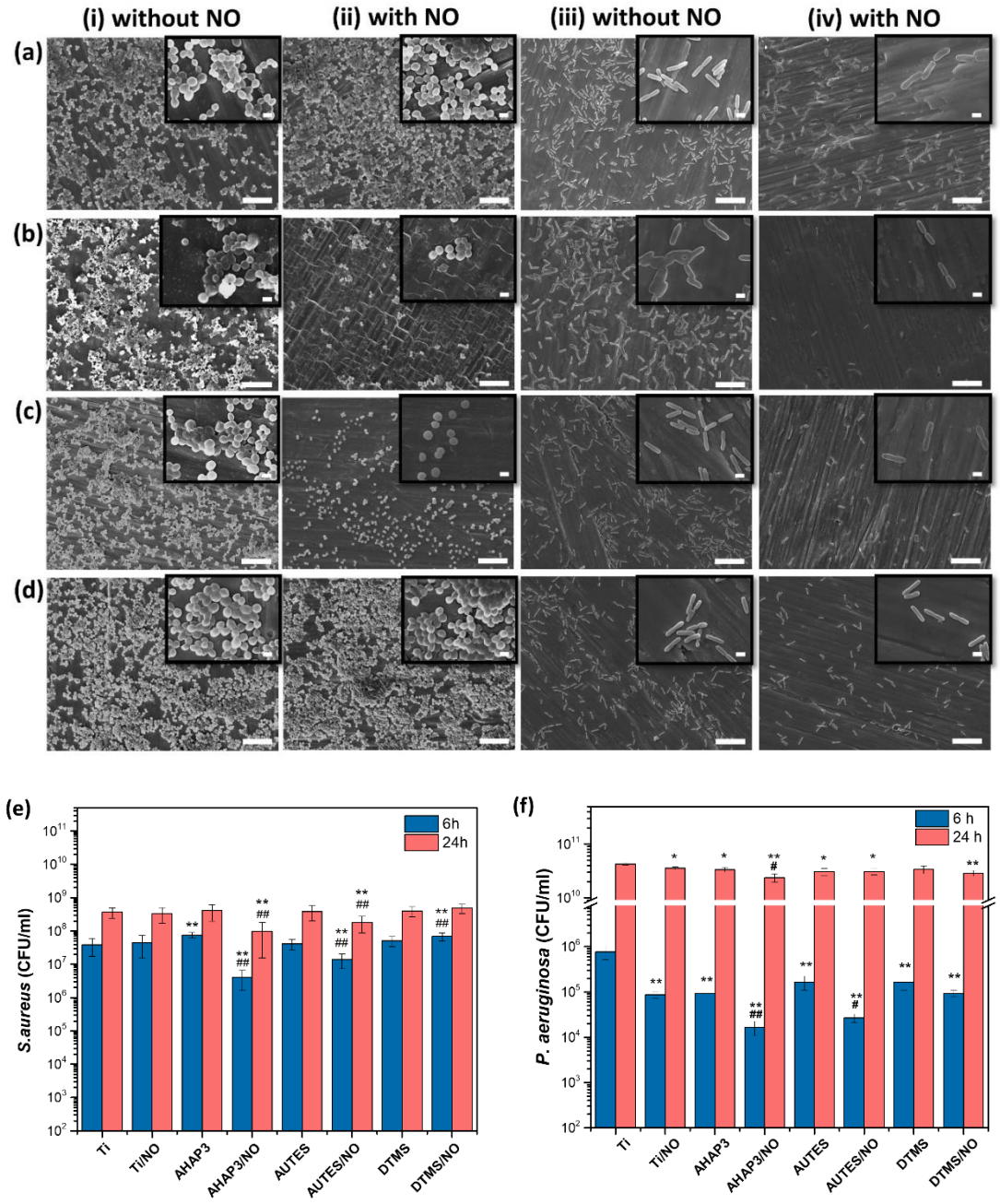

Figure 3.7: SEM images of (a(i) to d(ii)) *S. aureus* and (a(iii) to d(iv)) *P. aeruginosa* after 6 h growth on a(i and iii) Ti and (ii and iv)Ti/NO, b(i and iii) AHAP3 and (ii and iv)AHAP3/NO, c(i and iii) AUTES and (ii and iv)AUTES/NO, d(i and iii) DTMS and (ii and iv)DTMS/NO. Inserts in a-d are enlargements of the figures. The scale bar represents 10 µm and 1 µm in insets. (e) *S. aureus* and (f) *P. aeruginosa* colonies formation on

the surfaces after 6 h and 24 h incubation. * $p < 0.05$ and ** $p < 0.01$ from control, and # $p < 0.05$ and ## $p < 0.01$ from corresponding silane.

3.3.8 Cell Morphology

The morphology of human primary osteoblasts was studied on the various surfaces at 7 days post seeding using confocal laser scanning microscopy (**Figure 3.8**). As expected, the osteoblasts present on the control surfaces (pristine Ti (**Figure 3.8a(i)**) and DTMS (**Figure 3.8d(i)**) were well spread with a high contact area, a complex network of actin fibres and displayed characteristic cobblestone morphology associated with adherent functional osteoblasts. NO treatment of the control surfaces (pristine Ti (**Figure 3.8a(ii)**) and DTMS (**Figure 3.8d(ii)**) did not affect the morphology of the cells. On the AHAP3 (**Figure 3.8b(i)**) and the AUTES (**Figure 3.8c(i)**), the osteoblasts had a shrunken morphology, poor actin cytoskeletal formation and there were fewer cells. In direct comparison, qualitative analysis of the cell response to the AHAP3/NO and AUTES/NO surfaces revealed a more positive expression in terms of cell response. Qualitative analysis of these surfaces demonstrated that when cells were cultured in contact with AHAP3/NO (**Figure 3.8 b(ii)**) cells were well adhered and spread with a distinctive formation of stress fibres through the body of the cells. Cells cultured in contact with AUTES/NO (**Figure 3.8c(ii)**) demonstrated an elevated level of cell adhesion and actin formation compared to AHAP3 surfaces, and even showed formation of the characteristic cobblestone morphology that is associated with well adhered functional osteoblasts and was also apparent on the control surfaces.

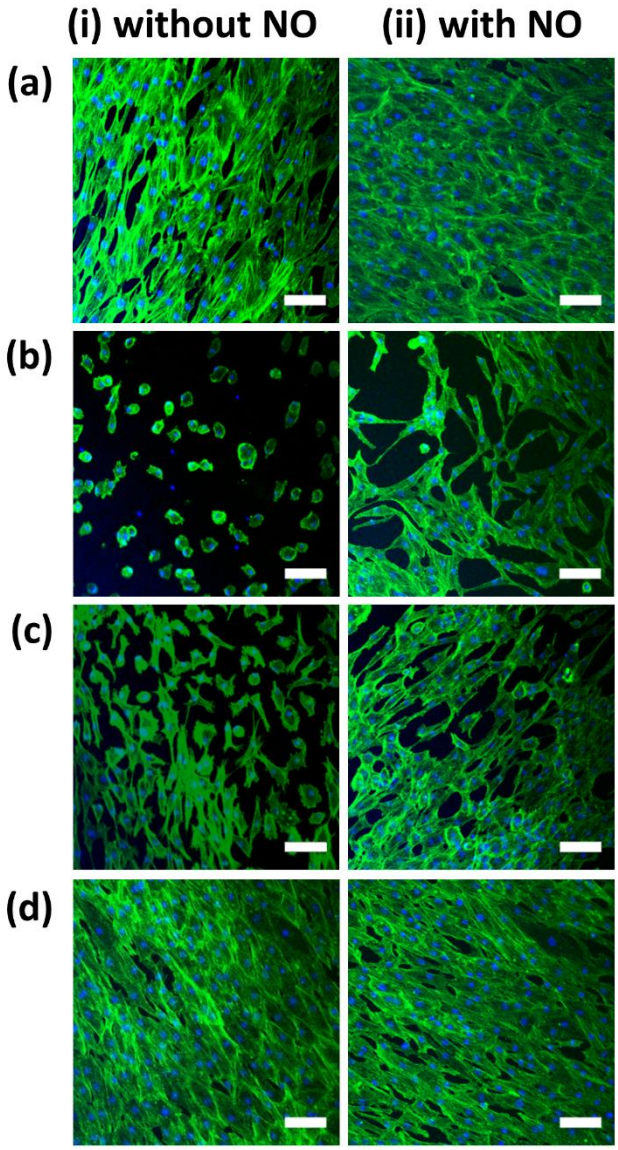

Figure 3.8 Fluorescence images of human osteoblasts spreading on a(i) Ti and (ii)Ti/NO, b(i) AHAP3 and (ii) AHAP3/NO, c(i) AUTES and (ii) AUTES/NO, d(i) DTMS and (ii) DTMS/NO after 7 days incubation. Representative images, n = 6 per group. Scale bar: 100 µm, F-actin (green) and nucleus (blue).

3.4 Conclusion

The prevention of bacterial adhesion and biofilm formation whilst promoting osteointegration remains a significant medical challenge. An efficient NO-releasing coating on Ti surfaces has been developed. A key focus of this study was to understand mechanistically how aminosilanes tether to the surface and how the nature of the aminosilane precursor affects the resultant NO releasing properties in terms of payload and release kinetics, whilst acting as an initiator for adherence and function of osteoblast cells. The ability of the variously modified surfaces to prevent biofilm formation was evaluated, with both the AHAP3/NO and AUTES/NO surfaces displaying similar antimicrobial efficacy despite having differing inherent NO loading capabilities. Of particular interest is that both AHAP3/NO and AUTES/NO surfaces were capable of prevention of biofilm formation while not displaying cytotoxicity towards human primary osteoblast cells.

Chapter 4 Antimicrobial Nitric Oxide Releasing Porous Titanium Foams

4.1 Introduction

Aseptic loosening and biomaterials related infection are the two leading causes of orthopaedic implant failure. Over 10% of implants require the second operation within 15 years of the initial surgery because of aseptic prosthesis loosening.[276] There are several unmet clinical needs pain this area that include complex bone reconstruction, large bony defects and patients with compromised bone metabolism and immune systems (for example people with bone cancers) that drive research in this area.[277] Ti and its alloys are widely for these applications, due to its good biocompatibility, mechanical property and corrosion resistance. Ti foams recently attracted more attentions, compared with Ti material itself, because of its advantage porous structures, giving better bonding strength at the implant-bone interfaces and match elastic modulus for improved osseointegration.[278-279] Porous titanium implants (foams) are promising materials for hard tissue regenerative applications as they have been proved to improve the bond between tissue and implants due to the interconnected pores which can facilitate the ingrowth of bone tissue.[280] Another advantage of using titanium foams in orthopaedic implant application is that the mechanical properties can be tailored to match the requirement of the bone defect as the mechanical properties are due to the pore size distribution and volume fraction.[281] Indeed, Yavari et al.[282] have recently shown that large surface area associated with porous titanium implants has led to an upregulation of osteogenic markers *in vitro* and has shown increased biomechanical properties *in vivo*.

Most manufacturing process used to fabricate porous metallic foams to date use additive manufacturing which requires expensive equipment. Within this chapter a novel titanium foams fabricated using a novel in house manufacturing technique and its feasibility for use for orthopaedic implants has been investigated. The Lost Carbonate Sintering (LCS) process is a representative space holder manufacturing process developed at Liverpool by Zhao et al.,[211] and is a cost-effective method used to manufacture metallic foams with highly controllable porosity, pore size and pore shape. This technique has been used for many applications in energy, aerospace and civil engineering,[212-215] but never studied in the biomedical arena. The porous metals produced by this route demonstrated mechanical properties in terms of elastic modulus and compressive strength.[211, 283]

In addition to the investigating the feasibility of using LCS manufactured titanium implants to provide materials that will demonstrate increased osteogenic function, these materials will also be modified with a surface coating to prevent implant associated infection, which is the other major cause of failure. Once bacteria adhere to an implanted biomaterial, they form biofilms which are notoriously difficult to remove and often the only solution is removal of the implant. Oral delivery of antibiotics to clear the infection is ineffective once a biofilm has formed and can be problematic given the rise in multidrug resistant bacterial.

NO, a free radical gas molecule, has been studied possessing functions in several physiological processes, including vascular relaxation, neurotransmission, immune response, wound healing, and bone remodelling.[111, 125, 284-286] NO is also part of the body's endogenous immune response to pathogens and has been heavily researched

as a broad-spectrum antimicrobial agent.[36, 94, 141, 156, 287] However, owing to the short half-life of NO, a suitable chemical donor that can control the payload and rate of delivery could make this a promising alternative to the use of antibiotics.[288] In the previous chapter, the functionalisation of flat titanium with two different aminosilanes with the subsequent tethering of diazeniumdioates onto the silanes has been studied. It has been demonstrated that the nature of the aminosilane precursors (AUTES and AHAP3) affects the resultant NO releasing properties in terms of payload and release kinetics, whilst acting as an initiator for adherence of osteoblast cells surfaces.[269] In this chapter, AUTES/NO was selected to be coating on LCS-fabricated Ti foams to understand the effects of microarchitecture on the antimicrobial efficacy. The NO payloads on Ti foams with different AUTES concentration treatment were performed by chemiluminescence at pH4. The biofilm prevention and antimicrobial activity were characterised on *E. coli* and *S. aureus* for 4 and 24 h culture.

4.2 Materials and Methods

4.2.1 Materials

Commercially pure Ti powder with an average particle size of 45 μm was purchased from Ecka Granules Metal Powder Ltd. (Wednesdbury, UK). Food grade sodium chloride (NaCl) with a particle size range of 425 – 710 μm was purchased from E&E Ltd. (Melbourne, Australia). 11-Aminoundecyltriethoxysilane (AUTES, > 95%) was purchased from Fluoro Chem. All common laboratory solvents and salts, including ethanol, acetic acid (HAc), nitric aicd (HNO_3), hydrochloric acid (HCl), disodium

phosphate and sodium acetate (NaAc), with analytic grade were from Merk KGGaA (Darmstadt, Germany) and used as received.

Sample nomenclature is as follows: (a) the clean Ti foam termed as m_Ti; (b) silanised m_Ti termed using the concentration value of AUTES in silanisation, for example m_Ti silanised in 1% concentration of AUTES termed as 1%AUTES; (c) Diazeniumdiolate functionalised samples are termed as m_Ti/NO, 1%AUTES/NO, 5%AUTES/NO, 10%AUTES/NO and 20%AUTES/NO. It should be clear here that there is no possible amine functionality on m_Ti which was used as a control group in the work, the nomenclature of m_Ti/NO is for consistency and readability.

4.2.2 Manufacturing of Ti Foams

Ti foams were obtained from Dr. Pengcheng Zhu who was using the Lost Carbonate Sintering process (LCS) as previously described by Zhao et al.[211, 215] Briefly, Ti and NaCl powders were mixed at a volume ratio of 4:6 for manufacturing porous samples with porosity of 60%. The mixture was sealed in a cylindrical steel tube, then compacted at 200 MPa by a hydraulic press and sintered at 790 °C for 4 h. A large porous Ti was obtained after removing all the NaCl particles by dissolution route in water. Then the as-produced Ti foam was cut into disc shapes, with a diameter of 6 mm and a height of 2 mm, by using an electrical discharge machine Prima E250 (ONA Ltd., Bristol, UK). The Ti foams were washed in HNO_3 and deionised water, then fully dried after autoclave sterilizing and stored in a desiccator before use. The LCS process is shown in **Figure 4.1**.

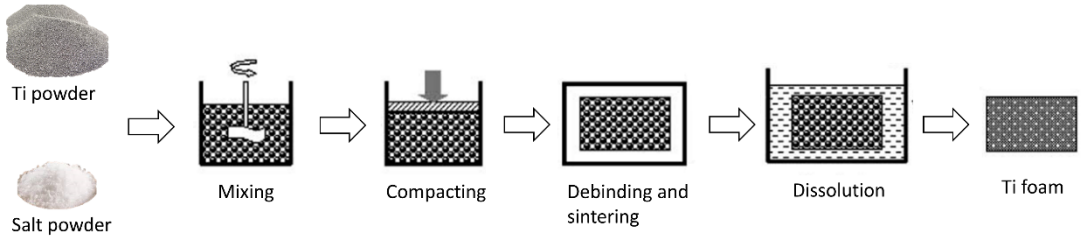

Figure 4.1: Schematic of the LCS process for manufacturing titanium foams. Image adapted from Zhao *et al*.[211] with permission from Elsevier.

4.2.3 Silanisation and Diazeniumdioate-Functionalisation

Cleaned Ti foams immersed in different concentration of 1%, 5%, 10% and 20 % (v/v) AUTES/ethanol solutions and slowly vacuumed to no bubble appeared in solution, subsequently shaken on a gyro-rocker (SSL3, Stuart) at 70 rpm for 4 h. Samples were then washed with ethanol 3 x 5 min to remove unreacted silane and cured in an oven at 80°C for another 4 h.

The treatment process of diazeniumdiolates functionalisation has been the same as described in **Chapter 3 section 3.2.3**.

4.2.4 Scanning Electron Microscopy (SEM)

The morphology of the Ti foam was examined by SEM. Sample m_Ti coated with gold by using Q150T ES sputter coater, images were subsequently captured on JSM 7001F field emission scanning electron microscope with a voltage of 10.0 kV. The energy dispersive X-ray spectroscopy (EDX) was used to characterise the elemental composition of m_Ti.

4.2.5 Brunauer-Emmett-Teller (BET)

The surface area of Ti foams was measured by Dr Pengcheng Zhu using a 3Flex 3500 gas sorption analyser at 77K.[213] m_Ti and silanised foams were degassed at 300°C under vacuum for 3 h before measurement. Each sample measured in triplicates.

4.2.6 Chemiluminescence

Nitric oxide release from Ti foams was measured using a Sievers 280i Chemiluminescence Nitric Oxide Analyser (NOA280i, GE, USA). The diazeniumdiolates functionalised samples (6 mm diameter, 2 mm thickness) were immersed in 5 ml of acetic acid buffer (pH 4) at room temperature in a three-neck round bottom flask. Nitrogen gas was continuously sparged though the buffer at a flow rate of 200 mL/min. A vacuum pump connected with the NOA is used to draw the mixed gases in to the reaction cell and maintains the pressure of the reaction cell. Nitric oxide release was measured at an interval of 1 s over more than 20 h. Each sample was measured in triplicate.

4.2.7 Antimicrobial Assays

4.2.7.1 LB Broth and Agar Plates Preparation

The LB broth and agar plates preparation have been the same as described in **Chapter 3 section 3.2.5.1**.

4.2.7.2 General Bacterial Culture

Escherichia coli (*E. coli*) ATCC 10536 and *Staphylococcus aureus* (*S. aureus*) ATCC 25923 were used to evaluate the antibacterial efficiency of the nitric oxide releasing foams. The operation has been the same as described in **Chapter 3 section 3.2.5.2**.

4.2.7.3 Biofilms Colony Forming Unit (CFU) Assay on Adhered Bacteria

The overnight cultures of *E. coli* and *S. aureus* were diluted to 1 x 10^6 CFU/mL in LB broth, according to the absorbance @600 nm and a 0.5 McFarland Standard.[289] Ti foams were placed in a 24 well-plate and 1 mL diluted bacterial solution was added to each well before incubating at 37 °C to allow bacteria growth and biofilm formation. After 4 h and 24 h incubation, foams were gently washed with PBS once to remove any unattached planktonic bacteria and then 1 mL of fresh LB broth was used to remove and re-suspend the biofilms. The bacterial CFU was determined after serial dilution of the bacterial suspension using the Miles and Misra method on LB agar plates.[271]

4.2.7.4 Antimicrobial Activity Assay on Planktonic Bacteria

The overnight cultures of *E. coli* and *S. aureus* were diluted to 1 x 10^6 CFU/mL in LB broth, according to the absorbance @600 nm and a 0.5 McFarland Standard.[289] Ti foams were placed in a 24 well-plate and 1 mL diluted bacterial solution was added to each well before incubating at 37 °C to allow bacteria growth. After 4 h and 24 h incubation, the liquids in the well-plates were removed to another aseptic well-plate and serial diluted with LB broth. The antimicrobial activity on planktonic bacteria was determined using the Miles and Misra method on LB agar plates.[271]

4.2.8 Immunofluorescence Live/Dead Assay

Bacterial cell viability was performed using Live/Dead assay kit (L3224, ThermoFisher). After 4 h incubation with bacteria, Ti foams were transferred to a new aseptic well-plate and washed with aseptic PBS to remove unattached bacteria. Removed the washing liquid and added 300 µL of combined reagent solution (includes 4 µM Ethidium homodimer-1 (EthD-1) solution and 2 µM calcein AM) into each well. Subsequently incubated the cells in dark at room temperature for 30 mins.

The images then were captured by confocal laser scanning microscopy (LSM 510, Zeiss, Germany). 3 images were taken per sample and representative images are shown. Images were processed using ImageJ 1.48 software.

4.2.9 Statistical Analysis

One-way analysis of variance (ANOVA) was used to analyse the differences among various treatment samples. The Student-Newman-Keuls (SNK) method was carried out to determine significance between treatment types. All data were collected in triplicate and displayed as Mean ± Standard Deviation. A value of $p < 0.05$ was taken as being statistically significant.

4.3 Results and Discussion

4.3.1 Characterisation of Ti Foam

4.3.1.1 Morphology and Elemental Analysis of Ti Foam

The morphology and pore structure of the titanium foams was measures using SEM, with the corresponding elemental analysis studied using EDX spectroscopy. The pore structure of the Ti foam was examined by SEM (shown in **Figure 4.2**). It can be seen clearly that the pores were distributed homogeneously in sizes of approximately 500 µm on the LCS m_Ti. Pores with sizes of 100-200 µm are also visible are found to interconnect large pores (shown in **Figure 4.2a**). This interconnectivity of pores can enable the potential tissue in-growth and vascularisation.[290-291] **Figure 4.2b** presents a magnified pore open wall region of **Figure 4.2a**, which reveals a roughed surface, as a result of the presence of the solid TiO_2 particles (in a size of ~10 µm). The microstructure of the prepared samples, containing pores with sizes from 100 to 500 µm, present the characteristics of hierarchical metallic foams, which can be used to

mimic natural bones and provide necessary supports for attachment, proliferation and differentiation of bone cells.[292-294]

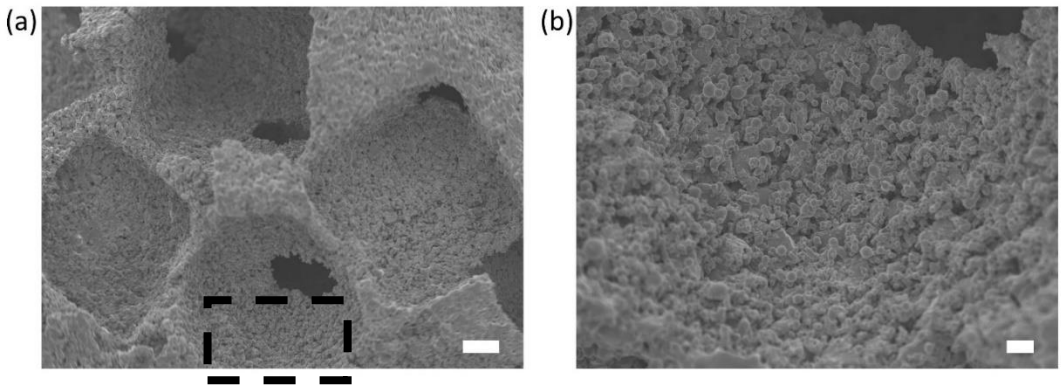

Figure 4.2: a) SEM images of the LCS m_Ti, the scale bar represents 100 µm. b) presents the dash rectangle region in a), the scale bar represents 20 µm.

The chemical analysis spectrum of m_Ti has been carried out by EDX as shown in **Figure 4.3**. Only Oxygen (O) and Titanium (Ti) elements have been detected, indicating the NaCl has been completely removed from the fabrication process. O displays weight percentage of 15.69% and atomic percentage of 35.78%. Ti displays weight percentage of 84.31% and atomic percentage of 64.22%. The atomic ratio of Ti/ O is 1.8, which is indicative of the formation of oxidation layer on m_Ti during LCS process.

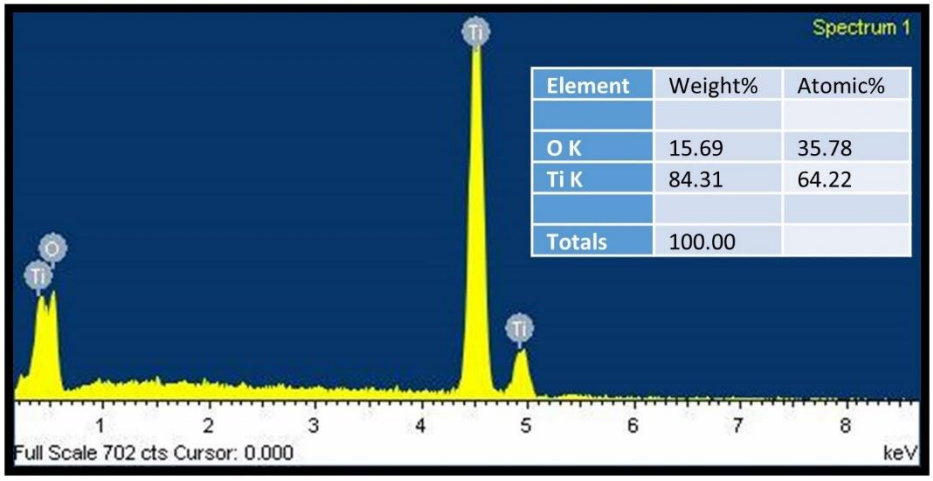

Figure 4.3: Elemental spectrum of m_Ti. The inserted table displays the element weight percentage and atomic percentage analysis on m_Ti.

4.3.1.2 Surface Area

The surface area of the Ti foams was evaluated using nitrogen adsorption isothermal analysis. The nitrogen adsorption isothermal plot of m_Ti, 5% AUTES and 20% AUTES measured at relative pressure (P/P_0), was shown in Figure 4.4. The BET surface area results were calculated based on the isotherm plot. The BET surface area of m_Ti was measured at 1.5 $m^2 g^{-1}$. The silanised samples of 5%AUTES and 20%AUTES displayed larger BET surface areas of 6.1 and 5.2 $m^2 g^{-1}$, respectively, indicating the increased silane concentration contribute to reduced surface areas.

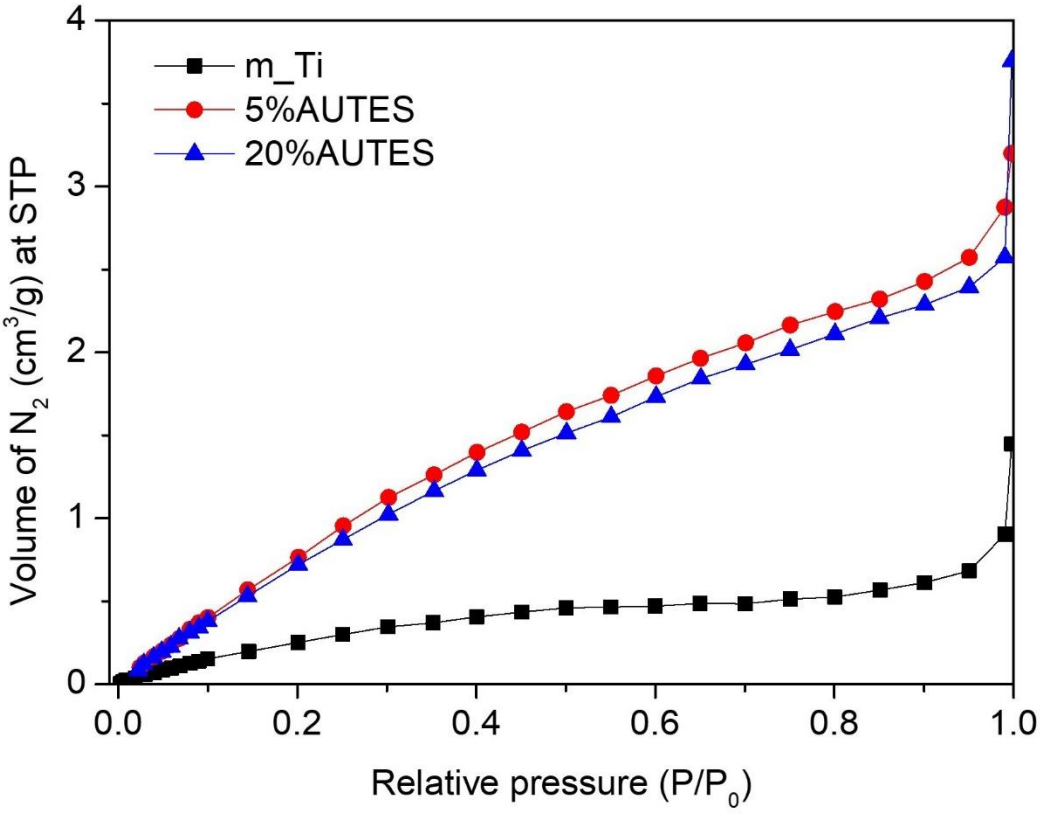

Figure 4.4: nitrogen adsorption isothermal plot of m_Ti (black, square), 5%AUTES (red, round) and 20%AUTES (blue, triangle).

4.3.2 Chemiluminescence: Measurement and Mechanism of NO Release

The NO payload from the diazeniumdiolates functionalised Ti foams was determined by using a chemiluminescence nitric oxide analyser in acetic acid buffer at pH 4. The NO releasing profiles of these Ti foams are shown in **Figure 4.5**. The kinetics of NO release, including the total concentration of NO (t[NO]), maximum instantaneous NO release concentration ($[NO]_m$), time required to reach $[NO]_m$ (t_m), and NO release duration (t_d), were determined from each modified foam, and the values are summarised in **Table 4.2**. It needs to be clarified here that the NO release profiles of the foams at pH 7.4 were not obtained due to the COVID19 lockdown.

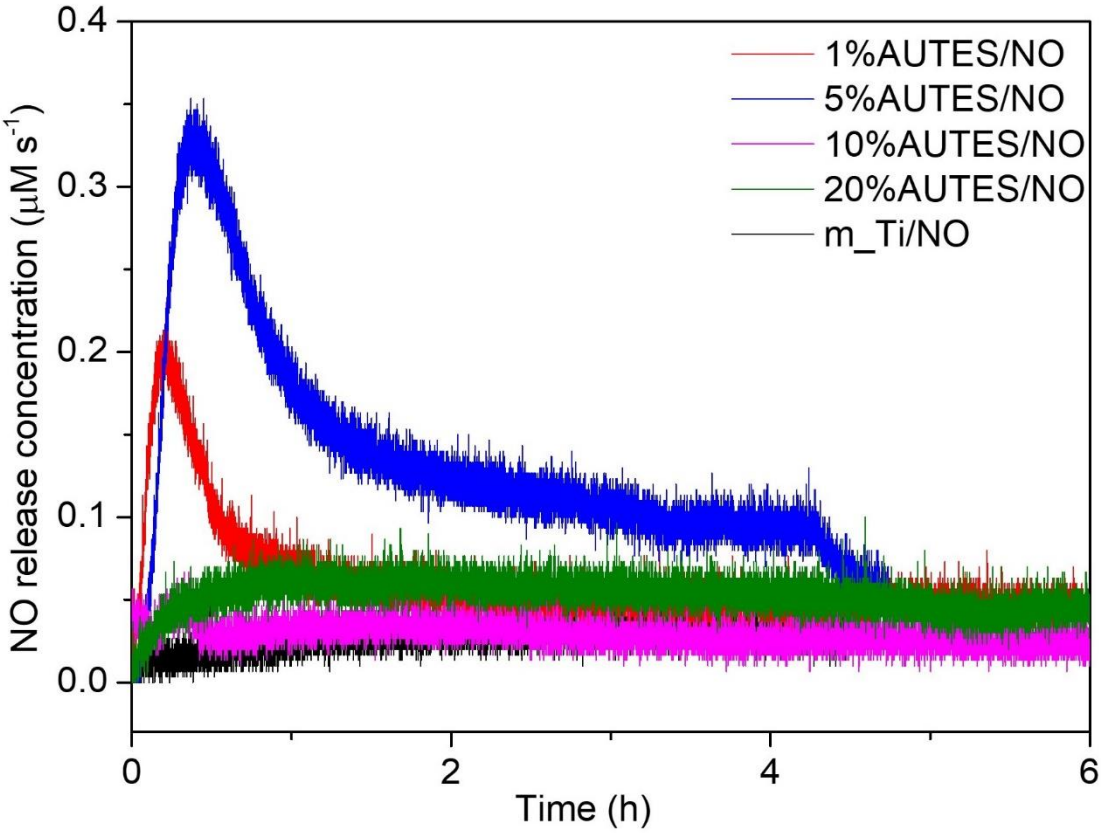

Figure 4.5: Chemiluminescence NO release profiles of diazeniumdiolates functionalised Ti foams overall 4 h at pH 4 at room temperature.

Table 4.2: Kinetic analysis of NO release Ti foams at pH 4.

pH	Sample	t[NO] (mM)	$[NO]_m$ ($\mu M \cdot s^{-1} \cdot cm^{-3}$)	t_m (min)	t_d (h)
4	1%AUTES/NO	1.2	4.0	13	6+
	5%AUTES/NO	2.3	6.2	22	5+
	10%AUTES/NO	0.9	1.1	28	10+
	20%AUTES/NO	2.0	1.5	79	14+
	m_Ti/NO	0.4	0.9	177	4+

NO release at pH 4

1%AUTES/NO release NO at a maximum instantaneous NO concentration of 4.0 $\mu M \cdot s^{-1} \cdot cm^{-3}$ at the 13 min with a total NO release concentration of 1.2 mM within 6 h.

5%AUTES/NO release NO at a maximum instantaneous NO concentration of 6.2 $\mu M \cdot s^{-1} \cdot cm^{-3}$ at the 22 min with a total NO release concentration of 2.3 mM within 5 h.

10%AUTES/NO release NO at a maximum instantaneous NO concentration of 1.1 $\mu M \cdot s^{-1} \cdot cm^{-3}$ at the 127 min with a total NO release concentration of 0.9 mM within 10 h.

20%AUTES/NO release NO at a maximum instantaneous NO concentration of 1.5 $\mu M \cdot s^{-1} \cdot cm^{-3}$ at the 79 min with a total NO release concentration of 2.0 mM within 14 h.

m_Ti/NO release NO at a maximum instantaneous NO concentration of 0.9 $\mu M \cdot s^{-1} \cdot cm^{-3}$ at the 177 min with a total NO release concentration of 0.4 mM within 16 h. As a control group, there is no amino binding site on m_Ti, therefore the NO payload measured from m_Ti/NO results from the physiosorbed NO gas molecules on m_Ti foam.

Mechanism of NO release from Ti foams

It can be seen that the Ti foams treated with different concentration of AUTES display different NO release profiles. When the concentration of AUTES was lower than 10%, all the foams display a burst release of NO., indicating a smooth fluid flow occurs in between the pores which can effectively release the NO. The NO payload of 5%AUTES/NO was of 2.3mM and is only about twice higher than that of 1%AUTES/NO with a value of 1.2mM, which theoretically supposed to be 5 times higher. This indicates that the silanisation efficiency on Ti foam is being hindered at these concentrations. The total NO payloads increased with increasing silane concentration up to 5% and then dropped when silanisation was higher than 10%. This indicates that, at these higher concentrations, multiple layers of the silane were forming which either prohibited more efficient NO loading onto the silane or resulted in blockage of the pore which prohibited effective release of NO. Interestingly however, for the 20%AUTES/NO foam a stable NO release for over 6 h is observed (as shown in **Figure**

4.5). This implies that a thick silanised layer has been formed on regions where the pores unblocked, leading to over twice higher of the NO payload of 20%AUTES/NO foam than 10%AUTES/NO foam.

Overall, the concentration of AUTES silane layer plays a key role in mediating the NO payloads and NO releasing life time. The effects of the different NO release amount and releasing period of these foams on microbiology tests will be further discussed in the following sections.

4.3.3 Antimicrobial Analysis

4.3.3.1 Biofilm Inhibition

Approximately 80% of biomaterial-associated infection in orthopaedic surgeries are caused by bacterial biofilm.[295] Therefore in this chapter, the antibiofilm response of the Ti foams has been evaluated against gram-negative *E. coli* and gram-positive *S. aureus*, which are relevant to orthopaedic implant infections.[296-297] The measurement of NO release at pH 7.4 has not been done due to COVID-19 lockdown, this will have to be done in the future. According to the previous NO release data analysis in Chapter 3, the NO release of Ti foams at pH 7.4 is assumed to follow the same trend ($t_{[NO]}$: 5% > 20% > 1% > 10%; $[NO]_m$: 5% > 1% > 20% > 10%) at pH 4 but with lower and longer releasing. The following analysis of the effects of different NO release samples on biofilm inhibition are based on this assumption.

The prevention of biofilm formation on the Ti foams has been measured by a biofilm CFU assay. All samples were incubated with bacteria for 4 and 24 h to allow the biofilm formation. The planktonic bacteria were washed off and the biofilm bacteria were then removed and counted as shown in **Figure 4.6**. NO releasing Ti foams

displayed effective antimicrobial activity against *E. coli* during the 4 and 24 h incubation periods as shown in **Figure 4.6(a)**. After 4 h incubation, compared with the control group m_Ti, sample m_Ti/NO presented ~0.5-log reduction on biofilm formation, 1%AUTES/NO presented ~1-log reduction, 5%AUTES/NO had the reduction at 1.6-log, while 10%AUTES/NO and 20%AUTES/NO showed ~0.6-log reduction. After 24 h incubation, control foams without NO have displayed significant number of colonies. All the AUTES/NO foams presented efficient biofilm prevention, which was shown as more than 2.4-log reduction (compared to m_Ti) and 0.9-log reduction (compared to m_Ti/NO), after 24 h incubation.

NO release Ti foams also displayed effective antimicrobial activity against *S. aureus* during the 4 and 24 h incubation periods as shown in **Figure 4.6(b)**. After 4 h incubation, compared with the control group m_Ti, sample m_Ti/NO presented ~2.4-log reduction on biofilm formation, 1%AUTES/NO presented ~1.5-log reduction, 5%AUTES/NO had 1.7-log reduction, 10%AUTES/NO displayed the largest reduction at ~1.9-log, and 20%AUTES/NO showed ~1.4-log reduction of biofilm formation. After 24 h incubation, control Ti foams without NO releasing have displayed significant number of colonies. All the AUTES/NO foams presented efficient biofilm prevention, with more than 2.2-log reduction (compared to m_Ti), after 24 h incubation. It should be noted that due to the lockdown, *S. aureus* biofilm CFU assay has been done for only one run. Hence not enough data for its analysis here. But it is predicted to have more biofilm prevention than *E. coli*, because the adhesion of *S. aureus* has displayed to be more susceptible than *E. coli* to NO release environment.[298-299]

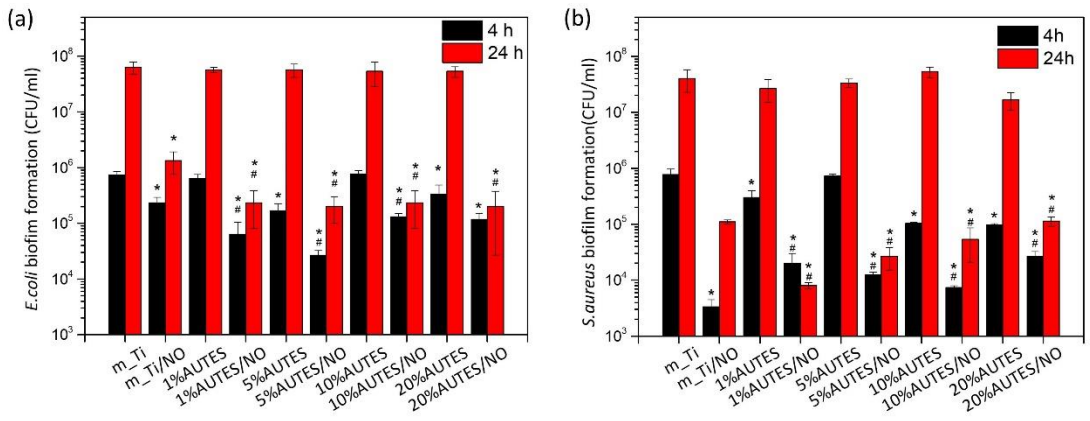

Figure 4.6: a) *E. coli* and b) *S. aureus* colonies formation on the NO release Ti foams after 4 and 24 h incubation. *p < 0.05 from control; #p <0.05 from the corresponding silane concentration with no diazeniumdiolates functionalisation. (NOTE: two runs on *E. coli* and one run on *S. aureus* have been done here)

The measurement of NO release at pH 7.4 has not been done due to COVID-19 lockdown, this will have to be done in the future. According to the previous NO release data analysis in Chapter 3, the NO release of Ti foams at pH 7.4 is assumed to follow the same trend (t[NO]: 5% > 20% > 1% > 10%; $[NO]_m$: 5% > 1% > 20% > 10%) at pH 4 but with lower and longer releasing. Based on this assumption, the prevention of biofilm formation on AUTES/NO foams is in agreement with the NO releasing profile. 1%AUTES/NO and 5%AUTES/NO displayed notably high burst NO release within the first half hour, implying the burst NO release efficiently kill *E. coli* at an early stage. Although 10%AUTES/NO displayed a long release last, the low $[NO]_m$ during the burst might not sufficient in killing *E. coli*.

It is of significantly interest that all AUTES/NO foams showed more than 2.4-log reduction of *E. coli* and *S. aureus* biofilm bacteria (after 24 h incubation. When comparing these results to the flat Ti samples in Chapter 3, the increased surface area from the Ti foam micro structure allows for a higher payload of NO, allowing for increased antimicrobial efficacy. This coupled with the increased potential for the porous scaffold to integrate, make these materials ideal for antimicrobial orthopaedic applications.

4.3.3.2 Antimicrobial Activity on Planktonic Bacteria

Planktonic bacteria play a key role in prevention of biofilm formation because it can freely attach onto the rest regimes of the implants in liquid environment. Bacteria cells are able to highly regulated alternate between the biofilm and the planktonic phase in their life cycles.[300] Therefore, the antimicrobial capacity of the NO release foams has been investigated and analysed using colonies formation assays, with results as shown in **Figure 4.7**. The measurement of NO release at pH 7.4 has not been done due to COVID-19 lockdown, this will have to be done in the future. According to the previous NO release data analysis in Chapter 3, the NO release of Ti foams at pH 7.4 is assumed to follow the same trend (t[NO]: 5% > 20% > 1% > 10%; $[NO]_m$: 5% > 1% > 20% > 10%) at pH 4 but with lower and longer releasing. The following analysis of planktonic bacterial growth inhibition are also based on this assumption.

NO release Ti foams displayed effective antimicrobial activity on planktonic *E. coli* during the 4 and 24 h incubation periods as shown in **Figure 4.7(a)**. After 4 h incubation, compared with the control group m_Ti, sample m_Ti/NO didn't presented significantly different reduction on planktonic *E. coli* proliferation, sample

1%AUTES/NO presented ~0.8-log reduction, sample 5%AUTES/NO had 0.6-log reduction, 10%AUTES/NO displayed 1.1-log reduction and 20%AUTES/NO showed no significantly different reduction on planktonic *E. coli* growth. After 24 h incubation, due to the fast recovery growth of *E. coli*, foams those without NO releasing have displayed significant number of colonies. All the AUTES/NO foams presented efficient prevention of planktonic *E. coli* growth. Furthermore, 5%AUTES/NO showed the highest prevention with 2.5-log and 1.2-log, respectively compared to m_Ti and m_Ti/NO, after 24 h.

NO release Ti foams also displayed effective antimicrobial activity on *S. aureus* during the 4 and 24 h incubation periods as shown in **Figure 4.7(b)**. After 4 h incubation, compared with the control group m_Ti, sample m_Ti/NO presented no significantly different reduction on planktonic *S. aureus* growth, sample 5%AUTES/NO had 1.1-log reduction which is the largest, while sample 1%AUTES/NO, sample 10%AUTES/NO and 20%AUTES/NO showed ~0.9-log reduction. After 24 h incubation, due to the fast recovery growth of bacteria, foams those without NO releasing have displayed significant number of colonies. 1%AUTES/NO and 5%AUTES/NO showed ~1 log reduction (compared to m_Ti) after 24 h incubation.

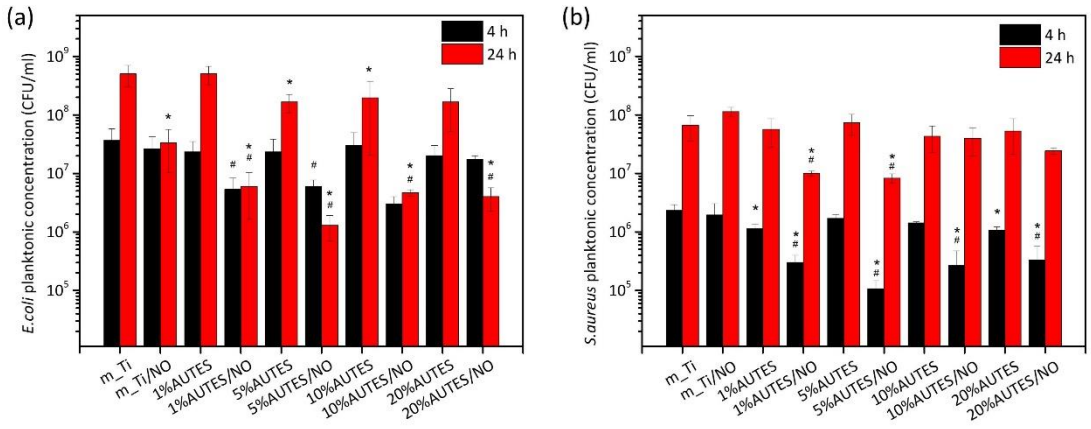

Figure 4.7: Planktonic a) *E. coli* and b) *S. aureus* colonies formation on the NO release Ti foams after 4 and 24 h incubation. *p < 0.05 from control; #p <0.05 from the corresponding silane concentration with no diazeniumdiolates functionalisation. (NOTE: two runs on both bacteria have been done here)

AUTES/NO foams displayed good growth inhibition against both planktonic *E. coli* and *S. aureus* in 4 and 24 h incubation time points. It can be seen that planktonic *E. coli* showed highly sensitive to NO released from the foams in the long-term incubation, which is corresponding to the NO releasing kinetic of AUTES/NO foams. In addition, planktonic *S. aureus* growth has been notably inhibited in 4 h incubation and around 1 log reduction (99% inhibition) after 24 h. Once again these, experiments need the necessary third set of repeats to confirm the trend.

4.3.3.3 Bacterial Cell Viability

Confocal microscopy was used to evaluate the effect of NO releasing from the foams on bacterial cell viability in 4 h culture. *E. coli* and *S. aureus* were stained with Live/Dead assays, where live and dead cells display green and red, respectively, with results shown in **Figure 4.8**. 1%AUTES/NO and 5%AUTES/NO, which displayed excellent biofilm prevention and planktonic bacterial growth inhibition, were selected to use in the test. m_Ti and m_Ti/NO were used as control groups.

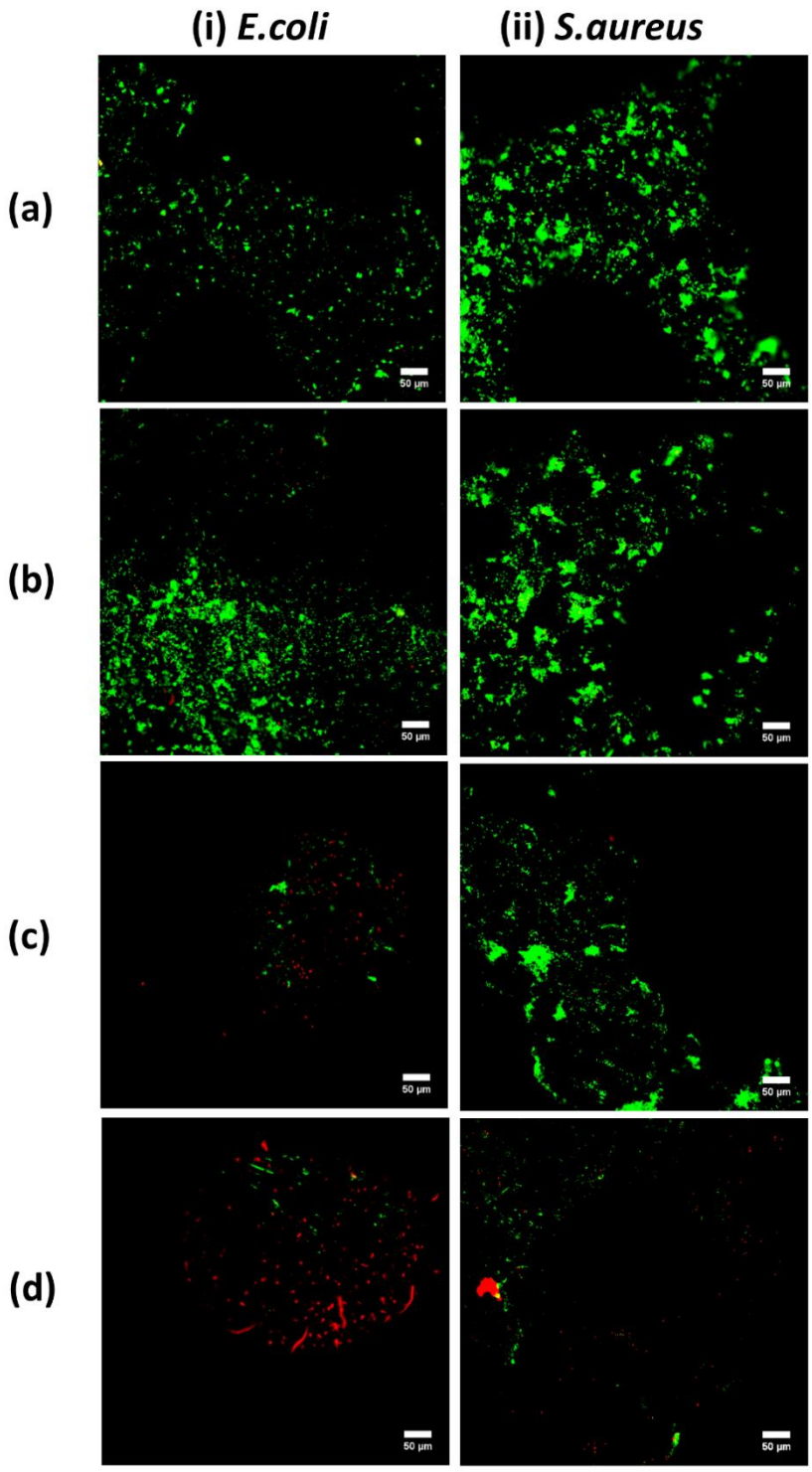

Figure 4.8: Fluorescence images of live/dead i) *E. coli* and ii) *S. aureus* on a) m_Ti, b) m_Ti/NO, c) 1%AUTES/NO and d) 5%AUTES/NO after 4 h incubation. Representative images, n=3 random spots per sample. Scale bar: 50 µm. Live bacteria: green, dead bacteria: red.

Cultures with m_Ti and m_Ti/NO (**Figure 4.8 a(i) and b(i)**) showed mainly live *E. coli* and exhibited fewer dead cells, compared with 1%AUTES/NO (**Figure 4.8 c(i)**) and 5%AUTES/NO (**Figure 4.8 d(i)**). It can be seen that with the increase of the silanisation concentration, leading to a higher NO payload contributes to the higher killing efficacy of the bacteria and the presentation of more dead cells (red stains) on 1%AUTES/NO and 5%AUTES/NO. These results are in corroboration with that of the biofilm and planktonic experiments given above.

m_Ti and m_Ti/NO (**Figure 4.8 a(ii) and b(ii)**) presented numerous live *S. aureus* on surfaces, while fewer live cells were seen on 1%AUTES/NO (not significantly less, **Figure 4.8 c(ii)**). On 5%AUTES/NO (**Figure 4.8 d(ii)**), more dispersed dead *S. aureus* (red) and less live *S. aureus* (green) cells were captured, implying the 5%AUTES/NO foam reduced cell viability of the attached *S. aureus*.

4.4 Conclusion

In this chapter, Ti foams have been fabricated with a novel LCS process to determine the feasibility of using this manufacturing technique for the fabrication of antimicrobial bone integrating implants. The best antimicrobial coating from the previous chapter has been selected and used to study the antimicrobial efficacy of the Ti foams with various concentration of the silane layer. NO releasing foams displayed high instantaneous NO release and steady long-term release when the concentration of silane is < 5%. The inhibition to the biofilm and planktonic bacterial growth correspond to the efficient releasing period and the instantaneous NO concentration of the NO release foams. Future work on this project will focus on determining the osteogenic potential of these scaffolds.

Chapter 5 Fabrication and Characterisation of Antimicrobial Guided Bone Regeneration (GBR) Electrospun Membranes

5.1 Introduction

Reconstruction of bone defects that are a result of trauma, infection, tumour resection or congenital malformations remain challenging in orthopaedic clinical practices.[301-302] Although human bone tissue has self-healing potential, the regeneration of osseous defects is often hindered by the invasion of non-functional soft tissue generated by the penetration of fibrous or epithelial tissue.[303] Guided Bone Regeneration (GBR) has been established as an effective therapy to circumvent this problem by using porous membranes that can simultaneously act as a physical barrier to prevent the ingrowth of fibrous tissue, whilst allowing for active tissue regeneration.[181, 304-305] The efficacy of the GBR approach depends on a few factors: the membranes should be flexible enough to overlay the tissue defect, provide the appropriate mechanical properties and degradation profile and mimic the natural extracellular matrix (ECM) in order to allow for cell adhesion and proliferation which can eliminate the need for surgical removal.[306-309]

Electrospinning is a promising technique for the fabrication of GBR membrane with notable advantages, including the availability of a wide range of polymers, the ability to control the diameter and alignment of fibres, space maintenance, high porosity, malleability and multifunctionality of the produced membranes.[236, 309-311] Many studies have investigated electrospun membranes fabricated from a combination of two or more ingredients, such as bioactive glass/polycaprolactone (PCL),[247, 312] poly(L-lactide) (PLLA)/chitosan[313] and collagen/chitosan/polyurethane (TPU) membrane,[314] with the purpose of achieving higher osteoconductivity, better

biodegradation and fitted mechanical properties that are not available in a single component. Although electrospun PCL membranes are used extensively for bone regeneration applications due to their excellent mechanical properties, its inherently high hydrophobicity prohibits proactive biological responses such as cell adhesion, migration, proliferation and differentiation.[315] Gelatine, a natural biopolymer derived from collagen, has good biocompatibility, non-immunogenicity, but low mechanical strength and fast degradation.[316] Hence, the combination of PCL/gelatine electrospun membranes can offer advantages of both polymers: mechanical strength, degradation and biocompatibility.

While tissue regeneration via GBR may be effective, potential implant failure can occur due to bacterial infections. Conventional treatment of these infections can include either systemic or localised delivery of antibiotics, which is problematic given the current rise in multidrug resistant bacteria. Thus, there is an urgent need to tackle infection with novel antimicrobials that do not lead to antimicrobial resistance, whilst allowing for active tissue regeneration. Nitric oxide (NO), is a promising alternative to antibiotics as it has shown potent antibacterial activity and will not lead to the development of antimicrobial resistance in bacteria due to the several pathways of inactivation.[287, 317] It has been previously demonstrated that *N*-diazeniumdiolates are an effective and versatile NO donor that can be easily tethered onto amino-functional groups that are capable of spontaneously releasing NO under physiological conditions.[36, 141]

This chapter reports on the fabrication of electrospun PCL/gelatine membranes tethered with the antimicrobial NO to allow for active GBR, whilst simultaneously

preventing infection. Electrospun nanofibrous membranes were first prepared by varying the ratios of PCL and gelatine. The composite membranes were then crosslinked with genipin a natural nontoxic agent which demonstrates lower cellular toxicity than the traditional crosslinking agents such as glutaraldehyde[318] and EDC/NHS.[319] This chapter is to study (i) modulation of the fibre morphology and NO payload profile of the membrane by varying the ratio of PCL:gelatine and the degree of crosslinking and (ii) decrease of bacterial adhesion by tethering of NO onto the membranes.

5.2 Materials and Methods

5.2.1 Materials

2, 2, 2-trifluoroethanol (TFE) solvent, gelatine (GT) (gel strength 300 g Bloom, Type A), Poly(*ε*-caprolactone) (PCL) (M_n: 80, 000 g·mol^{-1}), genipin (≥98%), Luria-Bertani (LB) broth and agar were purchased from Merk KGaA (Darmstadt, Germany) and used as received. All common, analytical grade laboratory solvents and salts, including ethanol, acetic acid (HAc), hydrochloric acid (HCl), disodium phosphate and sodium acetate (NaAc), were from Merk KGaA (Darmstadt, Germany) and used as received. The chemical structures of the selected polymers for electrospinning and the crosslinking agent are shown in **Figure 5.1**.

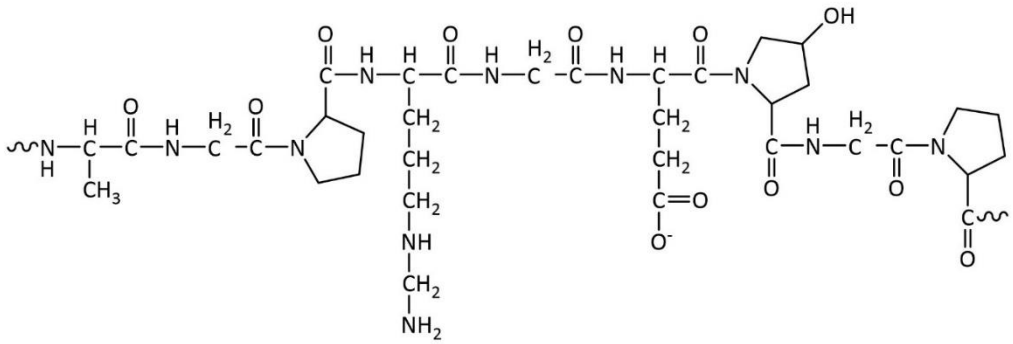

(A)

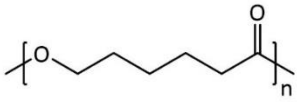

(B)

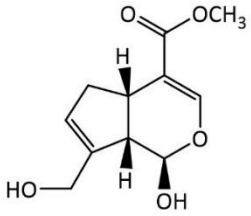

(C)

Figure 5.1: Chemical structure of selected polymers and crosslinker. (A): Gelatine (GT); (B): Poly(*ε*-caprolactone) (PCL); (C): Genipin.

Sample nomenclature is as follows: (a) In the liquid phase, solutions only containing PCL are termed as PCL; solutions only containing GT are termed as GT; solution containing PCL: GT termed as both shorts with numbers, for example, mixed solution with a PCL: GT mass ratio of 75:25 termed as P75G25. (b) For electrospun samples, use the same nomenclature as in (a). (c) The crosslinked samples, for example, crosslinked P75G25 is termed as c_P75G25. (d) Diazeniumdiolate functionalised samples are termed as PCL/NO, GT/NO, P25G75/NO, P50G50/NO, P75G25/NO, c_PCL/NO, c_GT/NO, c_P25G75/NO, c_P50G50/NO and c_P75G25/NO. Summarised in **Table 5.1**.

Table 5.1: Ingredients of the electrospun membranes and the usage of crosslinking agent.

Sample	*PCL/ wt%*	*Gelatine/ wt%*	*Genipin*
PCL	100	0	-
P75G25	75	25	-
P50G50	50	50	-
P25G75	25	75	-
GT	0	100	-
c_PCL	100	0	+
c_P75G25	75	25	+
c_P50G50	50	50	+
c_P25G75	25	75	+
c_GT	0	100	+

5.2.2 Electrospinning Solution Preparation

The polymer solutions of PCL and GT were prepared separately in TFE (10 % wt) by stirring at room temperature. After both polymers were dissolved completely in the solvent, the two solutions were blended at weight ratios (PCL solution: GT solution) of 75:25, 50:50 and 25:75. The mixture was turbid as a result of the phase separation of PCL and GT. Therefore, a few drops of HAc were added to the solution followed by further stirring (4 h) in order to obtain a homogenous PCL/GT solution for electrospinning.[320] The required amount of added HAc in reducing the phase separation was determined by measuring the light transmittance (%) of 5 ml P50G50 solution with a UV-vis spectrophotometer at a wavelength range from 400-800 nm after adding specific volumes of HAc.

5.2.3 Electrospinning

The parameters used in this chapter were based on a previous research.[320] The flow rate was subsequently optimised to produce beads-free fibres on an electrospinner (IME, Waalre, Netherland). After stirring for 4 h, polymer solutions were transferred into a 5 ml plastic syringe fitted with a blunt-ended needle (diameter of 0.4 mm, reciprocating motion speed of 10 mm/s over a distance of 50 mm) and the polymer solution flow rate was set to of 2 ml/h. A cylindrical grounded mandrel (diameter = 90 mm, height = 180 mm), coated with aluminium foil, at a distance of 185 mm away from the needle tip rotated at 200 RPM. A high voltage of 20 kV was applied between the needle and the collector. Membranes were collected after electrospinning for 120±10 mins in a climate control system with a relative humidity of 70% and temperature of 23 °C. The collected membranes were dried in the fume hood in air for 7 days to remove any remaining solvent.

The electrospun scaffolds were crosslinked for 24 h by immersion in 2% (*w*/*v*) genipin/ethanol solution. After crosslinking, these scaffolds were washed with ethanol 3 x 5 mins to remove residual genipin. The crosslinked scaffolds were dried in vacuum for 3 days to eliminate any leftover solvent. All the scaffolds were stored in a vacuum desiccator covered with foil until use to prevent degradation.

5.2.4 Synthesis of NO-Releasing Electrospun Membranes

Electrospun membranes were functionalised with diazeniumdiolates in an in-house built stainless-steel NO reactor as previously reported.[141] Briefly, the reactor chamber was purged with 6 bar argon (BOC, Guildford, UK) for 5 mins (3 x) and 10 mins (3 x) to remove atmospheric oxygen and water. Then nitric oxide (NO) (BOC, Guildford, UK) was introduced into the reactor at 5 bar for 3 days. At the end of this time, residual NO was removed by flushing the chamber with 6 bar argon for 5 mins (2 x) and 10 mins (2 x). Diazeniumdiolate functionalised membranes were then stored at -20°C until use. It should be noted that as PCL does not possess any amine functionality, there is no possibility of forming *N*-diazeniumdiolates, and as such it is the control group in NO release tests. The nomenclature is kept as PCL/NO for consistency and ease of readership.

5.2.5 Scanning Electron Microscopy (SEM)

The morphology of the fibres was examined by SEM. Membranes firstly were cut into 10 x 10 mm^2 and coated with gold by using Q150T ES sputter coater. Images were captured on a JSM 7001F field emission scanning electron microscope with a voltage of 10.0 kV. The diameter analysis of the fibres was performed by randomly picking up 20 fibres from each material enlargement SEM images and measuring in Image J.

5.2.6 Contact Angle

Surface wettability was determined by measuring static contact angles with Attension ThetaLite. The sessile drop method was used and contact angle measurement images were taken using OneAttension software (Biolin Scientific, Västra Frölunda, Sweden). The image began to be captured from when the drop contacted with the surfaces and was continuously captured for 10 seconds. All membranes were measured in triplicates.

5.2.7 Fourier-transform Infrared Spectroscopy (FTIR)

The FTIR spectra of the electrospun membranes was analysed using a PerkinElmer frontier IR system over the range of 500-4000 cm^{-1} at a scanning resolution of 4 cm^{-1}.

5.2.8 Chemiluminescence

Nitric oxide release from membranes was measured using a Sievers 280i Chemiluminescence Nitric Oxide Analyser (NOA280i, GE, USA). The diazeniumdiolate functionalised samples (10 x10 mm^2) were immersed in 5 ml of acetic acid buffer (pH 4) or phosphate buffered saline (PBS; pH 7.4) at room temperature in a three-neck round bottom flask. Nitrogen gas was continuously passed through the headspace of the vessel to bubble the buffer at a flow rate of 200 mL/min. A vacuum pump connected with the NOA was used to draw the mixed gases in to the reaction cell and maintain the pressure of the reaction cell. Nitric oxide release was measured at intervals of 1 s over more than 16 h. Each sample was measured in triplicate.

5.2.9 Antimicrobial Assays

5.2.9.1 LB Broth and Agar Plates Preparation

The LB broth and agar plates preparation have been the same as described in **Chapter 3 section 3.2.5.1**.

5.2.9.2 General Bacterial Culture

Escherichia coli (*E. coli*) ATCC 10536 and *Staphylococcus aureus* (*S. aureus*) ATCC 25923 were used to evaluate the antibacterial efficacy of the nitric oxide releasing membranes. The operation has been the same as described in **Chapter 3 section 3.2.5.2**.

5.2.9.3 Biofilms Colony Forming Unit (CFU) Assay on Adhered Bacteria

The overnight cultures of *E. coli* and *S. aureus* were diluted to 1 x 10^6 CFU/mL in LB broth, according to the absorbance @600 nm and a 0.5 McFarland Standard.[289] Membranes (cut into 10 x 10 mm^2) were placed in a 24 well-plate and 1 mL of diluted bacterial solution was added to each well before incubating at 37 °C to allow bacterial growth and biofilm formation. After 4 h incubation, membranes were gently washed with PBS once to remove any unattached planktonic bacteria and then 1 mL of fresh LB broth was used to remove and re-suspend the biofilms. The bacterial CFU was determined after serial dilution of the bacterial suspension using the Miles and Misra method on LB agar plates.[271]

5.2.9.4 Antimicrobial Activity Assay on Planktonic Bacteria

The overnight cultures of *E. coli* and *S. aureus* were diluted to 1 x 10^6 CFU/mL in LB broth, according to the absorbance @600 nm and a 0.5 McFarland Standard.[289] Membranes (cut into 10 x 10 mm^2) were placed in a 24 well-plate and 1 mL of diluted bacterial solution was added to each well before incubating at 37 °C to allow bacterial

growth. After 4 h incubation, the liquids in the well-plates were removed to another aseptic well-plate and serially diluted with LB broth. The antimicrobial activity against planktonic bacteria was determined using the Miles and Misra method on LB agar plates.[271]

5.2.10 Statistical Analysis

One-way analysis of variance (ANOVA) was used to analyse the differences among various treatment samples. The Student-Newman-Keuls (SNK) method was carried out to determine significance between treatment types. All data were collected in triplicate and displayed as Mean ± Standard Deviation. A value of $p < 0.05$ was taken as being statistically significant.

5.3 Results and Discussion

5.3.1 Phase Separation of Electrospinning Solutions

5.3.1.1 Preparation of Solutions

In this chapter, composite PCL/gelatine fibrous membranes with 5 different ratios were fabricated by electrospinning under consistent parameters such as voltage, flow rate, needle collector distance and humidity. Fabrication of consistent nanofibrous membranes was challenging given that phase separation occurs as gelatine is a hydrophilic polymer and dissolves easily in water and PCL is a hydrophobic polymer preferring organic solvents.[321]

TFE was used as a solvent to dissolve PCL and GT to form transparent solutions. The 5 different ratios of polymers, with mass ratios of PCL:GT at 100:0, 75:25, 50:50, 25:75 and 0:100, displayed different phase separation behaviours, depending on the relative proportions of the two polymer components (**Figure 5.2**). It is commonly

observed that the interaction between the two polymer chains with each other can lead to phase separation behaviour.[322-324] In this chapter, it was found that the mixed PCL and GT solutions become opaque and gradually separate into two phases after a period of time. Qualitative observation of the 3 mixed solutions, showed that P75G25 had the least phase separation in comparison to P5050 and P25G75 (**Figure 5.2**). There was a clear phase separation interface in both P50G50 and P25G75 solutions, with greater amounts of precipitate being observed after 24 h as the gelatine concentration was increased.

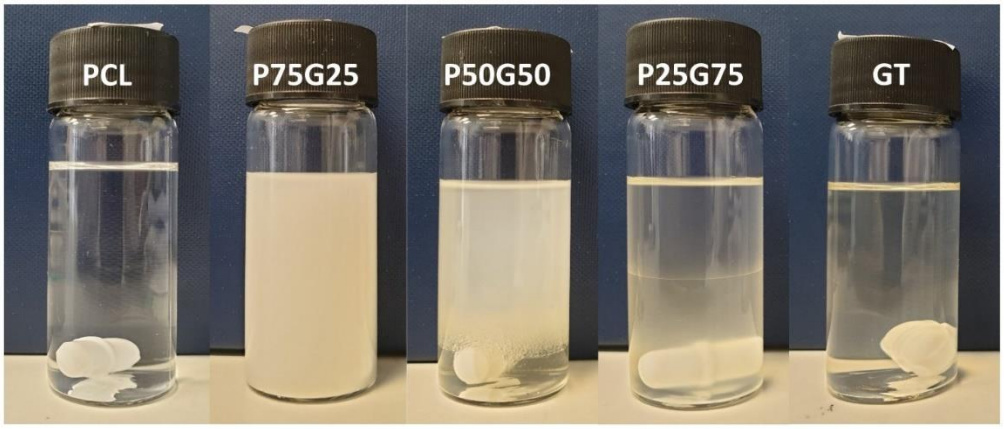

Figure 5.2: Photographs of the PCL:GT solutions (mass ratios of 100:0, 75:25, 50:50, 25:75 and 0:100) after being rested for 24 h at room temperature.

The solution P50G50 was left to rest for selected time periods over a 24 h interval (**Figure 5.3**). The turbidity of the mixture solution lasted for more than 6 h and a clear separation interface appeared after 24 h. This was important to observe as the electrospinning process takes place over a few hours, and as such any phase separation could most likely affect quality and the consistency of the fibres.

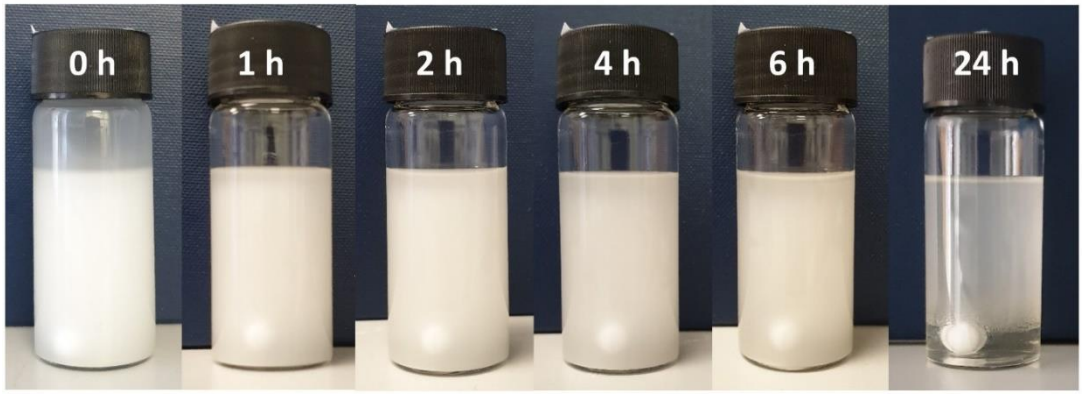

Figure 5.3: Photographs of the PCL:GT solutions at a mass ratio of 50:50 after being rested for the selected time periods (0, 1, 2, 4, 6 and 24 h) at room temperature.

5.3.1.2 Acetic-Acid Mediated Solutions

Acetic acid (HAc) was used to mitigate the effect of phase separation caused by the immiscibility of the polymer chains. Upon addition of HAc (20 µl), the PCL/GT solutions turned transparent and clear after stirring. There was no observed turbidity in solution after 1-week storage in a glass vial. The turbidity measured in terms of the light transmittance of the P50G50 solutions was observed to be mediated with different amounts of HAc (10 - 30 µl) as seen in **Figure 5.4**. The transmittance percentage of P50G50 was close to 0, due to the opacity of the mixed solution. With the increasing amount of HAc, P50G50 solution displayed higher transmittance, due to the increasing miscibility between PCL and GT polymer chains.

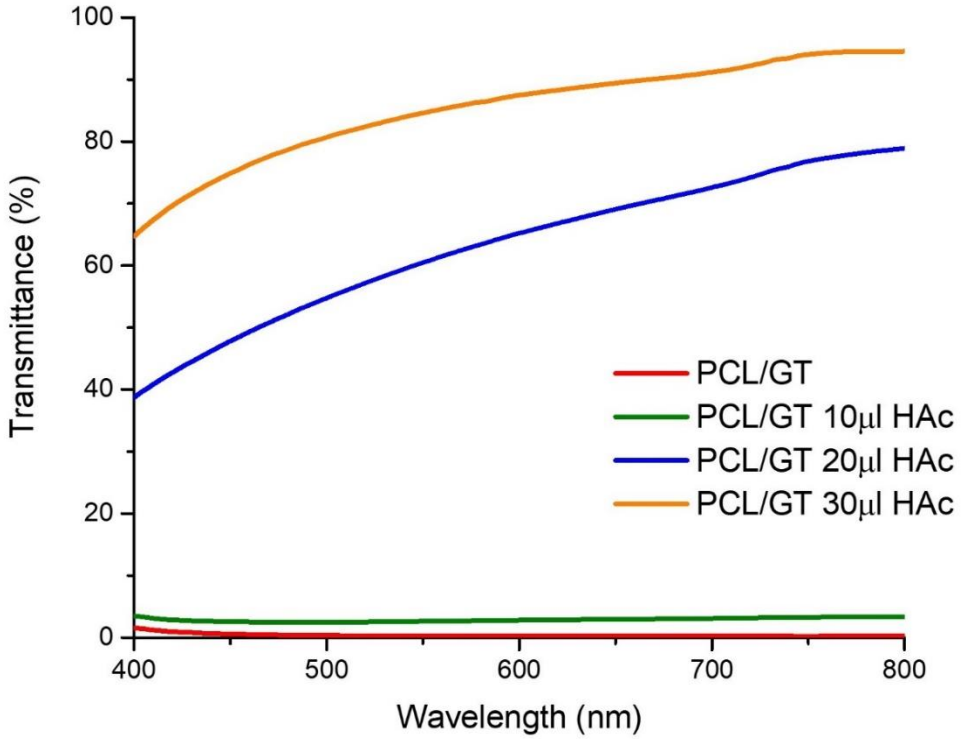

Figure 5.4: Light transmittance of the PCL/GT solution with a mass ratio of 50:50 before and after acetic acid mediating.

PCL and GT are inherently immiscible polymers and given that there is a sol-gel transition of GT, a mixture of these two polymers will result in the opacity of the solution, followed by gradual separation of the layers as seen in **Figure 5.2**. GT is known to its lowest solubility in mixture solution and therefore precipitate at its isoelectric point (IEP).[325-326] A change in pH by the addition of small amounts of HAc will move the pH of the solution away from the IEP. This will prevent the sol-gel transition of gelatine an make it more soluble in the mixture. This phase separation

behaviour also has been previously observed by others.[321, 327-328] The introduction of small amounts of acetic acid (0.2~0.6% v/v of TFE) increased the transmittance of the turbid mixture solution of P50G50. Therefore, an acetic acid mediated system has been utilised to achieve a lower pH value of the mixture solution than its IEP, resulting in effective reduction of the sol-gel transition. Moreover, at more acidic pH the amino groups in GT are more positively charged and therefore repel each other allowing for more entanglement with the PCL chains.[329]

5.3.2 Characterisation of Electrospun Fibres

5.3.2.1 Morphology of Fibres

The well dispersed PCL/GT solutions with different mass ratios of PCL and GT were electrospun successfully to obtain bead-free fibrous membranes (shown in **Figure 5.5 i)**. These electrospun fibres containing PCL were smooth. The average diameter of the fibres ranged from 0.7-1.2 μm (shown in **Table 5.2**). The diameter of the fibres was dependent on the ratios of the polymers to each other, with an increasing concentration of GT resulting in smaller fibre diameters. The pure GT samples (**Figure 5.5 i**) displayed agglutination between fibres. This agglutination can be explained by the fact that the electrospinning process can be a lengthy process which can result in the GT-induced phase separation, thereby affecting the fibre structure.

The SEM micrographs of the genipin-crosslinked nanofibrous membranes are shown in **Figure 5.5 ii**. The same trend in the fibre diameters (displayed in **Table 5.2**) of the non-crosslinked samples was seen once again; the samples with increasing ratios of GT displayed smaller fibres overall. There is no significant difference in the diameter of the fibres after crosslinking by genipin. Of high interest is that the c_GT fibrous membranes displayed less agglutinating when compared with the pre-crosslinking

GT. One explanation for this observation is that the genipin might slightly change the surface hydrophilicity of the GT membranes, resulting in the slower moisture absorbance from the c_GT membrane. A more in-depth discussion of the effect of crosslinking of genipin on the fibres is presented in the wettability section (**section 5.3.2.2**).

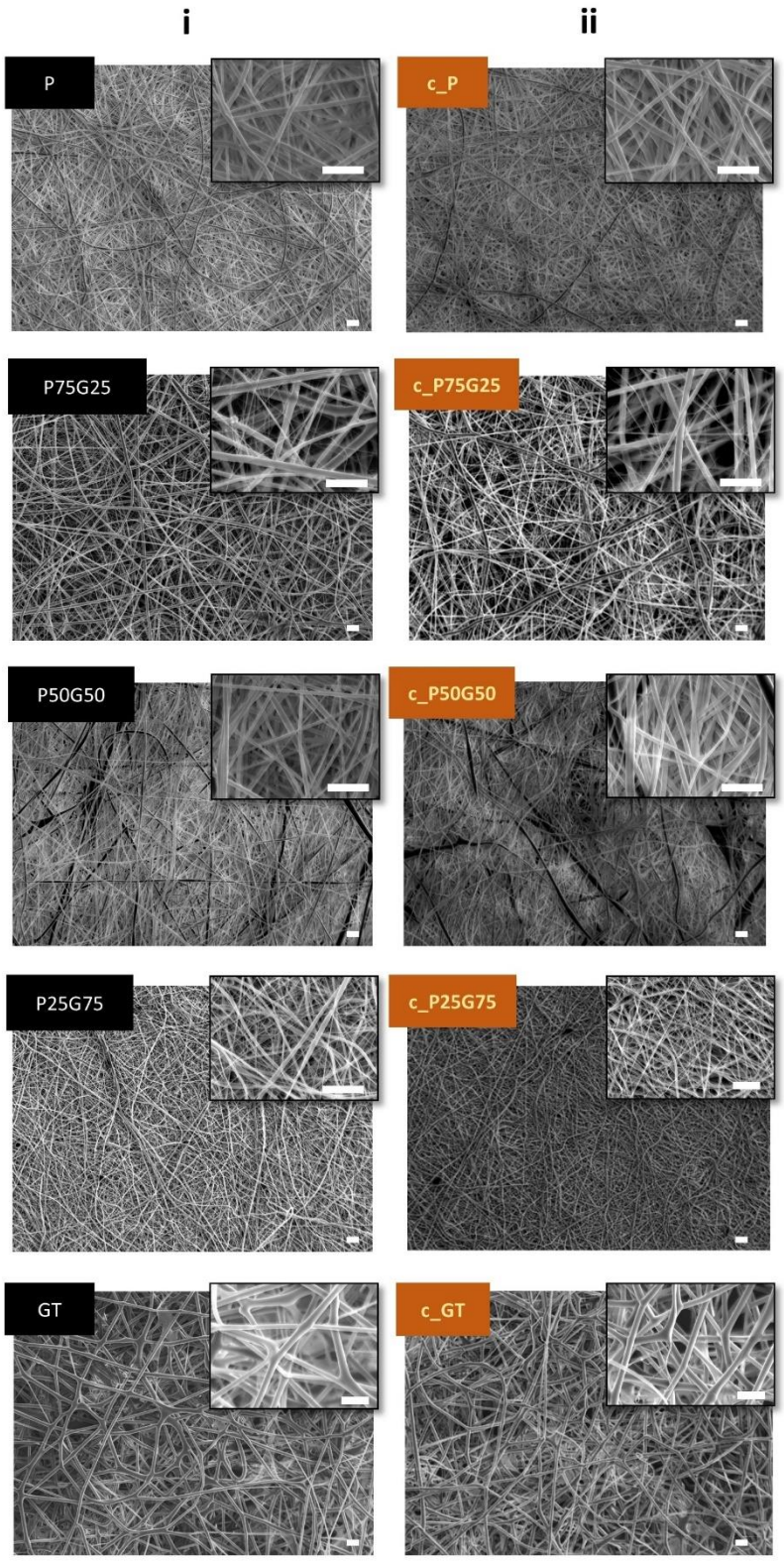

Figure 5.5: Scanning Electron Microscopy (SEM) of electrospun PCL/GT membranes, with a series mass ratio of 100:0, 75:25, 50:50, 25:75 and 0:100, (i) before and (ii)

after crosslinking in genipin. Inserts are enlargements of the figures. The scale bar represents 10 µm in figures and inserts.

Table 5.2: Fibre contents, crosslinking agent, and fibre diameter of electrospun membranes.

Sample	*PCL wt%*	*Gelatine wt%*	*genipin*	*Fibre diameter (µm)*
PCL	100	0	-	1±0.3
P75G25	75	25	-	1.2±0.4
P50G50	50	50	-	0.8±0.2
P25G75	25	75	-	0.7±0.2
GT	0	100	-	2±0.4
c_PCL	100	0	+	1.1±0.3
c_P75G25	75	25	+	1.1±0.5
c_P50G50	50	50	+	1.2±0.2
c_P25G75	25	75	+	0.6±0.1
c_GT	0	100	+	2.2±0.1

5.3.2.2 Wettability: Contact Angle

Static water contact angles using the sessile drop technique were performed to characterise the wettability of the electrospun nanofibres. In general, a more hydrophilic or wettable surface is known to have a more positive impact on

promoting cell adhesion.[330] The contact angles of both non-crosslinking and crosslinking electrospun membranes were measured for the initial 10 s of contact with a water droplet (**Figure 5.6**). PCL is known to be hydrophobic and has shown a contact angle of 130°. For the non-crosslinked samples, the addition of the more hydrophilic GT component in the electrospun fibrous membranes, causes a significant decrease in contact angle. This is attributed to the increase in the amine and carboxyl functionalities present in the GT polymer backbone.

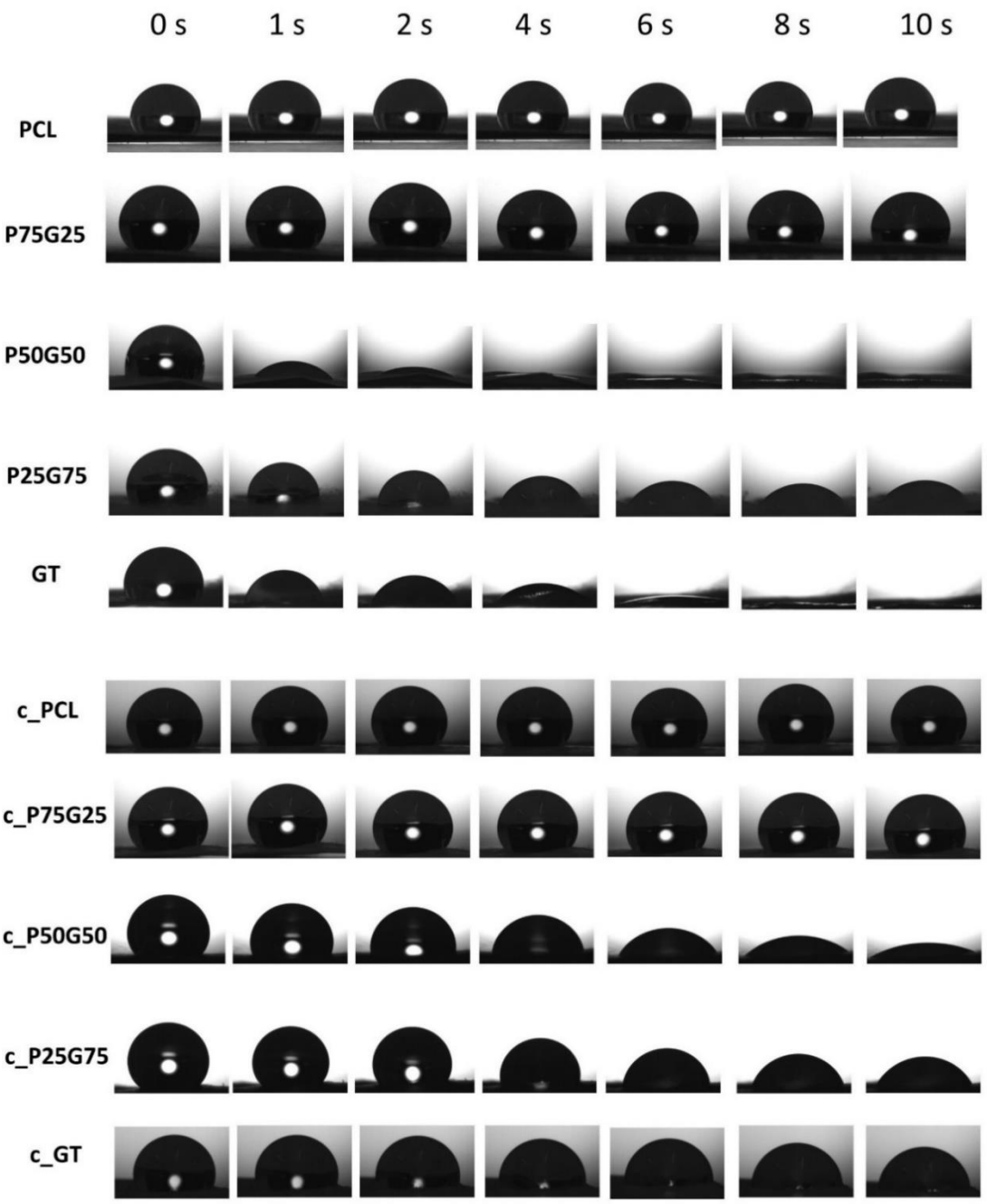

Figure 5.6: Optical images of water droplets on the electrospun membranes for the initial 10 s during the measurement of water contact angle. Images were taken every 1 s. Representative image of each sample selected from at least triplicates.

After crosslinking with genipin, the same trend of a steep decrease in contact angle is observed when going from pure PCL to pure gelatine, implying that the genipin has no effect on wettability of the electrospun fibrous membranes with higher PCL concentrations. Nevertheless, the shape of water drops maintains longer on c_P50G50, c_P25G75 and c_GT, when compared to P50G50, P25G75 and GT, respectively. On one hand, porous microstructure played a role in influencing the liquid-solid interface in contact angle measurement. Denser porous microstructures can be seen on c_P50G50, c_P25G75 and c_GT (enlarged images in **Figure 5.5**), resulting in surfaces with higher contact angles in the initial seconds. On the other, the surface wettability of these membranes with higher gelatine concentration was mediated by the crosslinking mechanism of genipin. The crosslinking mechanism of genipin includes two reactions (shown in **Figure 5.7**), involving different sites on the genipin molecule.[331] The first reaction is a nucleophilic substitution reaction between the $-NH_2$ and $-COOCH_3$, leading to a replacement of the ester group on the genipin molecule by a secondary amide linkage. The next reaction is a nucleophilic attack of the genipin C3 carbon atom from the primary amine group of gelatine to form an intermediate aldehyde group. The just formed secondary amine reacts with the aldehyde group to form a heterocyclic compound. The lack of change in water contact angle, which measured after seconds, between the non-crosslinked and crosslinked fibres was also observed by Zhang and coworkers[320, 332] who determined that only amino groups present in a small quantity were crosslinked leaving the carboxylic groups.

Reaction 1:

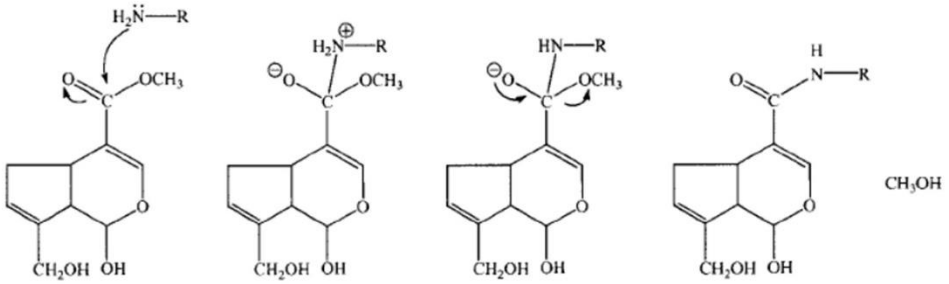

Reaction 2:

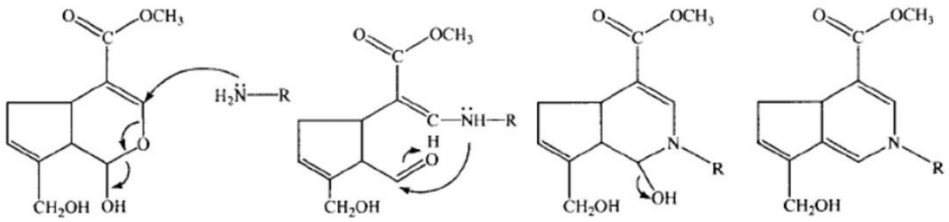

Figure 5.7: Crosslinking mechanism at different sites on genipin molecule with primary amine. Images reproduced from Butler *et al*.[331] with permission from John Wiley and Sons.

5.3.2.3 Chemistry Structure: FTIR

FTIR analysis was used to characterise the chemical bonds of PCL and GT in the membranes (**Figure 5.8**). PCL can be easily identified from its strong bands at ~2949 cm^{-1} (**Figure 5.7** dash line a) and 2865 cm^{-1} (**Figure 5.7** dash line b) corresponding to the stretching vibration of asymmetric and symmetric CH_2 bonds, respectively. The peak at 1727 cm^{-1} corresponds to the carbonyl stretching of PCL.[333] For GT, the FTIR spectrum displays peaks at ~1650 cm^{-1} (amide I, **Figure 5.7** dash line c) and ~1540 cm^{-1} (amide II, **Figure 5.7** dash line d) corresponding to the stretching vibration of C=O bond and the coupling vibrations of N-H and C-N, respectively.[321, 334] The FTIR

spectrum of the hybrid nanofibrous membranes include the characteristic peaks of both PCL and GT, confirming the presence of both polymers.

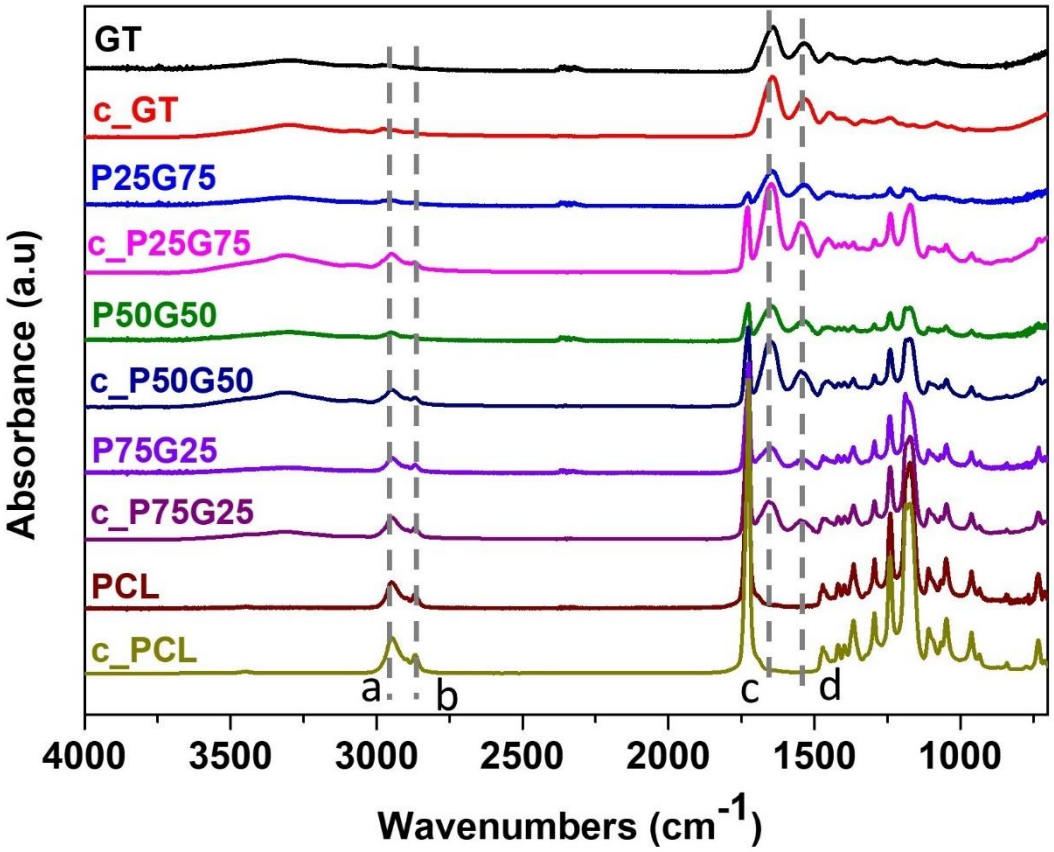

Figure 5.8: FTIR spectra of different electrospun fibrous membranes.

5.3.3 Chemiluminescence: Measurement and Mechanism of NO Release

The NO payload from the diazeniumdiolate-modified membranes was determined by using a chemiluminescence nitric oxide analyser in acetic acid and PBS buffers at pH 4 and 7.4, respectively. The NO release profiles of non-crosslinked electrospun membranes are shown in **Figure 5.9**. The kinetics of NO release, including the total

concentration of NO (t[NO]), maximum instantaneous NO release concentration ($[NO]_m$), time required to reach $[NO]_m$ (t_m), and NO release duration (t_d), were determined from each membrane, and the values are summarised in **Table 5.3**. The NO payload and release kinetics were dependent upon the gelatine content percentage of the membranes, the pH of the measuring buffers and crosslinking. But due to the COVID-19 lockdown, the release profiles of the crosslinking membranes were not able to be measured unfortunately.

GT/NO: At pH 4, GT/NO membranes released NO at a maximum instantaneous NO concentration of 27.6 $\mu M \cdot s^{-1} \cdot cm^{-2}$ at 3 min with a total NO release concentration of 40 mM within 16 h. At pH 7.4, the total NO release of GT/NO was less than at pH 4, with a concentration of 15 mM and a lower maximum instantaneous NO concentration of 10.4 $\mu M \cdot s^{-1} \cdot cm^{-2}$.

P25G75/NO: At pH 4, P25G75/NO membranes released NO at a maximum instantaneous NO concentration of 3.0 $\mu M \cdot s^{-1} \cdot cm^{-2}$ at 98 min with a total NO release concentration of 64 mM within 16 h. At pH 7.4, the total NO release of P25G75/NO was less than at pH 4, with a concentration of 8.4 mM and a lower maximum instantaneous NO concentration of 7.8 $\mu M \cdot s^{-1} \cdot cm^{-2}$.

P50G50/NO: At pH 4, P50G50/NO membranes released NO at a maximum instantaneous NO concentration of 9.7 $\mu M \cdot s^{-1} \cdot cm^{-2}$ at 5 min with a total NO release concentration of 37 mM within 16 h. At pH 7.4, the total NO release of P50G50/NO was less than at pH 4, with a concentration of 8.7 mM and a lower maximum instantaneous NO concentration of 6.1 $\mu M \cdot s^{-1} \cdot cm^{-2}$.

P75G25/NO: At pH 4, P75G25/NO membranes released NO at a maximum instantaneous NO concentration of 9.2 $\mu M \cdot s^{-1} \cdot cm^{-2}$ at 5 min with a total NO release concentration of 25 mM within 16 h. At pH 7.4, the total NO release of P75G25/NO was less than at pH 4, with a concentration of 0.3 mM and a lower maximum instantaneous NO concentration of 0.5 $\mu M \cdot s^{-1} \cdot cm^{-2}$.

PCL/NO: As there is no nitrogen in the backbone of PCL, it was expected that no diazeniumdiolate formation would take place and hence, no NO release. However, a small amount of NO has been measured at both pH 4 and 7.4, that is resulting from free NO gas molecules physisorbed on the surface of membranes.

The NO payload and release kinetics were dependent upon the ratio of gelatine content in the membranes and the pH of the measuring buffers. The GT/NO membranes released a lower total NO concentration than P25G75/NO at pH 4 but this trend was reversed at pH 7.4. This could be due to the loss of gelatine during sample preparation for chemiluminescence. That, it is of more challenge to fully remove GT membranes from the supported foil surfaces, when compare to the removal of PCL-contained membranes. With more time, an improved mean to ensure consistency of the membranes in size would be considered before chemiluminescence. Lower NO concentration was expected from the membranes at pH 4 based on the mechanistic study presented in **Chapter 3.** *N*-diazeniumdiolates formed on primary amine sites decompose to HNO and NO with the product ratio dependent on the pH and the basicity of the nitroso oxygen formed.[268] Therefore *N*-

diazeniumdiolates should decompose entirely to NO at pH 4 and a mixture of HNO an HNO at pH 7.4.

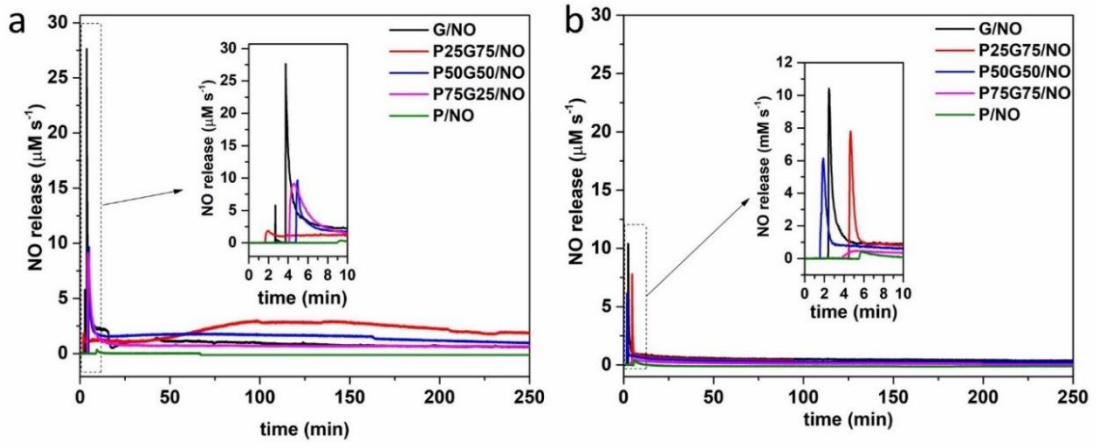

Figure 5.9: Chemiluminescence NO release profiles of diazeniumdiolate-functionalised membranes after 4 h and the inset is rescaling of the first 10 min at a) pH 4, and b) pH 7.4 at room temperature.

Table 5.3: NO release properties for diazeniumdiolate-functionalised membranes in pH 4 and 7.4.

pH	membrane	t[NO] (mM)	$[NO]_m$ ($\mu M \cdot s^{-1} \cdot cm^{-2}$)	t_m (min)	t_d (h)
4	GT/NO	40	27.6	3	16+
	P25G75/NO	64	3.0	98	16+
	P50G50/NO	37	9.7	5	16+
	P75G25/NO	25	9.2	5	16+
	PCL/NO	0.1	0.4	9	-
7.4	GT/NO	15	10.4	2.5	10+
	P25G75/NO	8.4	7.8	4.6	10+
	P50G50/NO	8.7	6.1	1.8	10+
	P75G25/NO	0.3	0.5	6	10+
	PCL/NO	0.07	0.4	6.1	-

5.3.4 Antimicrobial Analysis

5.3.4.1 Biofilm Inhibition

Bacterial biofilms cause up to 80% of nosocomial infections and once a biofilm forms, the infection is very difficult to eradicate.[295] One of the most effective means to prevent the formation of biofilm is to reduce or stop the initial adhesion of bacteria onto surfaces. Gram-negative *E. coli* and gram-positive *S. aureus*, which are relevant

to orthopaedic implant infections,[296-297] were selected to measure the antimicrobial activity of the NO releasing electrospun membranes.

Non-Crosslinked Membranes

The prevention of biofilm formation on the various non-crosslinked membranes at 4 h was determined by biofilm CFU assay, with the results shown in **Figure 5.10**. Bacteria were incubated on the surfaces for 4 h in LB broth to allow for biofilms to form, followed by the enumeration of the remaining viable bacterial colonies to analyse the efficacy of the NO-release. The result of the assay performed against *E. coli* is shown in **Figure 5.10 a**. GT/NO and P25G75/NO membranes both displayed a ~1.3-log reduction of *E. coli* adhesion. P50G50/NO displayed ~0.9-log reduction from 4×10^5 CFU/ml to 3×10^4 CFU/ml. Both P75G25/NO and PCL/NO membranes showed no significant difference of *E. coli* adhesion compared with P75G25 and PCL. The results of the biofilm CFU assay with *E. coli* are in agreement with the NO release profiles in **Figure 5.9** showing that NO release correlated directly to antimicrobial activity, i.e. GT/NO has the largest NO payload, followed by P25G75/NO and P50G50/NO.

The results of the biofilm CFU assay performed against *S. aureus* is shown in **Figure 5.10 b.** GT/NO and P25G75/NO both displayed a ~0.8-log reduction in *S. aureus* adhesion. The P50G50/NO displayed a less than 0.4-log reduction. However, both P75G25/NO and PCL/NO membrane displayed large reductions in *S. aureus* adhesion, ~1.1-log and ~1.5-log, respectively. The rationale for why these membranes perform better is unclear at the moment and extra experimental analysis has not been

possible due to the COVID-19 lockdown. The wettability, surface area and NO releasing concentration of membranes might synergistically affect biofilm inhibition on surfaces.

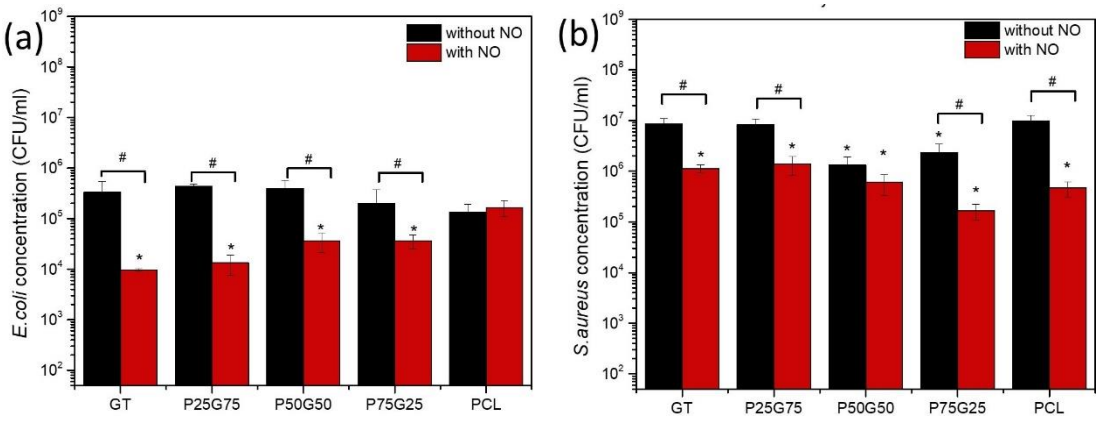

Figure 5.10: Viable bacterial colonies (CFU/mL) after 4 h of biofilm growth on non-crosslinked electrospun membranes of a) *E. coli* and b) *S. aureus*. **p* < 0.05 from PCL; #*p* <0.05 from the corresponding ratio with no diazeniumdiolate functionalisation. (Note: 3 runs for *E. coli* and 1 run for *S. aureus* have been done)

Crosslinked membranes

The prevention of biofilm formation on the various crosslinked membranes at 4 h was determined by biofilm CFU assay, with the results shown in **Figure 5.11**. The c_GT/NO displayed a reduction of *E. coli* adhesion from 1×10^5 CFU/ml to 1.5×10^3 CFU/ml, which corresponds to a ~2-log reduction (shown in **Figure 5.11 a**). c_P25G75/NO displayed the highest reduction of *E. coli* adhesion with ~3-log. The c_P50G50/NO, c_P75G25/NO and c_PCL/NO membranes showed no significant difference in *E. coli* adhesion compared with the control samples. It can be clearly

seen that crosslinking largely improved the antimicrobial efficacy of both c_GT/NO and c_P25G75/NO, which would be due to the increasing of NO payload after crosslinking.

The results of biofilm CFU assay with *S. aureus* on the crosslinked membranes (**Figure 5.11 b**) showed a similar trend with of that of *E. coli*. The c_GT/NO and c_P25G75/NO membranes displayed a ~4-log reduction which corresponds to the highest reduction for all the membranes. The c_P50G50/NO, P75G25/NO and PCL/NO membranes showed ~2-log reduction in *S. aureus* adhesion. Once again as with the *S. aureus* experiments above an improved antimicrobial efficacy of both c_GT/NO and c_P25G75/NO was observed probably due to the increasing of NO payload after crosslinking. Unfortunately, the chemiluminescence measurements of crosslinked membranes were not completed prior to lockdown and this is needed for a further discussion of the results. However, it can be hypothesised (based on what has been observed in **Chapter 3**) that crosslinking creates more secondary amines (amides) which are known to be more stable and have higher and longer NO releasing profiles in comparison to non-crosslinked membranes.

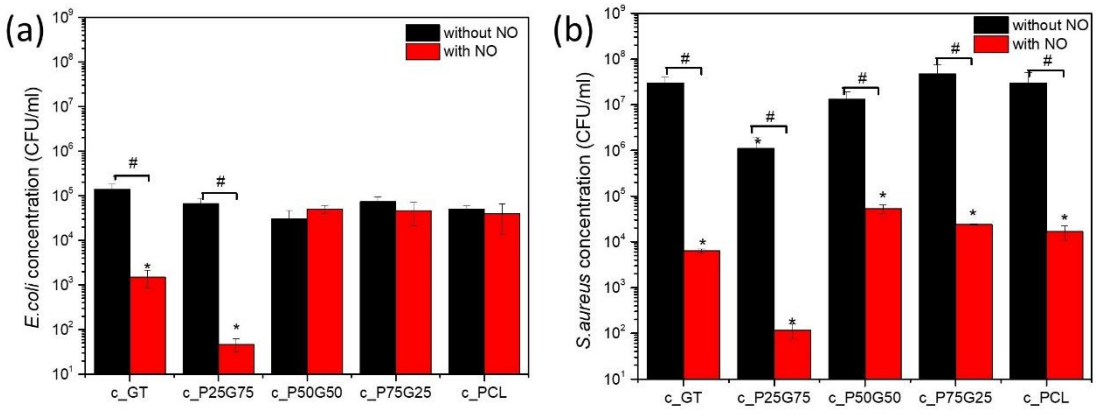

Figure 5.11: Viable bacterial colonies (CFU/mL) after 4 h of biofilm growth on crosslinked electrospun membranes of a) *E. coli* and b) *S. aureus*. *$p < 0.05$ from PCL; #$p < 0.05$ from the corresponding ratio with no diazeniumdiolates functionalisation. (Note: 2 runs for *E. coli* and 2 runs for *S. aureus*)

5.3.4.2 Antimicrobial Activity on Planktonic Bacteria

Non-Crosslinked Membranes

The prevention of planktonic bacterial growth in solution with the presence of the non-crosslinked electrospun membranes at 4 h was determined by using a spread plate CFU assay and the results are displayed in **Figure 5.12**. The antimicrobial activity of membranes tested against *E. coli* (**Figure 5.12 a**) directly correlate with the payload NO release presented in **Figure 5.9**. The GT/NO membrane displayed a reduction of planktonic *E. coli* growth from 3.5×10^5 CFU/ml to 3.5×10^3 CFU/ml, corresponding to a 2-log reduction. The P25G75/NO membrane displayed ~1.5-log reduction in planktonic *E. coli* growth. The P50G50/NO P75G25/NO membranes displayed a 1 log

and ~0.8 log reduction, respectively. PCL/NO showed no significant difference in the planktonic *E. coli* growth. The prevention of planktonic *E. coli* growth directly correlates to the NO payload results (**Figure 5.9**), i.e. the higher the payload the better the antimicrobial efficacy.

The results of prevention of planktonic *S. aureus* growth in solution in the presence of the non-crosslinked membranes (**Figure 5.12 b**) shows a different trend with of *E. coli* on NO release membranes at 4 h incubation. The GT/NO and P25G75/NO membranes displayed a~0.9 log reduction of planktonic *S. aureus* growth. The P50G50/NO, P75G25/NO, PCL/NO displayed 1.5, 1 and 0.7 log reduction, respectively. The investigation as to why *S. aureus* behaves differently to *E. coli* is not fully understood yet and COVID-19 lockdown has prevented us from exploring this further. Once again it is observed here that the GT membranes dissolve quite easily and are difficult to handle and thus may present a lower antimicrobial efficacy as a result.

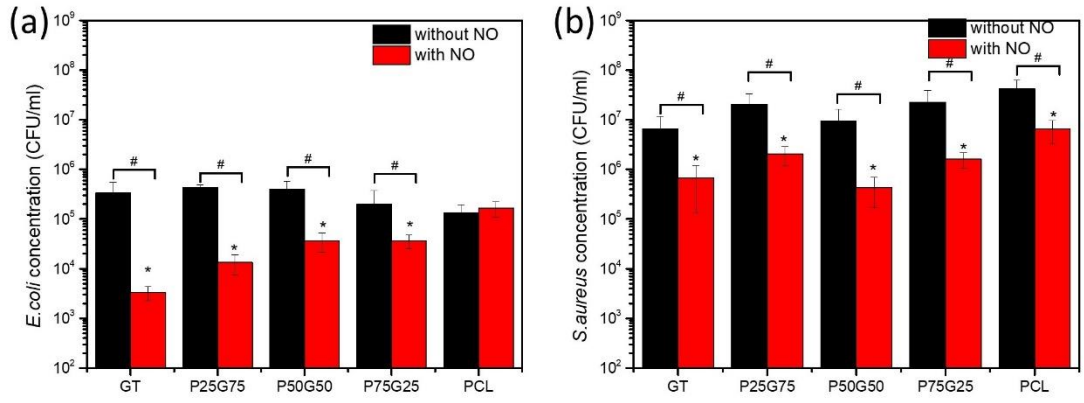

Figure 5.12: Planktonic a) *E. coli* and b) *S. aureus* growth in solution with the presence of the noncrosslinked electrospun membranes after 4 h incubation. *p < 0.05 from PCL; #p <0.05 from the corresponding ratio with no diazeniumdiolates functionalisation. (Note: 3 runs for *E. coli* and 1 run for *S. aureus*)

Crosslinked Membranes

The growth of planktonic bacteria at 4 h on crosslinked electrospun membranes is shown in **Figure 5.13**. The c_GT/NO membrane displayed a reduction of planktonic *E. coli* growth from 1×10^6 CFU/ml to 1.5×10^4 CFU/ml, which corresponds to a ~2-log reduction (shown in **Figure 5.13 a**). The c_P25G75/NO displayed the highest reduction of *E. coli* adhesion with ~3-log. The c_P50G50/NO, P75G25/NO and PCL/NO membranes showed less than 1 log reduction in planktonic *E. coli* growth. The crosslinking largely improved the antimicrobial efficiency of both c_GT/NO and c_P25G75/NO, by increasing the number of secondary amine (amide) functional

groups to facilitate increased NO loading which would be the rationale for the higher antimicrobial efficacy.

The results against *S. aureus* (**Figure 5.13 b**) show a similar trend as against *E. coli* on crosslinked NO release membranes at 4 h incubation. The c_GT/NO membrane displayed the highest reduction of planktonic *S. aureus* growth from 1×10^6 CFU/ml to 1×10^4 CFU/ml, which corresponds to a ~2-log reduction. The c_P25G75/NO membrane displayed 1.5-log reduction of planktonic *S. aureus* growth. The c_P50G50/NO, c_P75G25/NO and c_PCL/NO showed no reduction or no significant difference in planktonic *S. aureus* growth. Once again, it can be concluded that crosslinking largely improved the antimicrobial efficacy of both c_GT/NO and c_P25G75/NO, due to the increasing of NO payload after crosslinking. Unfortunately, the chemiluminescence measurements of crosslinked membranes were not finished before COVID-19 lockdown which prevents a more detailed discussion here.

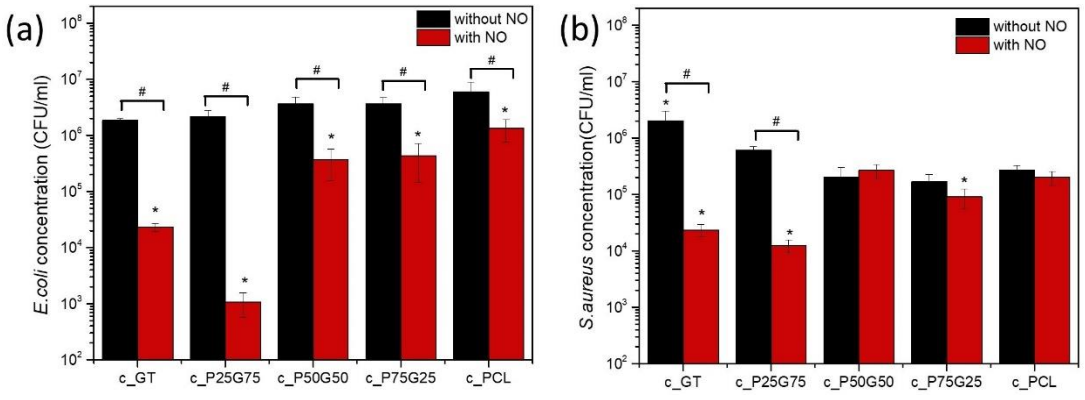

Figure 5.13: Planktonic a) *E. coli* and b) *S. aureus* growth in solution with the presence of the crosslinked electrospun membranes after 4 h incubation. *$p < 0.05$ from PCL;

#*p* <0.05 from the corresponding ratio with no diazeniumdiolates functionalisation. (Note: 2 runs for *E. coli* and 2 runs for *S. aureus*)

5.4 Conclusion

This chapter reports on the fabrication and the antimicrobial efficacy of crosslinked electrospun PCL/Gel membranes. The addition of acetic acid improved the phase separation issue during electrospinning which was instrumental to fabricating repeatable and reproducible membranes. SEM images indicated the fibre diameter of the membranes ranges from 0.7 to 1.2 µm. Genipin displayed no effect on the morphology of membranes but slightly decreased the hydrophilicity of the membranes at the initial contacting with water drop. The antimicrobial efficacy of the membranes was directly correlated to the mass ratio of gelatine in electrospun membranes. The higher the gelatine in the membrane the greater the NO loading which lead to a higher antimicrobial efficiency on *E. coli* and *S. aureus*. Moreover, crosslinking also had an effect on antimicrobial efficacy. Crosslinking provided more secondary amines which allowed for more stable and higher payloads of NO, thereby allowing for higher antimicrobial efficacy for both *E. coli* and *S. aureus*.

Chapter 6: Conclusions and Suggestions for Future Work

6.1 Conclusions

The aim of this thesis is to develop antimicrobial nitric oxide releasing materials for orthopaedic medical implants. The pathogenesis of many orthopaedic infections is related to the presence of biofilms on device surfaces, which are recalcitrant to conventional antibiotic therapy and causing antimicrobial resistance. In other word, the current clinical therapy for bacterial-related orthopaedic infections is the use of systematic antibiotics. Biofilm is a protective lifestyle of bacteria, and it has inherent tolerance to antibiotics therefore large doses of antibiotics are needed to achieve efficient treatment. The overuse of antibiotics has however resulted in rise of antimicrobial resistance of bacteria which necessitates larger doses and last resort antibiotics for treatment. However, the pipeline of antibiotics is depleting and there has been no new antibiotic developed for over 30 years.[335-336] As such, is of great importance to develop alternative antimicrobial treatments that do no relay on antibiotics.

The active agent selected during this thesis is NO as it is a potent antimicrobial agent that does not contribute to the development of antimicrobial resistance in bacteria. NO has been tethered onto the surfaces using an *N*-Diazeniumdiolate as a NO donor in this thesis. *N*-diazeniumdiolates are a versatile NO storage and delivery vehicle as the rate and payload of the therapeutic can be carefully controlled.

The objectives have been achieved via the work described in the preceding three experimental chapters. Various of fabrication and functionalisation techniques have been carried out to develop NO releasing implants which were able to prevent the

adhesion of bacteria and the subsequent inhibited formation of biofilm on surfaces. Three implants surfaces used in the thesis were commercial Ti, LCS Ti foams and electrospun PCL/gelatine electrospun membranes. Different characterisations have been employed to measure and analysis these materials. SEM/AFM performed the morphology and topography of the surfaces. Contact angle, XPS and FTIR were used to analysis the wettability and surface chemistry, further confirming the targeted synthesis. The NO releasing kinetic has been performed via chemiluminescence. Biofilm CFU assays and bacterial viability tests against *E. coli*, *S. aureus* and *P. aeruginosa* were taken to evaluate the antibiofilm/antimicrobial property of the materials. The bone-integrating was tested on human primary bone cells.

Firstly, in Chapter 3, NO releasing Ti surfaces were developed for antibiofilm and bone-integrating studies. Two different aminosilane precursors (AHAP3 and AUTES) were tethered onto commercially available flat Ti for subsequent functionalisation with NO. The structure of aminosilane precursors affected the resultants NO releasing properties in terms of payload and release kinetics, giving that both AHAP3/NO and AUTES/NO. The NO payloads and releasing kinetics were controlled in various ways, including the pK_a of the amine, the class of amine groups, the layers of aminosilane precursors, the pH value of the release medium and the structure of substrate materials with larger surface areas. Therefore, at pH 4, AUTES/NO displayed the highest instantaneous NO concentration of 17.4 $\mu M \cdot s^{-1} \cdot cm^{-1}$ and the highest sum NO amount of 1883.6 µM. At pH 7.4, AUTES/NO still given the highest instantaneous NO concentration with value of 10.2 $\mu M \cdot s^{-1} \cdot cm^{-1}$, while the total NO release amount has been showing reduce to 476.2 µM. The antibiofilm/antimicrobial property of the materials dependent upon the NO payloads and releasing kinetics.

Low level NO release (in the case of using aminosilanes as precursors) displayed antimicrobial activity with a biofilm inhibition rate of up to 2.4 log in a short-term culture (i.e. 4-6 h incubation). In addition, the constancy of NO releasing for longer time benefited to efficient biofilm inhibition as well as planktonic bacterial viability in 24 h bacterial culture. However, there was a similar antibiofilm efficiency of both coatings against *S. aureus* and *P. aeruginosa*. Furthermore, low level NO release presented good bone-integrating on human primary bone cells. Compared to AHAP3/NO, AUTES/NO presented more recovered cells, indicating its lower cytotoxicity towards human primary bone cells after 7 days in culture.

Secondly, in Chapter 4, Ti foams were fabricated with a novel LCS process, and the AUTES silnae coating (which was optimised the best performing silane in Chapter 3) have been used as aminosilane precursor for modifying the Ti foams. The layers of AUTES played roles on the NO releasing kinetics and the antimicrobial efficacy of the Ti foams. 5%AUTES/NO (the highest instantaneous NO release concentration of 6.2 $\mu M \cdot s^{-1} \cdot cm^{-1}$ and the largest sum NO payload of 2.3 mM at pH 4) displayed the optimal antibiofilm/antimicrobial properties against both *E. coli* and *S. aureus* after 4 and 24 h.

Thirdly, in Chapter 5, PCL/gelatine biodegradable electrospun membranes were fabricated using varying ratios of each polymer. The effect of crosslinking on the degradability of the coatings were also investigated. The addition of PCL and crosslinking process improved the microstructure and the wettability of the membranes. Gelatine has amino functionality in the backbone of the polymer and this was used as point to tether the diazeniumdiolate NO donor molecule. The

membranes were characterised and analysed for the antimicrobial efficacy. The crosslinked PCL/gelatine membranes displayed higher antimicrobial efficacy on with planktonic and biofilm bacteria (*S. aureus* and *E. coli*). Compared with using silane coatings high level NO release (in the case of using gelatine as the precursor) displayed high level biofilm inhibition and planktonic bactericidal in 4 h incubation.

In summary, three different bone implant models, ranging from flat titanium surfaces to porous titanium to electrospun membranes have been functionalised with the NO donor *N*-Diazeniumdiolate and have shown to be effective as antimicrobial materials for orthopaedic applications. These versatile materials are also promising as they use NO as the active agent that has not shown to develop resistance mechanisms in bacteria therefore contributing to the global epidemic of antimicrobial resistance.

6.2 Suggestions for Future Work

6.2.1 Race for the Surface: Bacterial-Mammalian Coculture Model

The two major barriers for a successful bone implant surgery are biomaterials-associated infections and tissue integration of the devices.[337] Biomaterial related infections mainly result from the adhesion of planktonic bacteria onto device surfaces, subsequently colonise the surfaces and form biofilms. As it is known, biofilm is difficult to treat once it forms, and it is able to obstruct the attachment of tissue cells and against the host immune system.[338-339] The successful tissue integrations dependent upon the interface reaction between device surfaces and tissue cells.[337] The competition between bacterial colonisation of implants and tissue cells integration with device surfaces was initially termed "the race for the surfaces" by Gristina in 1987.[337] If the race is won by the tissue cells, then the surfaces are dominantly occupied by tissue cells and bacteria have a lower probability to form biofilms on the surfaces. Therefore, to mimic this *in vivo* condition, *in vitro*, future work would involve the development of a bacteria-cell coculture model. The biofilm inhibition efficacy on both NO release flat Ti surface and Ti foams has been evaluated against *E. coli*, *S. aureus* and *P. aeruginosa*, and these antimicrobial conditions have been shown to be non-cytotoxic to primary human osteoblast cells on flat Ti surfaces.

6.2.2 Biodegradability and Mechanical Property of PCL/Gelatine Electrospun Membranes

This section is the incomplete work due to COVID19 lockdown. Biodegradation and mechanical property are two of the strategy requirements that need to be considered when designing biodegradable membranes for guided bone regeneration. These experiments would need to be undertaken to complete this

study. There are concerns with the use of biomaterials with quick degradation rate as there will be a rapid loss of mechanical stability in situ and subsequently allowing undesirable cell type entering the regeneration area.[340] Alternatively, a slow degradation could prevent tissue formation or result in stress shielding which would affect the integrity of the de novo tissue. As such this work needs to be extended in order to have the degradation rate of the membranes match the tissue regeneration rate.[341] Once optimised membranes in terms of degradation rate, mechanical stability and antimicrobial efficacy are optimised, *in vitro* cytocompatibility studies will need to be carried out.

6.2.3 Guided Stem Cell Differentiation of NO release PCL/Gelatine Electrospun Membranes

Endogenous NO plays role in governing various physiological process and it is a versatile signalling molecule in mediating cellular functions.[342] There is little or no research that has been carried on whether exogenous NO can affect the differentiation of mesenchymal stem cells. Once the NO releasing PCL/gelatine electrospun membranes have been optimised as in section 5.2.2, it is suggested to investigate study these membranes for guided bone regeneration using mesenchymal stem cells.

References

(1) Registry, N. J. *National Joint Registry 16th Annual Report 2019* **2018**.
(2) Raphel, J.; Holodniy, M.; Goodman, S. B.; Heilshorn, S. C. Multifunctional coatings to simultaneously promote osseointegration and prevent infection of orthopaedic implants. *Biomaterials* **2016,** *84*, 301-314.
(3) Campoccia, D.; Montanaro, L.; Arciola, C. R. The significance of infection related to orthopedic devices and issues of antibiotic resistance. *Biomaterials* **2006,** *27* (11), 2331-2339.
(4) Zmistowski, B.; Fedorka, C. J.; Sheehan, E.; Deirmengian, G.; Austin, M. S.; Parvizi, J. Prosthetic joint infection caused by gram-negative organisms. *The Journal of Arthroplasty* **2011,** *26* (6, Supplement), 104-108.
(5) Crémet, L.; Broquet, A.; Brulin, B.; Jacqueline, C.; Dauvergne, S.; Brion, R.; Asehnoune, K.; Corvec, S.; Heymann, D.; Caroff, N. Pathogenic potential of Escherichia coli clinical strains from orthopedic implant infections towards human osteoblastic cells. *Pathogens and Disease* **2015,** *73* (8).
(6) Stoodley, P.; Ehrlich, G. D.; Sedghizadeh, P. P.; Hall-Stoodley, L.; Baratz, M. E.; Altman, D. T.; Sotereanos, N. G.; Costerton, J. W.; Demeo, P. Orthopaedic biofilm infections. *Current Orthopaedic Practice* **2011,** *22* (6), 558-563.
(7) Anwar, H.; Dasgupta, M. K.; Costerton, J. W. Testing the susceptibility of bacteria in biofilms to antibacterial agents. *Antimicrob Agents Chemother* **1990,** *34* (11), 2043-2046.
(8) Potera, C. Antibiotic resistance: biofilm dispersing agent rejuvenates older antibiotics. *Environmental Health Perspectives* **2010,** *118* (7), A288-A288.
(9) O'Neill, J. Tackling drug-resistant infections globally: final report and recommendations 2016. *HM Government and Welcome Trust: UK* **2018**.
(10) Silver, L. L. Challenges of antibacterial discovery. *Clinical Microbiology Reviews* **2011,** *24* (1), 71.
(11) Akova, M. Epidemiology of antimicrobial resistance in bloodstream infections. *Virulence* **2016,** *7* (3), 252-266.
(12) Tenover, F. C. Mechanisms of antimicrobial resistance in bacteria. *The American Journal of Medicine* **2006,** *119* (6, Supplement 1), S3-S10.
(13) Wise, R.; Hart, T.; Cars, O.; Streulens, M.; Helmuth, R.; Huovinen, P.; Sprenger, M. Antimicrobial resistance. *BMJ* **1998,** *317* (7159), 609.
(14) Kumarasamy, K. K.; Toleman, M. A.; Walsh, T. R.; Bagaria, J.; Butt, F.; Balakrishnan, R.; Chaudhary, U.; Doumith, M.; Giske, C. G.; Irfan, S.; Krishnan, P.; Kumar, A. V.; Maharjan, S.; Mushtaq, S.; Noorie, T.; Paterson, D. L.; Pearson, A.; Perry, C.; Pike, R.; Rao, B.; Ray, U.; Sarma, J. B.; Sharma, M.; Sheridan, E.; Thirunarayan, M. A.; Turton, J.; Upadhyay, S.; Warner, M.; Welfare, W.; Livermore, D. M.; Woodford, N. Emergence of a new antibiotic resistance mechanism in India, Pakistan, and the UK: a molecular, biological, and epidemiological study. *The Lancet Infectious Diseases* **2010,** *10* (9), 597-602.
(15) Collignon, P. Antibiotic resistance: are we all doomed? *Internal Medicine Journal* **2015,** *45* (11), 1109-1115.
(16) Collignon, P.; Beggs, J. J.; Walsh, T. R.; Gandra, S.; Laxminarayan, R. Anthropological and socioeconomic factors contributing to global antimicrobial resistance: a univariate and multivariable analysis. *The Lancet Planetary Health* **2018,** *2* (9), e398-e405.
(17) Bozic, K. J.; Kurtz, S. M.; Lau, E.; Ong, K.; Chiu, V.; Vail, T. P.; Rubash, H. E.; Berry, D. J. The epidemiology of revision total knee arthroplasty in the United States. *Clinical Orthopaedics and Related Research* **2010,** *468* (1), 45-51.
(18) Organization, W. W. H. Antimicrobial resistance. https://www.who.int/news-room/fact-sheets/detail/antimicrobial-

resistance#:~:text=What%20is%20antimicrobial%20resistance%3F,%2C%20antimalarials%2C%20and%20anthelmintics).
(19) Organization, W. H. Antimicrobial resistance global report on surveillance: 2014 summary; World Health Organization: **2014**.
(20) Kang, C. I.; Kim, S. H.; Park, W. B.; Lee, K. D.; Kim, H. B.; Kim, E. C.; Oh, M. D.; Choe, K. W. Bloodstream infections caused by antibiotic-resistant gram-negative bacilli: risk factors for mortality and impact of inappropriate initial antimicrobial therapy on outcome. *Antimicrobial Agents and Chemotherapy* **2005,** *49* (2), 760.
(21) Francis, J. S.; Doherty, M. C.; Lopatin, U.; Johnston, C. P.; Sinha, G.; Ross, T.; Cai, M.; Hansel, N. N.; Perl, T.; Ticehurst, J. R.; Carroll, K.; Thomas, D. L.; Nuermberger, E.; Bartlett, J. G. Severe community-onset pneumonia in healthy adults caused by methicillin-resistant Staphylococcus aureus carrying the panton-valentine leukocidin genes. *Clinical Infectious Diseases* **2005,** *40* (1), 100-107.
(22) Reygaert, W. C. An overview of the antimicrobial resistance mechanisms of bacteria. *AIMS Microbiol* **2018,** *4* (3), 482-501.
(23) Martinez, J. L. General principles of antibiotic resistance in bacteria. *Drug Discovery Today: Technologies* **2014,** *11*, 33-39.
(24) Cox, G.; Wright, G. D. Intrinsic antibiotic resistance: mechanisms, origins, challenges and solutions. *International Journal of Medical Microbiology* **2013,** *303* (6), 287-292.
(25) van Hoek, A.; Mevius, D.; Guerra, B.; Mullany, P.; Roberts, A.; Aarts, H. Acquired antibiotic resistance genes: an overview. *Frontiers in Microbiology* **2011,** *2* (203).
(26) Rice, L. B. Antimicrobial resistance in gram-positive bacteria. *American Journal of Infection Control* **2006,** *34* (5, Supplement), S11-S19.
(27) Chancey, S. T.; Zähner, D.; Stephens, D. S. Acquired inducible antimicrobial resistance in gram-positive bacteria. *Future Microbiology* **2012,** *7* (8), 959-978.
(28) Stewart, P. S.; William Costerton, J. Antibiotic resistance of bacteria in biofilms. *The Lancet* **2001,** *358* (9276), 135-138.
(29) Marrie, T. J.; Nelligan, J.; Costerton, J. W. A scanning and transmission electron microscopic study of an infected endocardial pacemaker lead. *Circulation* **1982,** *66* (6).
(30) Donlan, R. M.; Costerton, J. W. Biofilms: survival mechanisms of clinically relevant microorganisms. *Clinical Microbiology Reviews* **2002,** *15* (2), 167.
(31) Donlan, R. M. Biofilms and device-associated infections. *Emerging Infectious Diseases* **2001,** *7* (2).
(32) Elliott, T. S. J.; Moss, H. A.; Tebbs, S. E.; Wilson, I. C.; Bonser, R. S.; Graham, T. R.; Burke, L. P.; Faroqui, M. H. Novel approach to investigate a source of microbial contamination of central venous catheters. *European Journal of Clinical Microbiology and Infectious Diseases* **1997,** *16* (3), 210-213.
(33) Raad, I. I.; Sabbagh, M. F.; Rand, K. H.; Sherertz, R. J. Quantitative tip culture methods and the diagnosis of central venous catheter-related infections. *Diagnostic Microbiology and Infectious Disease* **1992,** *15* (1), 13-20.
(34) Stickler, D. J. Bacterial biofilms and the encrustation of urethral catheters. *Biofouling* **1996,** *9* (4), 293-305.
(35) McLaughlin, B.; Stapleton; Matheson; Dart. Bacterial biofilm on contact lenses and lens storage cases in wearers with microbial keratitis. *Journal of Applied Microbiology* **1998,** *84* (5), 827-838.
(36) Aveyard, J.; Deller, R. C.; Lace, R.; Williams, R. L.; Kaye, S. B.; Kolegraff, K. N.; Curran, J. M.; D'Sa, R. A. Antimicrobial nitric oxide releasing contact lens gels for the treatment of microbial keratitis. *ACS Applied Materials and Interfaces* **2019,** *11* (41), 37491-37501.
(37) Rieger, U.; Mesina, J.; Kalbermatten, D.; Haug, M.; Frey, H.; Pico, R.; Frei, R.; Pierer, G.; Lüscher, N.; Trampuz, A. Bacterial biofilms and capsular contracture in patients with breast implants. *British Journal of Surgery* **2013,** *100* (6), 768-774.

(38) Calderone, R. A.; Clancy, C. J. *Candida and candidiasis*, American Society for Microbiology Press: **2011**.
(39) Bauer, T.; Torres, A.; Ferrer, R.; Heyer, C.; Schultze-Werninghaus, C.; Rasche, K. Biofilm formation in endotracheal tubes. association between pneumonia and the persistence of pathogens. *Monaldi archives for chest disease* **2002,** *57* (1), 84-87.
(40) Garvin, K. L.; Hanssen, A. D. Infection after total hip arthroplasty. Past, present, and future. *JBJS* **1995,** *77* (10).
(41) Espeland, E.; Wetzel, R. Complexation, stabilization, and uv photolysis of extracellular and surface-bound glucosidase and alkaline phosphatase: implications for biofilm microbiota. *Microbial ecology* **2001,** *42* (4), 572-585.
(42) Leid, J. G.; Shirtliff, M. E.; Costerton, J. W.; Stoodley; Paul. Human leukocytes adhere to, penetrate, and respond to *Staphylococcus aureus* biofilms. *Infection and Immunity* **2002,** *70* (11), 6339.
(43) Le Magrex-Debar, E.; Lemoine, J.; Gellé, M. P.; Jacquelin, L. F.; Choisy, C. Evaluation of biohazards in dehydrated biofilms on foodstuff packaging. *International Journal of Food Microbiology* **2000,** *55* (1), 239-243.
(44) McNeill, K.; Hamilton, I. R. Acid tolerance response of biofilm cells of Streptococcus mutans. *FEMS Microbiology Letters* **2003,** *221* (1), 25-30.
(45) Teitzel, G. M.; Parsek, M. R. Heavy metal resistance of biofilm and planktonic *Pseudomonas aeruginosa*. *Applied and Environmental Microbiology* **2003,** *69* (4), 2313.
(46) Galanakos, S. P.; Papadakis, S. A.; Kateros, K.; Papakostas, I.; Macheras, G. Biofilm and orthopaedic practice: the world of microbes in a world of implants. *Orthopaedics and Trauma* **2009,** *23* (3), 175-179.
(47) Jones, H. C.; Roth, I. L.; Sanders, W. M. Electron microscopic study of a slime layer. *Journal of Bacteriology* **1969,** *99* (1), 316.
(48) Anwar, H.; Strap, J. L.; Chen, K.; Costerton, J. W. Dynamic interactions of biofilms of mucoid Pseudomonas aeruginosa with tobramycin and piperacillin. *Antimicrobial Agents and Chemotherapy* **1992,** *36* (6), 1208.
(49) Dufour, D.; Leung, V.; Lévesque, C. M. Bacterial biofilm: structure, function, and antimicrobial resistance. *Endodontic Topics* **2010,** *22* (1), 2-16.
(50) Lewis, K. Persister cells, dormancy and infectious disease. *Nature Reviews Microbiology* **2007,** *5* (1), 48-56.
(51) Lewis, K. Riddle of biofilm resistance. *Antimicrobial Agents and Chemotherapy* **2001,** *45* (4), 999.
(52) Lebeaux, D.; Ghigo, J. M.; Beloin, C. Biofilm-related infections: bridging the gap between clinical management and fundamental aspects of recalcitrance toward antibiotics. *Microbiology and Molecular Biology Reviews* **2014,** *78* (3), 510.
(53) Costerton, J. W.; Stewart, P. S.; Greenberg, E. P. Bacterial biofilms: a common cause of persistent infections. *Science* **1999,** *284* (5418), 1318.
(54) Fine, D. H.; Furgang, D.; Barnett, M. L. Comparative antimicrobial activities of antiseptic mouthrinses against isogenic planktonic and biofilm forms of actinobacillus actinomycetemcomitans. *Journal of Clinical Periodontology* **2001,** *28* (7), 697-700.
(55) Frank, K. L.; Reichert, E. J.; Piper, K. E.; Patel, R. In vitro effects of antimicrobial agents on planktonic and biofilm forms of staphylococcus lugdunensis clinical isolates. *Antimicrobial Agents and Chemotherapy* **2007,** *51* (3), 888.
(56) Reller, L. B.; Weinstein, M.; Jorgensen, J. H.; Ferraro, M. J. Antimicrobial susceptibility testing: a review of general principles and contemporary practices. *Clinical Infectious Diseases* **2009,** *49* (11), 1749-1755.
(57) Høiby, N.; Bjarnsholt, T.; Givskov, M.; Molin, S.; Ciofu, O. Antibiotic resistance of bacterial biofilms. *International Journal of Antimicrobial Agents* **2010,** *35* (4), 322-332.

(58) Singh, S. B.; Young, K.; Silver, L. L. What is an “ideal” antibiotic? discovery challenges and path forward. *Biochemical Pharmacology* **2017,** *133*, 63-73.
(59) González-Chávez, S. A.; Arévalo-Gallegos, S.; Rascón-Cruz, Q. Lactoferrin: structure, function and applications. *International Journal of Antimicrobial Agents* **2009,** *33* (4), 301.e1-301.e8.
(60) Düring, K.; Porsch, P.; Mahn, A.; Brinkmann, O.; Gieffers, W. The non-enzymatic microbicidal activity of lysozymes. *FEBS Letters* **1999,** *449* (2-3), 93-100.
(61) Tikhonov, V. E.; Stepnova, E. A.; Babak, V. G.; Yamskov, I. A.; Palma-Guerrero, J.; Jansson, H. B.; Lopez-Llorca, L. V.; Salinas, J.; Gerasimenko, D. V.; Avdienko, I. D.; Varlamov, V. P. Bactericidal and antifungal activities of a low molecular weight chitosan and its N-/2(3)-(dodec-2-enyl)succinoyl/-derivatives. *Carbohydrate Polymers* **2006,** *64* (1), 66-72.
(62) Juneja, V. K.; Dwivedi, H. P.; Yan, X. Novel natural food antimicrobials. *Annual Review of Food Science and Technology* **2012,** *3* (1), 381-403.
(63) Barnby-Smith, F. M. Bacteriocins: Applications in food preservation. *Trends in Food Science and Technology* **1992,** *3*, 133-137.
(64) Fleming, A. The discovery of penicillin. *British Medical Bulletin* **1944,** *2* (1), 4-5.
(65) Jabes, D. The antibiotic R&D pipeline: an update. *Current Opinion in Microbiology* **2011,** *14* (5), 564-569.
(66) Hagihara, M.; Crandon, J. L.; Nicolau, D. P. The efficacy and safety of antibiotic combination therapy for infections caused by gram-positive and gram-negative organisms. *Expert Opinion on Drug Safety* **2012,** *11* (2), 221-233.
(67) Zhao, L.; Chu, P. K.; Zhang, Y.; Wu, Z. Antibacterial coatings on titanium implants. *Journal of Biomedical Materials Research Part B: Applied Biomaterials* **2009,** *91B* (1), 470-480.
(68) Melaiye, A.; Youngs, W. J. Silver and its application as an antimicrobial agent. *Expert Opinion on Therapeutic Patents* **2005,** *15* (2), 125-130.
(69) Boholm, M.; Arvidsson, R. Controversy over antibacterial silver: implications for environmental and sustainability assessments. *Journal of Cleaner Production* **2014,** *68*, 135-143.
(70) Gambardella, C.; Costa, E.; Piazza, V.; Fabbrocini, A.; Magi, E.; Faimali, M.; Garaventa, F. Effect of silver nanoparticles on marine organisms belonging to different trophic levels. *Marine Environmental Research* **2015,** *111*, 41-49.
(71) Zheng, K.; Setyawati, M. I.; Leong, D. T.; Xie, J. Antimicrobial gold nanoclusters. *ACS Nano* **2017,** *11* (7), 6904-6910.
(72) Grass, G.; Rensing, C.; Solioz, M. Metallic copper as an antimicrobial surface. *Applied and Environmental Microbiology* **2011,** *77* (5), 1541.
(73) Campbell, A. A.; Song, L.; Li, X. S.; Nelson, B. J.; Bottoni, C.; Brooks, D. E.; DeJong, E. S. Development, characterization, and anti-microbial efficacy of hydroxyapatite-chlorhexidine coatings produced by surface-induced mineralization. *Journal of Biomedical Materials Research* **2000,** *53* (4), 400-407.
(74) Morra, M.; Cassinelli, C.; Cascardo, G.; Carpi, A.; Fini, M.; Giavaresi, G.; Giardino, R. Adsorption of cationic antibacterial on collagen-coated titanium implant devices. *Biomedicine and Pharmacotherapy* **2004,** *58* (8), 418-422.
(75) Heasman, P. A.; Heasman, L.; Stacey, F.; McCracken, G. I. Local delivery of chlorhexidine gluconate (PerioChipTM) in periodontal maintenance patients. *Journal of Clinical Periodontology* **2001,** *28* (1), 90-95.
(76) Uçkay, I.; Hoffmeyer, P.; Lew, D.; Pittet, D. Prevention of surgical site infections in orthopaedic surgery and bone trauma: state-of-the-art update. *Journal of Hospital Infection* **2013,** *84* (1), 5-12.
(77) Yin, J. M.; Liu, Z. T.; Zhao, S. C.; Guo, Y. J. Diagnosis, management, and prevention of prosthetic joint infections *Front Biosci (Landmark Ed)* [Online], **2013**, p. 1349-1357.

(78) Campoccia, D.; Montanaro, L.; Arciola, C. R. A review of the biomaterials technologies for infection-resistant surfaces. *Biomaterials* **2013,** *34* (34), 8533-8554.
(79) Lichter, J. A.; Van Vliet, K. J.; Rubner, M. F. Design of antibacterial surfaces and interfaces: polyelectrolyte multilayers as a multifunctional platform. *Macromolecules* **2009,** *42* (22), 8573-8586.
(80) Patti, J. M.; Allen, B. L.; McGavin, M. J.; Höök, M. Mscramm-mediated adherence of microorganisms to host tissues. *Annual Review of Microbiology* **1994,** *48* (1), 585-617.
(81) Montanaro, L.; Speziale, P.; Campoccia, D.; Ravaioli, S.; Cangini, I.; Pietrocola, G.; Giannini, S.; Arciola, C. R. Scenery of Staphylococcus implant infections in orthopedics. *Future Microbiology* **2011,** *6* (11), 1329-1349.
(82) Muszanska, A. K.; Rochford, E. T. J.; Gruszka, A.; Bastian, A. A.; Busscher, H. J.; Norde, W.; van der Mei, H. C.; Herrmann, A. Antiadhesive polymer brush coating functionalized with antimicrobial and RGD peptides to reduce biofilm formation and enhance tissue integration. *Biomacromolecules* **2014,** *15* (6), 2019-2026.
(83) Humblot, V.; Yala, J. F.; Thebault, P.; Boukerma, K.; Héquet, A.; Berjeaud, J. M.; Pradier, C. M. The antibacterial activity of Magainin I immobilized onto mixed thiols self-assembled monolayers. *Biomaterials* **2009,** *30* (21), 3503-3512.
(84) Ge, X.; Leng, Y.; Lu, X.; Ren, F.; Wang, K.; Ding, Y.; Yang, M. Bacterial responses to periodic micropillar array. *Journal of Biomedical Materials Research Part A* **2015,** *103* (1), 384-396.
(85) Yang, M.; Ding, Y.; Ge, X.; Leng, Y. Control of bacterial adhesion and growth on honeycomb-like patterned surfaces. *Colloids and Surfaces B: Biointerfaces* **2015,** *135*, 549-555.
(86) Montanaro, L.; Poggi, A.; Visai, L.; Ravaioli, S.; Campoccia, D.; Speziale, P.; Arciola, C. R. Extracellular DNA in biofilms. *The International Journal of Artificial Organs* **2011,** *34* (9), 824-831.
(87) Arciola, C. R.; Montanaro, L.; Costerton, J. W. New Trends in Diagnosis and Control Strategies for Implant Infections. *The International Journal of Artificial Organs* **2011,** *34* (9), 727-736.
(88) Chromek, M.; Slamová, Z.; Bergman, P.; Kovács, L.; Podracká, L. u.; Ehrén, I.; Hökfelt, T.; Gudmundsson, G. H.; Gallo, R. L.; Agerberth, B.; Brauner, A. The antimicrobial peptide cathelicidin protects the urinary tract against invasive bacterial infection. *Nature Medicine* **2006,** *12* (6), 636-641.
(89) Punyani, S.; Singh, H. Preparation of iodine containing quaternary amine methacrylate copolymers and their contact killing antimicrobial properties. *Journal of Applied Polymer Science* **2006,** *102* (2), 1038-1044.
(90) Darouiche, R. O.; Mansouri, M. D.; Gawande, P. V.; Madhyastha, S. Antimicrobial and antibiofilm efficacy of triclosan and DispersinB® combination. *Journal of Antimicrobial Chemotherapy* **2009,** *64* (1), 88-93.
(91) Mansouri, M. D.; Hull, R. A.; Stager, C. E.; Cadle, R. M.; Darouiche, R. O. In vitro activity and durability of a combination of an antibiofilm and an antibiotic against vascular catheter colonization. *Antimicrobial Agents and Chemotherapy* **2013,** *57* (1), 621.
(92) Banerjee, M.; Mallick, S.; Paul, A.; Chattopadhyay, A.; Ghosh, S. S. Heightened reactive oxygen species generation in the antimicrobial activity of a three component iodinated chitosan−silver nanoparticle composite. *Langmuir* **2010,** *26* (8), 5901-5908.
(93) Amitai, G.; Andersen, J.; Wargo, S.; Asche, G.; Chir, J.; Koepsel, R.; Russell, A. J. Polyurethane-based leukocyte-inspired biocidal materials. *Biomaterials* **2009,** *30* (33), 6522-6529.
(94) Nablo, B. J.; Prichard, H. L.; Butler, R. D.; Klitzman, B.; Schoenfisch, M. H. Inhibition of implant-associated infections via nitric oxide release. *Biomaterials* **2005,** *26* (34), 6984-6990.

(95) Fu, J.; Ji, J.; Yuan, W.; Shen, J. Construction of anti-adhesive and antibacterial multilayer films via layer-by-layer assembly of heparin and chitosan. *Biomaterials* **2005,** *26* (33), 6684-6692.
(96) Yang, Y.; Qi, P. K.; Yang, Z. L.; Huang, N. Nitric oxide based strategies for applications of biomedical devices. *Biosurface and Biotribology* **2015,** *1* (3), 177-201.
(97) Kumar, S.; Singh, R. K.; Bhardwaj, T. R. Therapeutic role of nitric oxide as emerging molecule. *Biomedicine and Pharmacotherapy* **2017,** *85*, 182-201.
(98) Rees, D. D.; Palmer, R. M.; Moncada, S. Role of endothelium-derived nitric oxide in the regulation of blood pressure. *Proceedings of the National Academy of Sciences* **1989,** *86* (9), 3375.
(99) Schäffer, M. R.; Tantry, U.; Gross, S. S.; Wasserkrug, H. L.; Barbul, A. Nitric oxide regulates wound healing. *Journal of Surgical Research* **1996,** *63* (1), 237-240.
(100) Bogdan, C. Nitric oxide and the immune response. *Nature Immunology* **2001,** *2* (10), 907-916.
(101) Wink, D. A.; Hines, H. B.; Cheng, R. Y. S.; Switzer, C. H.; Flores-Santana, W.; Vitek, M. P.; Ridnour, L. A.; Colton, C. A. Nitric oxide and redox mechanisms in the immune response. *Journal of Leukocyte Biology* **2011,** *89* (6), 873-891.
(102) Kalyanaraman, H.; Schall, N.; Pilz, R. B. Nitric oxide and cyclic GMP functions in bone. *Nitric Oxide* **2018,** *76*, 62-70.
(103) Kalyanaraman, H.; Ramdani, G.; Joshua, J.; Schall, N.; Boss, G. R.; Cory, E.; Sah, R. L.; Casteel, D. E.; Pilz, R. B. A Novel, Direct NO donor regulates osteoblast and osteoclast functions and increases bone mass in ovariectomized mice. *Journal of Bone and Mineral Research* **2017,** *32* (1), 46-59.
(104) Williams, D. L. H. A chemist's view of the nitric oxide story. *Organic and Biomolecular Chemistry* **2003,** *1* (3), 441-449.
(105) Griffith, O. W.; Stuehr, D. J. Nitric oxide synthases: properties and catalytic mechanism. *Annual Review of Physiology* **1995,** *57* (1), 707-734.
(106) Schairer, D. O.; Chouake, J. S.; Nosanchuk, J. D.; Friedman, A. J. The potential of nitric oxide releasing therapies as antimicrobial agents. *Virulence* **2012,** *3* (3), 271-279.
(107) Nurhasni, H.; Cao, J.; Choi, M.; Kim, I.; Lee, B. L.; Jung, Y.; Yoo, J. W. Nitric oxide-releasing poly(lactic-co-glycolic acid)-polyethylenimine nanoparticles for prolonged nitric oxide release, antibacterial efficacy, and in vivo wound healing activity. *International Journal of Nanomedicine* **2015,** *10*, 3065-3080.
(108) Hetrick, E. M.; Shin, J. H.; Stasko, N. A.; Johnson, C. B.; Wespe, D. A.; Holmuhamedov, E.; Schoenfisch, M. H. Bactericidal efficacy of nitric oxide-releasing silica nanoparticles. *ACS Nano* **2008,** *2* (2), 235-246.
(109) Wink, D. A.; Kasprzak, K. S.; Maragos, C. M.; Elespuru, R. K.; Misra, M.; Dunams, T. M.; Cebula, T. A.; Koch, W. H.; Andrews, A. W.; Allen, J. S.; et, a. DNA deaminating ability and genotoxicity of nitric oxide and its progenitors. *Science* **1991,** *254* (5034), 1001.
(110) Carpenter, A. W.; Schoenfisch, M. H. Nitric oxide release: Part II. Therapeutic applications. *Chemical Society Reviews* **2012,** *41* (10), 3742-3752.
(111) Privett, B. J.; Broadnax, A. D.; Bauman, S. J.; Riccio, D. A.; Schoenfisch, M. H. Examination of bacterial resistance to exogenous nitric oxide. *Nitric Oxide* **2012,** *26* (3), 169-173.
(112) Quinn, J. F.; Whittaker, M. R.; Davis, T. P. Delivering nitric oxide with nanoparticles. *Journal of Controlled Release* **2015,** *205*, 190-205.
(113) Miller, C.; McMullin, B.; Ghaffari, A.; Stenzler, A.; Pick, N.; Roscoe, D.; Ghahary, A.; Road, J.; Av-Gay, Y. Gaseous nitric oxide bactericidal activity retained during intermittent high-dose short duration exposure. *Nitric Oxide* **2009,** *20* (1), 16-23.

(114) Miller, C. C.; Hergott, C. A.; Rohan, M.; Arsenault-Mehta, K.; Döring, G.; Mehta, S. Inhaled nitric oxide decreases the bacterial load in a rat model of Pseudomonas aeruginosa pneumonia. *Journal of Cystic Fibrosis* **2013,** *12* (6), 817-820.
(115) Arora, D. P.; Hossain, S.; Xu, Y.; Boon, E. M. Nitric oxide regulation of bacterial biofilms. *Biochemistry* **2015,** *54* (24), 3717-3728.
(116) Barraud, N.; Storey, M. V.; Moore, Z. P.; Webb, J. S.; Rice, S. A.; Kjelleberg, S. Nitric oxide-mediated dispersal in single- and multi-species biofilms of clinically and industrially relevant microorganisms. *Microbial Biotechnology* **2009,** *2* (3), 370-378.
(117) Wo, Y.; Brisbois, E. J.; Bartlett, R. H.; Meyerhoff, M. E. Recent advances in thromboresistant and antimicrobial polymers for biomedical applications: just say yes to nitric oxide (NO). *Biomaterials Science* **2016,** *4* (8), 1161-1183.
(118) Barraud, N.; Hassett, D. J.; Hwang, S. H.; Rice, S. A.; Kjelleberg, S.; Webb, J. S. Involvement of nitric oxide in biofilm dispersal of Pseudomonas aeruginosa. *Journal of Bacteriology* **2006,** *188* (21), 7344.
(119) Neufeld, B. H.; Reynolds, M. M. Critical nitric oxide concentration for Pseudomonas aeruginosa biofilm reduction on polyurethane substrates. *Biointerphases* **2016,** *11* (3), 031012.
(120) Duan, J.; Kasper, D. L. Oxidative depolymerization of polysaccharides by reactive oxygen/nitrogen species. *Glycobiology* **2011,** *21* (4), 401-409.
(121) Yang, L.; Feura, E. S.; Ahonen, M. J. R.; Schoenfisch, M. H. Nitric oxide–releasing macromolecular scaffolds for antibacterial applications. *Advanced Healthcare Materials* **2018,** *7* (13), 1800155.
(122) Teitelbaum, S. L. Bone resorption by osteoclasts. *Science* **2000,** *289* (5484), 1504.
(123) Van'T Hof, R. J.; Ralston, S. H. Nitric oxide and bone. *Immunology* **2001,** *103* (3), 255-261.
(124) Meesters, D. M.; Neubert, S.; Wijnands, K. A. P.; Heyer, F. L.; Zeiter, S.; Ito, K.; Brink, P. R. G.; Poeze, M. Deficiency of inducible and endothelial nitric oxide synthase results in diminished bone formation and delayed union and nonunion development. *Bone* **2016,** *83*, 111-118.
(125) Klein-Nulend, J.; van Oers, R. F. M.; Bakker, A. D.; Bacabac, R. G. Nitric oxide signaling in mechanical adaptation of bone. *Osteoporosis International* **2014,** *25* (5), 1427-1437.
(126) Wimalawansa, S. J. Rationale for using nitric oxide donor therapy for prevention of bone loss and treatment of osteoporosis in humans. *Annals of the New York Academy of Sciences* **2007,** *1117* (1), 283-297.
(127) Diwan, A. D.; Wang, M. X.; Jang, D.; Zhu, W.; Murrell, G. A. C. Nitric Oxide Modulates Fracture Healing. *Journal of Bone and Mineral Research* **2000,** *15* (2), 342-351.
(128) Baldik, Y.; Diwan, A. D.; Appleyard, R. C.; Ming Fang, Z.; Wang, Y.; Murrell, G. A. C. Deletion of iNOS gene impairs mouse fracture healing. *Bone* **2005,** *37* (1), 32-36.
(129) van; t Hof, R. J.; Armour, K. J.; Smith, L. M.; Armour, K. E.; Wei, X. Q.; Liew, F. Y.; Ralston, S. H. Requirement of the inducible nitric oxide synthase pathway for IL-1-induced osteoclastic bone resorption. *Proceedings of the National Academy of Sciences* **2000,** *97* (14), 7993.
(130) O'Shaughnessy, M. C.; Polak, J. M.; Afzal, F.; Hukkanen, M. V. J.; Huang, P.; MacIntyre, I.; Buttery, L. D. K. Nitric oxide mediates 17β-estradiol-stimulated human and rodent osteoblast proliferation and differentiation. *Biochemical and Biophysical Research Communications* **2000,** *277* (3), 604-610.
(131) Collin-Osdoby, P.; Rothe, L.; Bekker, S.; Anderson, F.; Osdoby, P. Decreased nitric oxide levels stimulate osteoclastogenesis and bone resorption both in vitro and in vivo on the chick chorioallantoic membrane in association with neoangiogenesis. *Journal of Bone and Mineral Research* **2000,** *15* (3), 474-488.

(132) Rubin, J.; Murphy, T.; Nanes, M. S.; Fan, X. Mechanical strain inhibits expression of osteoclast differentiation factor by murine stromal cells. *American Journal of Physiology-Cell Physiology* **2000,** *278* (6), C1126-C1132.
(133) Otsuka, E.; Hirano, K.; Matsushita, S.; Inoue, A.; Shigehisa, H.; Yamaguchi, A.; Hagiwara, H. Effects of nitric oxide from exogenous nitric oxide donors on osteoblastic metabolism. *European Journal of Pharmacology* **1998,** *349* (2), 345-350.
(134) Mancini, L.; Moradi-Bidhendi, N.; Becherini, L.; Martineti, V.; MacIntyre, I. The biphasic effects of nitric oxide in primary rat osteoblasts are cGMP dependent. *Biochemical and Biophysical Research Communications* **2000,** *274* (2), 477-481.
(135) Nichols, S. P.; Storm, W. L.; Koh, A.; Schoenfisch, M. H. Local delivery of nitric oxide: Targeted delivery of therapeutics to bone and connective tissues. *Advanced Drug Delivery Reviews* **2012,** *64* (12), 1177-1188.
(136) Kanaoka, K.; Kobayashi, Y.; Hashimoto, F.; Nakashima, T.; Shibata, M.; Kobayashi, K.; Kato, Y.; Sakai, H. A common downstream signaling activity of osteoclast survival factors that prevent nitric oxide-promoted osteoclast apoptosis*. *Endocrinology* **2000,** *141* (8), 2995-3005.
(137) Drago, R. S.; Karstetter, B. R. The reaction of nitrogen (II) oxide with various primary and secondary amines. *Journal of the American Chemical Society* **1961,** *83* (8), 1819-1822.
(138) Hrabie, J. A.; Keefer, L. K. Chemistry of the nitric oxide-releasing diazeniumdiolate ("nitrosohydroxylamine") functional group and its oxygen-substituted derivatives. *Chemical Reviews* **2002,** *102* (4), 1135-1154.
(139) Maragos, C. M.; Morley, D.; Wink, D. A.; Dunams, T. M.; Saavedra, J. E.; Hoffman, A.; Bove, A. A.; Isaac, L.; Hrabie, J. A.; Keefer, L. K. Complexes of .NO with nucleophiles as agents for the controlled biological release of nitric oxide. Vasorelaxant effects. *Journal of Medicinal Chemistry* **1991,** *34* (11), 3242-3247.
(140) Hrabie, J. A.; Klose, J. R.; Wink, D. A.; Keefer, L. K. New nitric oxide-releasing zwitterions derived from polyamines. *The Journal of Organic Chemistry* **1993,** *58* (6), 1472-1476.
(141) Fleming, G.; Aveyard, J.; Fothergill, J. L.; McBride, F.; Raval, R.; D'Sa, R. A. Nitric oxide releasing polymeric coatings for the prevention of biofilm formation. *Polymers* **2017,** *9* (11), 601.
(142) Stasko, N. A.; Schoenfisch, M. H. Dendrimers as a scaffold for nitric oxide release. *Journal of the American Chemical Society* **2006,** *128* (25), 8265-8271.
(143) Keefer, L. K. Progress toward clinical application of the nitric oxide–releasing diazeniumdiolates. *Annual Review of Pharmacology and Toxicology* **2003,** *43* (1), 585-607.
(144) Williams, D. L. H. The chemistry of S-nitrosothiols. *Accounts of chemical research* **1999,** *32* (10), 869-876.
(145) Wang, P. G.; Xian, M.; Tang, X.; Wu, X.; Wen, Z.; Cai, T.; Janczuk, A. J. Nitric oxide donors: chemical activities and biological applications. *Chemical Reviews* **2002,** *102* (4), 1091-1134.
(146) Divakaran, S.; Loscalzo, J. The role of nitroglycerin and other nitrogen oxides in cardiovascular therapeutics. *Journal of the American College of Cardiology* **2017,** *70* (19), 2393.
(147) Matthews, E. K.; Seaton, E. D.; Forsyth, M. J.; Humphrey, P. P. A. Photon pharmacology of an iron-sulphur cluster nitrosyl compound acting on smooth muscle. *British Journal of Pharmacology* **1994,** *113* (1), 87-94.
(148) Keefer, L. K.; Nims, R. W.; Davies, K. M.; Wink, D. A. "NONOates" (1-substituted diazen-1-ium-1,2-diolates) as nitric oxide donors: Convenient nitric oxide dosage forms. In *Methods in Enzymology*; Academic Press: **1996**; pp 281-293.
(149) Ignarro, L. J.; Lippton, H.; Edwards, J. a.; Baricos, W. H.; Hyman, A. L.; Kadowitz, P. J.; Gruetter, C. A. Mechanism of vascular smooth muscle relaxation by organic nitrates, nitrites, nitroprusside and nitric oxide: evidence for the involvement of S-nitrosothiols as active

intermediates. *Journal of Pharmacology and Experimental Therapeutics* **1981,** *218* (3), 739-749.
(150) Daiber, A.; Wenzel, P.; Oelze, M.; Münzel, T. New insights into bioactivation of organic nitrates, nitrate tolerance and cross-tolerance. *Clinical Research in Cardiology* **2008,** *97* (1), 12-20.
(151) Hogg, N. Biological chemistry and clinical potential of S-nitrosothiols. *Free Radical Biology and Medicine* **2000,** *28* (10), 1478-1486.
(152) Scatena, R.; Bottoni, P.; Martorana, G. E.; Giardina, B. Nitric oxide donor drugs: an update on pathophysiology and therapeutic potential. *Expert Opinion on Investigational Drugs* **2005,** *14* (7), 835-846.
(153) Richardson, G.; Benjamin, N. Potential therapeutic uses for S-nitrosothiols. *Clinical Science* **2001,** *102* (1), 99-105.
(154) Carpenter, A. W.; Reighard, K. P.; Saavedra, J. E.; Schoenfisch, M. H. O 2-Protected diazeniumdiolate-modified silica nanoparticles for extended nitric oxide release from dental composites. *Biomaterials Science* **2013,** *1* (5), 456-459.
(155) Nandurdikar, R. S.; Maciag, A. E.; Holland, R. J.; Cao, Z.; Shami, P. J.; Anderson, L. M.; Keefer, L. K.; Saavedra, J. E. Structural modifications modulate stability of glutathione-activated arylated diazeniumdiolate prodrugs. *Bioorganic and Medicinal Chemistry* **2012,** *20* (9), 3094-3099.
(156) Li, M.; Aveyard, J.; Fleming, G.; Curran, J. M.; McBride, F.; Raval, R.; D'Sa, R. A. Nitric oxide releasing titanium surfaces for antimicrobial bone-integrating orthopedic implants. *ACS Applied Materials and Interfaces* **2020,** *12* (20), 22433-22443.
(157) Shin, J. H.; Metzger, S. K.; Schoenfisch, M. H. Synthesis of nitric oxide-releasing silica nanoparticles. *Journal of the American Chemical Society* **2007,** *129* (15), 4612-4619.
(158) Sayari, A.; Hamoudi, S. Periodic mesoporous silica-based organic–inorganic nanocomposite materials. *Chemistry of Materials* **2001,** *13* (10), 3151-3168.
(159) Stein, A.; Melde, B. J.; Schroden, R. C. Hybrid inorganic–organic mesoporous silicates—nanoscopic reactors coming of age. *Advanced Materials* **2000,** *12* (19), 1403-1419.
(160) Zhang, H.; Annich, G. M.; Miskulin, J.; Stankiewicz, K.; Osterholzer, K.; Merz, S. I.; Bartlett, R. H.; Meyerhoff, M. E. Nitric oxide-releasing fumed silica particles: synthesis, characterization, and biomedical application. *Journal of the American Chemical Society* **2003,** *125* (17), 5015-5024.
(161) Polizzi, M. A.; Stasko, N. A.; Schoenfisch, M. H. Water-soluble nitric oxide-releasing gold nanoparticles. *Langmuir* **2007,** *23* (9), 4938-4943.
(162) Tan, L.; Wan, A.; Li, H. Quantum dots-poly(N-isopropylacrylamide) hybrid nanogel diazeniumdiolates as donors and real-time probes of nitric oxide. *Materials Chemistry and Physics* **2013,** *138* (2), 956-962.
(163) Di Meo, C.; Capitani, D.; Mannina, L.; Brancaleoni, E.; Galesso, D.; De Luca, G.; Crescenzi, V. Synthesis and NMR characterization of new hyaluronan-based NO donors. *Biomacromolecules* **2006,** *7* (4), 1253-1260.
(164) Wan, A.; Gao, Q.; Li, H. Effects of molecular weight and degree of acetylation on the release of nitric oxide from chitosan-nitric oxide adducts. *Journal of Applied Polymer Science* **2010,** *117* (4), 2183-2188.
(165) Jin, H.; Yang, L.; Ahonen, M. J. R.; Schoenfisch, M. H. Nitric oxide-releasing cyclodextrins. *Journal of the American Chemical Society* **2018,** *140* (43), 14178-14184.
(166) Ahonen, M. J. R.; Suchyta, D. J.; Zhu, H.; Schoenfisch, M. H. Nitric oxide-releasing alginates. *Biomacromolecules* **2018,** *19* (4), 1189-1197.
(167) Lu, Y.; Slomberg, D. L.; Schoenfisch, M. H. Nitric oxide-releasing chitosan oligosaccharides as antibacterial agents. *Biomaterials* **2014,** *35* (5), 1716-1724.

(168) Liu, T.; Zhang, D.; Yang, X.; Li, C. Silica/polymer microspheres and hollow polymer microspheres as scaffolds for nitric oxide release in PBS buffer and bovine serum. *Polymer Chemistry* **2015,** *6* (9), 1512-1520.
(169) Huang, S. L.; Kee, P. H.; Kim, H.; Moody, M. R.; Chrzanowski, S. M.; MacDonald, R. C.; McPherson, D. D. Nitric oxide-loaded echogenic liposomes for nitric oxide delivery and inhibition of intimal hyperplasia. *Journal of the American College of Cardiology* **2009,** *54* (7), 652.
(170) Suchyta, D. J.; Schoenfisch, M. H. Controlled release of nitric oxide from liposomes. *ACS Biomaterials Science and Engineering* **2017,** *3* (9), 2136-2143.
(171) Anguita-Alonso, P.; Giacometti, A.; Cirioni, O.; Ghiselli, R.; Orlando, F.; Saba, V.; Scalise, G.; Sevo, M.; Tuzova, M.; Patel, R.; Balaban, N. RNAIII-inhibiting-peptide-loaded polymethylmethacrylate prevents in vivo Staphylococcus aureus biofilm formation. *Antimicrobial Agents and Chemotherapy* **2007,** *51* (7), 2594.
(172) Stensballe, J.; Tvede, M.; Looms, D.; Lippert, F. K.; Dahl, B.; Tønnesen, E.; Rasmussen, L. S. Infection risk with nitrofurazone-impregnated urinary catheters in trauma patients. *Annals of Internal Medicine* **2007,** *147* (5), 285-293.
(173) Sadrearhami, Z.; Shafiee, F. N.; Ho, K. K. K.; Kumar, N.; Krasowska, M.; Blencowe, A.; Wong, E. H. H.; Boyer, C. Antibiofilm nitric oxide-releasing polydopamine coatings. *ACS Applied Materials and Interfaces* **2019,** *11* (7), 7320-7329.
(174) Riccio, D. A.; Schoenfisch, M. H. Nitric oxide release: Part I. Macromolecular scaffolds. *Chemical Society Reviews* **2012,** *41* (10), 3731-3741.
(175) Smith, D. J.; Chakravarthy, D.; Pulfer, S.; Simmons, M. L.; Hrabie, J. A.; Citro, M. L.; Saavedra, J. E.; Davies, K. M.; Hutsell, T. C.; Mooradian, D. L.; Hanson, S. R.; Keefer, L. K. Nitric Oxide-releasing polymers containing the [N(O)NO]- group. *Journal of Medicinal Chemistry* **1996,** *39* (5), 1148-1156.
(176) Nablo, B. J.; Schoenfisch, M. H. Poly(vinyl chloride)-coated sol−gels for studying the effects of nitric oxide release on bacterial adhesion. *Biomacromolecules* **2004,** *5* (5), 2034-2041.
(177) Ho, K. K. K.; Ozcelik, B.; Willcox, M. D. P.; Thissen, H.; Kumar, N. Facile solvent-free fabrication of nitric oxide (NO)-releasing coatings for prevention of biofilm formation. *Chemical Communications* **2017,** *53* (48), 6488-6491.
(178) Koh, A.; Riccio, D. A.; Sun, B.; Carpenter, A. W.; Nichols, S. P.; Schoenfisch, M. H. Fabrication of nitric oxide-releasing polyurethane glucose sensor membranes. *Biosensors and Bioelectronics* **2011,** *28* (1), 17-24.
(179) Buser, D.; Dahlin, C.; Schenk, R. Guided bone regeneration. *Chicago Quintessence* **1994**.
(180) Bottino, M. C.; Thomas, V.; Janowski, G. M. A novel spatially designed and functionally graded electrospun membrane for periodontal regeneration. *Acta Biomaterialia* **2011,** *7* (1), 216-224.
(181) Dahlin, C.; Linde, A.; Gottlow, J.; Nyman, S. Healing of bone defects by guided tissue regeneration. *Plastic and Reconstructive Surgery* **1988,** *81* (5).
(182) Piattelli, A.; Scarano, A.; Paolantonio, M. Bone formation inside the material interstices of e-PTFE membranes: a light microscopical and histochemical study in man. *Biomaterials* **1996,** *17* (17), 1725-1731.
(183) Piattelli, A.; Podda, G.; Scarano, A. Clinical and histological results in alveolar ridge enlargement using coralline calcium carbonate. *Biomaterials* **1997,** *18* (8), 623-627.
(184) Scantlebury, T. V. 1982-1992: A decade of technology development for guided tissue regeneration. *Journal of Periodontology* **1993,** *64* (11S), 1129-1137.
(185) Geetha, M.; Singh, A. K.; Asokamani, R.; Gogia, A. K. Ti based biomaterials, the ultimate choice for orthopaedic implants – A review. *Progress in Materials Science* **2009,** *54* (3), 397-425.

(186) Williams, D. F. On the mechanisms of biocompatibility. *Biomaterials* **2008,** *29* (20), 2941-2953.
(187) Viceconti, M.; Muccini, R.; Bernakiewicz, M.; Baleani, M.; Cristofolini, L. Large-sliding contact elements accurately predict levels of bone–implant micromotion relevant to osseointegration. *Journal of Biomechanics* **2000,** *33* (12), 1611-1618.
(188) Zhang, J.; Xu, Q.; Huang, C.; Mo, A.; Li, J.; Zuo, Y. Biological properties of an anti-bacterial membrane for guided bone regeneration: an experimental study in rats. *Clinical Oral Implants Research* **2010,** *21* (3), 321-327.
(189) Hutmacher, D.; Hürzeler, M. B.; Schliephake, H. A review of material properties of biodegradable and bioresorbable polymers and devices for GTR and GBR applications. *International Journal of Oral and Maxillofacial Implants* **1996,** *11* (5), 667-678.
(190) Brunette, D. M.; Tengvall, P.; Textor, M.; Thomsen, P. *Titanium in medicine: material science, surface science, engineering, biological responses and medical applications*, Springer Science and Business Media: **2012**.
(191) Liu, X.; Chu, P. K.; Ding, C. Surface modification of titanium, titanium alloys, and related materials for biomedical applications. *Materials Science and Engineering: R: Reports* **2004,** *47* (3), 49-121.
(192) Morra, M. Biochemical modification of titanium surfaces: peptides and ECM proteins. *European Cells and Materials Journal* **2006,** *12* (1), 15.
(193) Xiao, S. J.; Kenausis, G.; Textor, M. Biochemical modification of titanium surfaces. In *Titanium in Medicine: Material Science, Surface Science, Engineering, Biological Responses and Medical Applications*; Brunette, D. M.; Tengvall, P.; Textor, M.; Thomsen, P., Eds.; Springer Berlin Heidelberg: Berlin, Heidelberg, **2001**; pp 417-455.
(194) Iwasaki, Y.; Saito, N. Immobilization of phosphorylcholine polymers to Ti-supported vinyldimethylsilyl monolayers and reduction of albumin adsorption. *Colloids and Surfaces B: Biointerfaces* **2003,** *32* (1), 77-84.
(195) Tosatti, S.; Paul, S. M. D.; Askendal, A.; VandeVondele, S.; Hubbell, J. A.; Tengvall, P.; Textor, M. Peptide functionalized poly(l-lysine)-g-poly(ethylene glycol) on titanium: resistance to protein adsorption in full heparinized human blood plasma. *Biomaterials* **2003,** *24* (27), 4949-4958.
(196) Matinlinna, J. P.; Areva, S.; Lassila, L. V. J.; Vallittu, P. K. Characterization of siloxane films on titanium substrate derived from three aminosilanes. *Surface and Interface Analysis* **2004,** *36* (9), 1314-1322.
(197) Söderholm, K. J. M.; Lambrechts, P.; Sarrett, D.; Abe, Y.; Yang, M. C. K.; Labella, R.; Yildiz, E.; Willems, G. Clinical wear performance of eight experimental dental composites over three years determined by two measuring methods. *European Journal of Oral Sciences* **2001,** *109* (4), 273-281.
(198) Bronzino, J. D. *Biomedical Engineering Handbook 2*, Springer Science and Business Media: 2000; Vol. 2.
(199) Plueddemann, E. P. Adhesion through silane coupling agents. *The Journal of Adhesion* **1970,** *2* (3), 184-201.
(200) Arkles, B.; Steinmetz, J.; Zazyczny, J.; Mehta, P. Silanes and other coupling agents. *Ed. KL Mittal, VSP* **1992**, 91-104.
(201) Matinlinna, J. P.; Lassila, L. V. J.; Özcan, M.; Yli-Urpo, A.; Vallittu, P. K. An introduction to silanes and their clinical applications in dentistry. *International Journal of Prosthodontics* **2004,** *17* (2), 155-164.
(202) Asenath Smith, E.; Chen, W. How to prevent the loss of surface functionality derived from aminosilanes. *Langmuir* **2008,** *24* (21), 12405-12409.
(203) Zhu, M.; Lerum, M. Z.; Chen, W. How to prepare reproducible, homogeneous, and hydrolytically stable aminosilane-derived layers on silica. *Langmuir* **2012,** *28* (1), 416-423.

(204) Matinlinna, J. P.; Laajalehto, K.; Laiho, T.; Kangasniemi, I.; Lassila, L. V. J.; Vallittu, P. K. Surface analysis of Co–Cr–Mo alloy and Ti substrates silanized with trialkoxysilanes and silane mixtures. *Surface and Interface Analysis* **2004,** *36* (3), 246-253.
(205) Kanan, S. M.; Tze, W. T. Y.; Tripp, C. P. Method to double the surface concentration and control the orientation of adsorbed (3-aminopropyl)dimethylethoxysilane on silica powders and glass slides. *Langmuir* **2002,** *18* (17), 6623-6627.
(206) Wu, S.; Liu, X.; Yeung, K. W. K.; Liu, C.; Yang, X. Biomimetic porous scaffolds for bone tissue engineering. *Materials Science and Engineering: R: Reports* **2014,** *80*, 1-36.
(207) Karageorgiou, V.; Kaplan, D. Porosity of 3D biomaterial scaffolds and osteogenesis. *Biomaterials* **2005,** *26* (27), 5474-5491.
(208) Fujibayashi, S.; Neo, M.; Kim, H. M.; Kokubo, T.; Nakamura, T. Osteoinduction of porous bioactive titanium metal. *Biomaterials* **2004,** *25* (3), 443-450.
(209) Marin, E.; Fedrizzi, L.; Zagra, L. Porous metallic structures for orthopaedic applications: a short review of materials and technologies. *European Orthopaedics and Traumatology* **2010,** *1* (3-4), 103-109.
(210) Van Bael, S.; Chai, Y. C.; Truscello, S.; Moesen, M.; Kerckhofs, G.; Van Oosterwyck, H.; Kruth, J. P.; Schrooten, J. The effect of pore geometry on the in vitro biological behavior of human periosteum-derived cells seeded on selective laser-melted Ti6Al4V bone scaffolds. *Acta Biomaterialia* **2012,** *8* (7), 2824-2834.
(211) Zhao, Y. Y.; Fung, T.; Zhang, L. P.; Zhang, F. L. Lost carbonate sintering process for manufacturing metal foams. *Scripta Materialia* **2005,** *52* (4), 295-298.
(212) Lu, X.; Zhao, Y. Effect of flow regime on convective heat transfer in porous copper manufactured by lost carbonate sintering. *International Journal of Heat and Fluid Flow* **2019,** *80*, 108482.
(213) Zhu, P.; Wu, Z.; Zhao, Y. Hierarchical porous Cu with high surface area and fluid permeability. *Scripta Materialia* **2019,** *172*, 119-124.
(214) Diao, K.; Zhang, L.; Zhao, Y. Measurement of tortuosity of porous Cu using a diffusion diaphragm cell. *Measurement* **2017,** *110*, 335-338.
(215) Zhu, P.; Zhao, Y. Mass transfer performance of porous nickel manufactured by lost carbonate sintering process. *Advanced Engineering Materials* **2017,** *19* (12), 1700392.
(216) Liao, S.; Wang, W.; Uo, M.; Ohkawa, S.; Akasaka, T.; Tamura, K.; Cui, F.; Watari, F. A three-layered nano-carbonated hydroxyapatite/collagen/PLGA composite membrane for guided tissue regeneration. *Biomaterials* **2005,** *26* (36), 7564-7571.
(217) Park, Y. J.; Lee, Y. M.; Park, S. N.; Lee, J. Y.; Ku, Y.; Chung, C. P.; Lee, S. J. Enhanced guided bone regeneration by controlled tetracycline release from poly(L-lactide) barrier membranes. *Journal of Biomedical Materials Research* **2000,** *51* (3), 391-397.
(218) Teng, S. H.; Lee, E. J.; Yoon, B. H.; Shin, D. S.; Kim, H. E.; Oh, J. S. Chitosan/nanohydroxyapatite composite membranes via dynamic filtration for guided bone regeneration. *Journal of Biomedical Materials Research Part A* **2009,** *88A* (3), 569-580.
(219) Yang, F.; Both, S. K.; Yang, X.; Walboomers, X. F.; Jansen, J. A. Development of an electrospun nano-apatite/PCL composite membrane for GTR/GBR application. *Acta Biomaterialia* **2009,** *5* (9), 3295-3304.
(220) Rashtchian, M.; Hivechi, A.; Bahrami, S. H.; Milan, P. B.; Simorgh, S. Fabricating alginate/poly(caprolactone) nanofibers with enhanced bio-mechanical properties via cellulose nanocrystal incorporation. *Carbohydrate Polymers* **2020,** *233*, 115873.
(221) Wei, Q. *Functional nanofibers and their applications*, Elsevier: 2012.
(222) Islam, M. S.; Ang, B. C.; Andriyana, A.; Afifi, A. M. A review on fabrication of nanofibers via electrospinning and their applications. *SN Applied Sciences* **2019,** *1* (10), 1248.
(223) Bhardwaj, N.; Kundu, S. C. Electrospinning: A fascinating fiber fabrication technique. *Biotechnology Advances* **2010,** *28* (3), 325-347.

(224) Holzwarth, J. M.; Ma, P. X. Biomimetic nanofibrous scaffolds for bone tissue engineering. *Biomaterials* **2011,** *32* (36), 9622-9629.
(225) Sill, T. J.; von Recum, H. A. Electrospinning: Applications in drug delivery and tissue engineering. *Biomaterials* **2008,** *29* (13), 1989-2006.
(226) Bhattarai, R. S.; Bachu, R. D.; Boddu, S. H.; Bhaduri, S. Biomedical applications of electrospun nanofibers: Drug and nanoparticle delivery. *Pharmaceutics* **2019,** *11* (1), 5.
(227) Yousefzadeh, M. 12 - Modeling and simulation of the electrospinning process. In *Electrospun Nanofibers*; Afshari, M., Ed.; Woodhead Publishing: 2017; pp 277-301.
(228) Taylor, G. I.; Van Dyke, M. D. Electrically driven jets. *Proceedings of the Royal Society of London. A. Mathematical and Physical Sciences* **1969,** *313* (1515), 453-475.
(229) Yarin, A. L.; Koombhongse, S.; Reneker, D. H. Bending instability in electrospinning of nanofibers. *Journal of Applied Physics* **2001,** *89* (5), 3018-3026.
(230) Buchko, C. J.; Chen, L. C.; Shen, Y.; Martin, D. C. Processing and microstructural characterization of porous biocompatible protein polymer thin films. *Polymer* **1999,** *40* (26), 7397-7407.
(231) Yuan, X.; Zhang, Y.; Dong, C.; Sheng, J. Morphology of ultrafine polysulfone fibers prepared by electrospinning. *Polymer International* **2004,** *53* (11), 1704-1710.
(232) Wang, X.; Um, I. C.; Fang, D.; Okamoto, A.; Hsiao, B. S.; Chu, B. Formation of water-resistant hyaluronic acid nanofibers by blowing-assisted electro-spinning and non-toxic post treatments. *Polymer* **2005,** *46* (13), 4853-4867.
(233) Deitzel, J. M.; Kleinmeyer, J.; Harris, D.; Beck Tan, N. C. The effect of processing variables on the morphology of electrospun nanofibers and textiles. *Polymer* **2001,** *42* (1), 261-272.
(234) Doshi, J.; Reneker, D. H. Electrospinning process and applications of electrospun fibers. *Journal of Electrostatics* **1995,** *35* (2), 151-160.
(235) Jiang, H.; Fang, D.; Hsiao, B. S.; Chu, B.; Chen, W. Optimization and characterization of dextran membranes prepared by electrospinning. *Biomacromolecules* **2004,** *5* (2), 326-333.
(236) Huang, L.; Nagapudi, K.; P.Apkarian, R.; Chaikof, E. L. Engineered collagen–PEO nanofibers and fabrics. *Journal of Biomaterials Science, Polymer Edition* **2001,** *12* (9), 979-993.
(237) Kim, B.; Park, H.; Lee, S. H.; Sigmund, W. M. Poly(acrylic acid) nanofibers by electrospinning. *Materials Letters* **2005,** *59* (7), 829-832.
(238) Son, W. K.; Youk, J. H.; Lee, T. S.; Park, W. H. The effects of solution properties and polyelectrolyte on electrospinning of ultrafine poly(ethylene oxide) fibers. *Polymer* **2004,** *45* (9), 2959-2966.
(239) Chen, V. J.; Ma, P. X. Nano-fibrous poly(l-lactic acid) scaffolds with interconnected spherical macropores. *Biomaterials* **2004,** *25* (11), 2065-2073.
(240) Demir, M. M.; Yilgor, I.; Yilgor, E.; Erman, B. Electrospinning of polyurethane fibers. *Polymer* **2002,** *43* (11), 3303-3309.
(241) Koski, A.; Yim, K.; Shivkumar, S. Effect of molecular weight on fibrous PVA produced by electrospinning. *Materials Letters* **2004,** *58* (3), 493-497.
(242) Jun, Z.; Youling, Y.; Kehua, W.; Jian, S.; Sicong, L. Surface modification of segmented poly(ether urethane) by grafting sulfo ammonium zwitterionic monomer to improve hemocompatibilities. *Colloids and Surfaces B: Biointerfaces* **2003,** *28* (1), 1-9.
(243) De Vrieze, S.; Van Camp, T.; Nelvig, A.; Hagström, B.; Westbroek, P.; De Clerck, K. The effect of temperature and humidity on electrospinning. *Journal of Materials Science* **2009,** *44* (5), 1357-1362.
(244) Casper, C. L.; Stephens, J. S.; Tassi, N. G.; Chase, D. B.; Rabolt, J. F. Controlling surface morphology of electrospun polystyrene fibers: effect of humidity and molecular weight in the electrospinning process. *Macromolecules* **2004,** *37* (2), 573-578.

(245) Ding, J.; Zhang, J.; Li, J.; Li, D.; Xiao, C.; Xiao, H.; Yang, H.; Zhuang, X.; Chen, X. Electrospun polymer biomaterials. *Progress in Polymer Science* **2019,** *90*, 1-34.
(246) Agarwal, S.; Wendorff, J. H.; Greiner, A. Use of electrospinning technique for biomedical applications. *Polymer* **2008,** *49* (26), 5603-5621.
(247) Hidalgo Pitaluga, L.; Trevelin Souza, M.; Dutra Zanotto, E.; Santocildes Romero, M. E.; Hatton, P. V. Electrospun F18 bioactive glass/PCL—poly (ε-caprolactone)—membrane for guided tissue regeneration. *Materials* **2018,** *11* (3), 400.
(248) Colley, H. E.; Said, Z.; Santocildes-Romero, M. E.; Baker, S. R.; D'Apice, K.; Hansen, J.; Madsen, L. S.; Thornhill, M. H.; Hatton, P. V.; Murdoch, C. Pre-clinical evaluation of novel mucoadhesive bilayer patches for local delivery of clobetasol-17-propionate to the oral mucosa. *Biomaterials* **2018,** *178*, 134-146.
(249) Clitherow, K. H.; Binaljadm, T. M.; Hansen, J.; Spain, S. G.; Hatton, P. V.; Murdoch, C. Medium-chain fatty acids released from polymeric electrospun patches inhibit Candida albicans growth and reduce the biofilm viability. *ACS Biomaterials Science and Engineering* **2020,** *6* (7), 4087-4095.
(250) Flemming, H. C.; Wingender, J.; Szewzyk, U.; Steinberg, P.; Rice, S. A.; Kjelleberg, S. Biofilms: an emergent form of bacterial life. *Nature Reviews Microbiology* **2016,** *14* (9), 563.
(251) Penesyan, A.; Gillings, M.; Paulsen, I. T. Antibiotic discovery: combatting bacterial resistance in cells and in biofilm communities. *Molecules* **2015,** *20* (4), 5286-5298.
(252) Arciola, C. R.; Campoccia, D.; Speziale, P.; Montanaro, L.; Costerton, J. W. Biofilm formation in Staphylococcus implant infections. A review of molecular mechanisms and implications for biofilm-resistant materials. *Biomaterials* **2012,** *33* (26), 5967-5982.
(253) Zaat, S. A. J.; Broekhuizen, C. A. N.; Riool, M. Host tissue as a niche for biomaterial-associated infection. *Future Microbiology* **2010,** *5* (8), 1149-1151.
(254) Hsieh, P. H.; Lee, M. S.; Hsu, K. Y.; Chang, Y. H.; Shih, H. N.; Ueng, S. W. Gram-negative prosthetic joint infections: risk factors and outcome of treatment. *Clinical Infectious Diseases* **2009,** *49* (7), 1036-1043.
(255) Green, S. A.; Ripley, M. J. Chronic osteomyelitis in pin tracks. *Journal of Bone and Joint Surgery* **1984,** *66* (7), 1092-1098.
(256) Parameswaran, A. D.; Roberts, C. S.; Seligson, D.; Voor, M. Pin tract infection with contemporary external fixation: how much of a problem? *Journal of Orthopaedic Trauma* **2003,** *17* (7).
(257) Feng, Q. L.; Wu, J.; Chen, G. Q.; Cui, F. Z.; Kim, T. N.; Kim, J. O. A mechanistic study of the antibacterial effect of silver ions on Escherichia coli and Staphylococcus aureus. *Journal of Biomedical Materials Research* **2000,** *52* (4), 662-668.
(258) Xu, Z.; Li, M.; Li, X.; Liu, X.; Ma, F.; Wu, S.; Yeung, K. W. K.; Han, Y.; Chu, P. K. Antibacterial activity of silver doped titanate nanowires on Ti implants. *ACS Applied Materials and Interfaces* **2016,** *8* (26), 16584-16594.
(259) Wang, Y. W.; Cao, A.; Jiang, Y.; Zhang, X.; Liu, J. H.; Liu, Y.; Wang, H. Superior antibacterial activity of zinc oxide/graphene oxide composites originating from high zinc concentration localized around bacteria. *ACS Applied Materials and Interfaces* **2014,** *6* (4), 2791-2798.
(260) Zhou, Z. H.; Zhang, Y.; Hu, Y. F.; Wahl, L. M.; Cisar, J. O.; Notkins, A. L. The broad antibacterial activity of the natural antibody repertoire is due to polyreactive antibodies. *Cell Host and Microbe* **2007,** *1* (1), 51-61.
(261) Glinel, K.; Jonas, A. M.; Jouenne, T.; Leprince, J.; Galas, L.; Huck, W. T. S. Antibacterial and antifouling polymer brushes incorporating antimicrobial peptide. *Bioconjugate Chemistry* **2009,** *20* (1), 71-77.
(262) Kazemzadeh-Narbat, M.; Noordin, S.; Masri, B. A.; Garbuz, D. S.; Duncan, C. P.; Hancock, R. E. W.; Wang, R. Drug release and bone growth studies of antimicrobial peptide-loaded

calcium phosphate coating on titanium. *Journal of Biomedical Materials Research Part B: Applied Biomaterials* **2012,** *100B* (5), 1344-1352.
(263) Barraud, N.; J. Kelso, M.; A. Rice, S.; Kjelleberg, S. Nitric oxide: a key mediator of biofilm dispersal with applications in infectious diseases. *Current Pharmaceutical Design* **2015,** *21* (1), 31-42.
(264) Keefer, L. K. Fifty years of diazeniumdiolate research. from laboratory curiosity to broad-spectrum biomedical advances. *ACS Chemical Biology* **2011,** *6* (11), 1147-1155.
(265) Ignarro Louis, J.; Napoli, C.; Loscalzo, J. Nitric oxide donors and cardiovascular agents modulating the bioactivity of nitric oxide. *Circulation Research* **2002,** *90* (1), 21-28.
(266) Bharadwaj, G.; Benini, P. G. Z.; Basudhar, D.; Ramos-Colon, C. N.; Johnson, G. M.; Larriva, M. M.; Keefer, L. K.; Andrei, D.; Miranda, K. M. Analysis of the HNO and NO donating properties of alicyclic amine diazeniumdiolates. *Nitric Oxide* **2014,** *42*, 70-78.
(267) Miranda, K. M.; Katori, T.; Torres de Holding, C. L.; Thomas, L.; Ridnour, L. A.; McLendon, W. J.; Cologna, S. M.; Dutton, A. S.; Champion, H. C.; Mancardi, D.; Tocchetti, C. G.; Saavedra, J. E.; Keefer, L. K.; Houk, K. N.; Fukuto, J. M.; Kass, D. A.; Paolocci, N.; Wink, D. A. Comparison of the NO and HNO donating properties of diazeniumdiolates: primary amine adducts release HNO in vivo. *Journal of Medicinal Chemistry* **2005,** *48* (26), 8220-8228.
(268) Salmon, D. J.; Torres de Holding, C. L.; Thomas, L.; Peterson, K. V.; Goodman, G. P.; Saavedra, J. E.; Srinivasan, A.; Davies, K. M.; Keefer, L. K.; Miranda, K. M. HNO and NO release from a primary amine-based diazeniumdiolate as a function of pH. *Inorganic Chemistry* **2011,** *50* (8), 3262-3270.
(269) Chen, R.; Hunt, J. A.; Fawcett, S.; D'sa, R.; Akhtar, R.; Curran, J. M. The optimization and production of stable homogeneous amine enriched surfaces with characterized nanotopographical properties for enhanced osteoinduction of mesenchymal stem cells. *Journal of Biomedical Materials Research Part A* **2018,** *106* (7), 1862-1877.
(270) Curran, J. M.; Chen, R.; Hunt, J. A. The guidance of human mesenchymal stem cell differentiation in vitro by controlled modifications to the cell substrate. *Biomaterials* **2006,** *27* (27), 4783-4793.
(271) Miles, A. A.; Misra, S. S.; Irwin, J. O. The estimation of the bactericidal power of the blood. *Epidemiology and Infection* **2009,** *38* (6), 732-749.
(272) Fawcett, S. A.; Curran, J. M.; Chen, R.; Rhodes, N. P.; Murphy, M. F.; Wilson, P.; Ranganath, L.; Dillon, J. P.; Gallagher, J. A.; Hunt, J. A. Defining the properties of an array of $–NH_2$-modified substrates for the induction of a mature osteoblast/osteocyte phenotype from a primary human osteoblast population using controlled nanotopography and surface chemistry. *Calcified Tissue International* **2017,** *100* (1), 95-106.
(273) Ragsdale, R. O.; Karstetter, B. R.; Drago, R. S. Decomposition of the adducts of diethylamine and isopropylamine with nitrogen (II) oxide. *Inorganic Chemistry* **1965,** *4* (3), 420-422.
(274) Arkles, B.; Steinmetz, J. R.; Zazyczny, J.; Mehta, P. Factors contributing to the stability of alkoxysilanes in aqueous solution. *Journal of Adhesion Science and Technology* **1992,** *6* (1), 193-206.
(275) Zhang, F.; Sautter, K.; Larsen, A. M.; Findley, D. A.; Davis, R. C.; Samha, H.; Linford, M. R. Chemical vapor deposition of three aminosilanes on silicon dioxide: surface characterization, stability, effects of silane concentration, and cyanine dye adsorption. *Langmuir* **2010,** *26* (18), 14648-14654.
(276) Drees, P.; Eckardt, A.; Gay, R. E.; Gay, S.; Huber, L. C. Mechanisms of Disease: molecular insights into aseptic loosening of orthopedic implants. *Nature Clinical Practice Rheumatology* **2007,** *3* (3), 165-171.
(277) van Hengel, I. A. J.; Riool, M.; Fratila-Apachitei, L. E.; Witte-Bouma, J.; Farrell, E.; Zadpoor, A. A.; Zaat, S. A. J.; Apachitei, I. Selective laser melting porous metallic implants

with immobilized silver nanoparticles kill and prevent biofilm formation by methicillin-resistant Staphylococcus aureus. *Biomaterials* **2017,** *140*, 1-15.
(278) Chen, L. J.; He, H.; Li, Y. M.; Li, T.; Guo, X. P.; Wang, R. F. Finite element analysis of stress at implant–bone interface of dental implants with different structures. *Transactions of Nonferrous Metals Society of China* **2011,** *21* (7), 1602-1610.
(279) Pałka, K.; Adamek, G.; Jakubowicz, J. Compression behavior of Ti foams with spherical and polyhedral pores *Advanced Engineering Materials* **2016,** *18* (8), 1511-1518.
(280) Otsuki, B.; Takemoto, M.; Fujibayashi, S.; Neo, M.; Kokubo, T.; Nakamura, T. Pore throat size and connectivity determine bone and tissue ingrowth into porous implants: Three-dimensional micro-CT based structural analyses of porous bioactive titanium implants. *Biomaterials* **2006,** *27* (35), 5892-5900.
(281) Singh, R.; Lee, P. D.; Dashwood, R. J.; Lindley, T. C. Titanium foams for biomedical applications: a review. *Materials Technology* **2010,** *25* (3-4), 127-136.
(282) Amin Yavari, S.; van der Stok, J.; Chai, Y. C.; Wauthle, R.; Tahmasebi Birgani, Z.; Habibovic, P.; Mulier, M.; Schrooten, J.; Weinans, H.; Zadpoor, A. A. Bone regeneration performance of surface-treated porous titanium. *Biomaterials* **2014,** *35* (24), 6172-6181.
(283) Lu, M.; Zhao, Y., Mechanical properties of LCS porous steel: comparison between the dissolution and decomposition routes. Minerals, Metals and Materials Society/AIME, 420 Commonwealth Dr., P. O. Box …: 2010.
(284) Wink, D. A.; Mitchell, J. B. Chemical biology of nitric oxide: insights into regulatory, cytotoxic, and cytoprotective mechanisms of nitric oxide. *Free Radical Biology and Medicine* **1998,** *25* (4), 434-456.
(285) Palmer, R. M. J.; Ferrige, A. G.; Moncada, S. Nitric oxide release accounts for the biological activity of endothelium-derived relaxing factor. *Nature* **1987,** *327* (6122), 524-526.
(286) Collin-Osdoby, P.; Nickols, G. A.; Osdoby Dr, P. Bone cell function, regulation, and communication: A role for nitric oxide. *Journal of Cellular Biochemistry* **1995,** *57* (3), 399-408.
(287) Nablo, B. J.; Rothrock, A. R.; Schoenfisch, M. H. Nitric oxide-releasing sol–gels as antibacterial coatings for orthopedic implants. *Biomaterials* **2005,** *26* (8), 917-924.
(288) Feelisch, M. The use of nitric oxide donors in pharmacological studies. *Naunyn-Schmiedeberg's archives of pharmacology* **1998,** *358* (1), 113-122.
(289) McFarland, J. The nephelometer:an instrument for estimating the number of bacteria in suspensions used for calculating the opsonic index and for vaccines. *Journal of the American Medical Association* **1907,** *XLIX* (14), 1176-1178.
(290) Clemow, A. J. T.; Weinstein, A. M.; Klawitter, J. J.; Koeneman, J.; Anderson, J. Interface mechanics of porous titanium implants. *Journal of Biomedical Materials Research* **1981,** *15* (1), 73-82.
(291) Zardiackas, L. D.; Parsell, D. E.; Dillon, L. D.; Mitchell, D. W.; Nunnery, L. A.; Poggie, R. Structure, metallurgy, and mechanical properties of a porous tantalum foam. *Journal of Biomedical Materials Research* **2001,** *58* (2), 180-187.
(292) Hollister, S. J. Porous scaffold design for tissue engineering. *Nature Materials* **2005,** *4* (7), 518-524.
(293) Wen, C.; Yamada, Y.; Shimojima, K.; Chino, Y.; Hosokawa, H.; Mabuchi, M. Novel titanium foam for bone tissue engineering. *Journal of materials research* **2002,** *17* (10), 2633-2639.
(294) Müller, U.; Imwinkelried, T.; Horst, M.; Sievers, M.; Graf-Hausner, U. Do human osteoblasts grow into open-porous titanium. *European Cells and Materials* **2006,** *11*, 8-15.
(295) de la Fuente-Núñez, C.; Korolik, V.; Bains, M.; Nguyen, U.; Breidenstein, E. B. M.; Horsman, S.; Lewenza, S.; Burrows, L.; Hancock, R. E. W. Inhibition of bacterial biofilm formation and swarming motility by a small synthetic cationic peptide. *Antimicrobial Agents and Chemotherapy* **2012,** *56* (5), 2696.

(296) Crémet, L.; Corvec, S.; Bémer, P.; Bret, L.; Lebrun, C.; Lesimple, B.; Miegeville, A. F.; Reynaud, A.; Lepelletier, D.; Caroff, N. Orthopaedic-implant infections by Escherichia coli: Molecular and phenotypic analysis of the causative strains. *Journal of Infection* **2012,** *64* (2), 169-175.
(297) Inzana, J. A.; Schwarz, E. M.; Kates, S. L.; Awad, H. A. Biomaterials approaches to treating implant-associated osteomyelitis. *Biomaterials* **2016,** *81*, 58-71.
(298) Cardozo, V. F.; Lancheros, C. A. C.; Narciso, A. M.; Valereto, E. C. S.; Kobayashi, R. K. T.; Seabra, A. B.; Nakazato, G. Evaluation of antibacterial activity of nitric oxide-releasing polymeric particles against Staphylococcus aureus and Escherichia coli from bovine mastitis. *International Journal of Pharmaceutics* **2014,** *473* (1), 20-29.
(299) Charville, G. W.; Hetrick, E. M.; Geer, C. B.; Schoenfisch, M. H. Reduced bacterial adhesion to fibrinogen-coated substrates via nitric oxide release. *Biomaterials* **2008,** *29* (30), 4039-4044.
(300) McDougald, D.; Rice, S. A.; Barraud, N.; Steinberg, P. D.; Kjelleberg, S. Should we stay or should we go: mechanisms and ecological consequences for biofilm dispersal. *Nature Reviews Microbiology* **2012,** *10* (1), 39-50.
(301) Dimitriou, R.; Jones, E.; McGonagle, D.; Giannoudis, P. V. Bone regeneration: current concepts and future directions. *BMC Medicine* **2011,** *9* (1), 66.
(302) Dimitriou, R.; Mataliotakis, G. I.; Calori, G. M.; Giannoudis, P. V. The role of barrier membranes for guided bone regeneration and restoration of large bone defects: current experimental and clinical evidence. *BMC Medicine* **2012,** *10* (1), 81.
(303) Lee, Y. J.; Lee, J. H.; Cho, H. J.; Kim, H. K.; Yoon, T. R.; Shin, H. Electrospun fibers immobilized with bone forming peptide-1 derived from BMP7 for guided bone regeneration. *Biomaterials* **2013,** *34* (21), 5059-5069.
(304) Salata, L. A.; Hatton, P. V.; Devlin, A. J.; Craig, G. T.; Brook, I. M. In vitro and in vivo evaluation of e-PTFE and alkali-cellulose membranes for guided bone regeneration. *Clinical Oral Implants Research* **2001,** *12* (1), 62-68.
(305) Retzepi, M.; Donos, N. Guided Bone Regeneration: biological principle and therapeutic applications. *Clinical Oral Implants Research* **2010,** *21* (6), 567-576.
(306) Rajzer, I.; Menaszek, E.; Kwiatkowski, R.; Planell, J. A.; Castano, O. Electrospun gelatin/poly(ε-caprolactone) fibrous scaffold modified with calcium phosphate for bone tissue engineering. *Materials Science and Engineering: C* **2014,** *44*, 183-190.
(307) Binulal, N. S.; Natarajan, A.; Menon, D.; Bhaskaran, V. K.; Mony, U.; Nair, S. V. PCL–gelatin composite nanofibers electrospun using diluted acetic acid–ethyl acetate solvent system for stem cell-based bone tissue engineering. *Journal of Biomaterials Science, Polymer Edition* **2014,** *25* (4), 325-340.
(308) Yoshimoto, H.; Shin, Y. M.; Terai, H.; Vacanti, J. P. A biodegradable nanofiber scaffold by electrospinning and its potential for bone tissue engineering. *Biomaterials* **2003,** *24* (12), 2077-2082.
(309) Li, C.; Vepari, C.; Jin, H. J.; Kim, H. J.; Kaplan, D. L. Electrospun silk-BMP-2 scaffolds for bone tissue engineering. *Biomaterials* **2006,** *27* (16), 3115-3124.
(310) Liang, D.; Hsiao, B. S.; Chu, B. Functional electrospun nanofibrous scaffolds for biomedical applications. *Advanced Drug Delivery Reviews* **2007,** *59* (14), 1392-1412.
(311) Fernandes, J. S.; Gentile, P.; Martins, M.; Neves, N. M.; Miller, C.; Crawford, A.; Pires, R. A.; Hatton, P.; Reis, R. L. Reinforcement of poly-l-lactic acid electrospun membranes with strontium borosilicate bioactive glasses for bone tissue engineering. *Acta Biomaterialia* **2016,** *44*, 168-177.
(312) Santocildes-Romero, M. E.; Goodchild, R. L.; Hatton, P. V.; Crawford, A.; Reaney, I. M.; Miller, C. A. Preparation of composite electrospun membranes containing strontium-substituted bioactive glasses for bone tissue regeneration. *Macromolecular Materials and Engineering* **2016,** *301* (8), 972-981.

(313) Cao, W.; Li, H.; Zhang, J.; Li, D.; Acheampong, D. O.; Chen, Z.; Wang, M. Periplasmic expression optimization of VEGFR2 D3 adopting response surface methodology: Antiangiogenic activity study. *Protein Expression and Purification* **2013,** *90* (2), 55-66.
(314) Huang, C.; Chen, R.; Ke, Q.; Morsi, Y.; Zhang, K.; Mo, X. Electrospun collagen–chitosan–TPU nanofibrous scaffolds for tissue engineered tubular grafts. *Colloids and Surfaces B: Biointerfaces* **2011,** *82* (2), 307-315.
(315) Kim, C. H.; Khil, M. S.; Kim, H. Y.; Lee, H. U.; Jahng, K. Y. An improved hydrophilicity via electrospinning for enhanced cell attachment and proliferation. *Journal of Biomedical Materials Research Part B: Applied Biomaterials* **2006,** *78B* (2), 283-290.
(316) Ghasemi-Mobarakeh, L.; Prabhakaran, M. P.; Morshed, M.; Nasr-Esfahani, M. H.; Ramakrishna, S. Electrospun poly(ε-caprolactone)/gelatin nanofibrous scaffolds for nerve tissue engineering. *Biomaterials* **2008,** *29* (34), 4532-4539.
(317) Singha, P.; Pant, J.; Goudie, M. J.; Workman, C. D.; Handa, H. Enhanced antibacterial efficacy of nitric oxide releasing thermoplastic polyurethanes with antifouling hydrophilic topcoats. *Biomaterials Science* **2017,** *5* (7), 1246-1255.
(318) Schiffman, J. D.; Schauer, C. L. Cross-linking chitosan nanofibers. *Biomacromolecules* **2007,** *8* (2), 594-601.
(319) Hsieh, S. C.; Tang, C. M.; Huang, W. T.; Hsieh, L. L.; Lu, C. M.; Chang, C. J.; Hsu, S. H. Comparison between two different methods of immobilizing NGF in poly(DL-lactic acid-co-glycolic acid) conduit for peripheral nerve regeneration by EDC/NHS/MES and genipin. *Journal of Biomedical Materials Research Part A* **2011,** *99A* (4), 576-585.
(320) Ren, K.; Wang, Y.; Sun, T.; Yue, W.; Zhang, H. Electrospun PCL/gelatin composite nanofiber structures for effective guided bone regeneration membranes. *Materials Science and Engineering: C* **2017,** *78*, 324-332.
(321) Feng, B.; Tu, H.; Yuan, H.; Peng, H.; Zhang, Y. Acetic-acid-mediated miscibility toward electrospinning homogeneous composite nanofibers of GT/PCL. *Biomacromolecules* **2012,** *13* (12), 3917-3925.
(322) van de Witte, P.; Dijkstra, P. J.; van den Berg, J. W. A.; Feijen, J. Phase separation processes in polymer solutions in relation to membrane formation. *Journal of Membrane Science* **1996,** *117* (1), 1-31.
(323) Kim, J. S.; Ho, P. K. H.; Murphy, C. E.; Friend, R. H. Phase separation in polyfluorene-based conjugated polymer blends: lateral and vertical analysis of blend spin-cast thin films. *Macromolecules* **2004,** *37* (8), 2861-2871.
(324) Dobry, A.; Boyer-Kawenoki, F. Phase separation in polymer solution. *Journal of Polymer Science* **1947,** *2* (1), 90-100.
(325) Wong, D. W. S.; Camirand, W. M.; Pavlath, A. E.; Parris, N.; Friedman, M. Structures and functionalities of milk proteins. *Critical Reviews in Food Science and Nutrition* **1996,** *36* (8), 807-844.
(326) Pelegrine, D. H. G.; Gasparetto, C. A. Whey proteins solubility as function of temperature and pH. *LWT - Food Science and Technology* **2005,** *38* (1), 77-80.
(327) Gupta, A. N.; Bohidar, H. B.; Aswal, V. K. Surface patch binding induced intermolecular complexation and phase separation in aqueous solutions of similarly charged gelatin−chitosan molecules. *The Journal of Physical Chemistry B* **2007,** *111* (34), 10137-10145.
(328) Liu, X.; Ma, P. X. Phase separation, pore structure, and properties of nanofibrous gelatin scaffolds. *Biomaterials* **2009,** *30* (25), 4094-4103.
(329) Xue, J.; He, M.; Liu, H.; Niu, Y.; Crawford, A.; Coates, P. D.; Chen, D.; Shi, R.; Zhang, L. Drug loaded homogeneous electrospun PCL/gelatin hybrid nanofiber structures for anti-infective tissue regeneration membranes. *Biomaterials* **2014,** *35* (34), 9395-9405.
(330) D'Sa, R. A.; Raj, J.; Dickinson, P. J.; McCabe, F.; Meenan, B. J. Human fetal osteoblast response on poly(methyl methacrylate)/polystyrene demixed thin film blends: surface

chemistry vs topography effects. *ACS Applied Materials and Interfaces* **2016,** *8* (24), 14920-14931.
(331) Butler, M. F.; Ng, Y. F.; Pudney, P. D. A. Mechanism and kinetics of the crosslinking reaction between biopolymers containing primary amine groups and genipin. *Journal of Polymer Science Part A: Polymer Chemistry* **2003,** *41* (24), 3941-3953.
(332) Chong, E. J.; Phan, T. T.; Lim, I. J.; Zhang, Y. Z.; Bay, B. H.; Ramakrishna, S.; Lim, C. T. Evaluation of electrospun PCL/gelatin nanofibrous scaffold for wound healing and layered dermal reconstitution. *Acta Biomaterialia* **2007,** *3* (3), 321-330.
(333) Elzein, T.; Nasser-Eddine, M.; Delaite, C.; Bistac, S.; Dumas, P. FTIR study of polycaprolactone chain organization at interfaces. *Journal of Colloid and Interface Science* **2004,** *273* (2), 381-387.
(334) Ki, C. S.; Baek, D. H.; Gang, K. D.; Lee, K. H.; Um, I. C.; Park, Y. H. Characterization of gelatin nanofiber prepared from gelatin–formic acid solution. *Polymer* **2005,** *46* (14), 5094-5102.
(335) Davies, S. C.; Fowler, T.; Watson, J.; Livermore, D. M.; Walker, D. Annual Report of the Chief Medical Officer: infection and the rise of antimicrobial resistance. *The Lancet* **2013,** *381* (9878), 1606-1609.
(336) Payne, D. J.; Gwynn, M. N.; Holmes, D. J.; Pompliano, D. L. Drugs for bad bugs: confronting the challenges of antibacterial discovery. *Nature Reviews Drug Discovery* **2007,** *6* (1), 29-40.
(337) Gristina, A. G. Biomaterial-centered infection: microbial adhesion versus tissue integration. *Science* **1987,** *237* (4822), 1588.
(338) Gristina, A. G.; Rovere, G. D.; Shoji, H.; Nicastro, J. F. An in vitro study of bacterial response to inert and reactive metals and to methyl methacrylate. *Journal of Biomedical Materials Research* **1976,** *10* (2), 273-281.
(339) Gristina, A. G.; Naylor, P. T.; Myrvik, Q. N. Musculoskeletal infection, microbial adhesion, and antibiotic resistance. *Infectious disease clinics of North America* **1990,** *4* (3), 391-408.
(340) Tatakis, D. N.; Promsudthi, A.; Wikesjö, U. M. E. Devices for periodontal regeneration. *Periodontology 2000* **1999,** *19* (1), 59-73.
(341) Bottino, M. C.; Thomas, V.; Schmidt, G.; Vohra, Y. K.; Chu, T. M. G.; Kowolik, M. J.; Janowski, G. M. Recent advances in the development of GTR/GBR membranes for periodontal regeneration—A materials perspective. *Dental Materials* **2012,** *28* (7), 703-721.
(342) Fuseler, J. W.; Valarmathi, M. T. Nitric oxide modulates postnatal bone marrow-derived mesenchymal stem cell migration. *Frontiers in Cell and Developmental Biology* **2016,** *4* (133).